NTNU

Norwegian University of
Science and Technology

Performance Evaluation of a Multi-Branch Liquid-Gas Pipe Separator using Computational Fluid Dynamics

Helene Sund Refsnes

Petroleum Geoscience and Engineering
Submission date: June 2018
Supervisor: Milan Stanko, IGP
Co-supervisor: Mariana J.C. Diaz Arias, IGP

Norwegian University of Science and Technology
Department of Geoscience and Petroleum

Preface

This master thesis was written at the Department of Geoscience and Petroleum (IPT) at the Norwegian University of Science and Technology (NTNU) in Trondheim, Norway. It was prepared as part of the course ”TPG4920 - Petroleum Engineering - Master’s thesis” during the spring of 2018.

I would like to thank my supervisor, Milan Stanko, and my co-supervisor, Mariana J.C. Diaz Arias, for their guidance, advice and help throughout the project. I would also like to thank Gilberto Nuñez for taking his time to help me with technical issues and give useful input and help on numerical simulations. Audun Faanes arranged a meeting at Equinor where I got valuable information and advice on future work, in which I am grateful.

Regards,
Helene Sund Refsnes

June 2018

Summary

The present thesis aims to evaluate the performance of a multi-branch gas-liquid separator by means of 3D computational fluid dynamics (CFD). Thus, numerical simulations of the two-phase system were performed using various operating conditions to determine the potential of such a separator in terms of separation efficiency and slug handling capacity. The separation efficiency was measured by quantifying the liquid carry over and gas blowby.

The capability of 4 multiphase models in a commercial software to represent realistic flow distributions and separation of an oil-gas mixture in the multi-branch separator was evaluated. The inhomogeneous mixture model was the multiphase model providing the most realistic results and best convergence behaviour and was employed for simulations performed to quantify the performance of the separator.

The effect of the pressure difference between the two outlets on separation performance was analyzed using multiple different pressures in the gas outlet. A small variation in outlet pressure was found to have a large effect on the flow distribution. Optimal operating conditions regarding the pressure difference between the two outlets have been found. Inlet conditions with various volume fractions showed a small effect on the gas separation performance and no effect on the liquid separation performance and flow distribution.

Hydrodynamic slug flow at two different frequencies was studied. A high separation performance, similar to simulations with stable inlet conditions, was seen for the high-frequency slugs while the longer slugs resulted in a slightly reduced performance. Thus, the multi-branch separator showed well slug-handling abilities for the studied slug flow conditions.

Sammendrag

Målet for denne oppgaven er å evaluere separasjonsegenskapene til en rørbasert gass/væske-separator ved hjelp av 3D numerisk fluiddynamikk (*Computational Fluid Dynamics* - CFD). Numeriske simuleringer av tofasesystemet ble utført under ulike operasjonsbetingelser for å bestemme potensialet til en slik separator i form av separasjonsytelse og bufferkapasitet ved slug-strømning. Separasjonsytelsen ble målt ut ifra mengden olje ført ut gjennom gassutløpet og mengden gass ført ut gjennom væskeutløpet.

Fire flerfasemodeller i en kommersiell programvare ble evaluert etter evnen til å produsere en realistisk separasjon og realistiske strømningsmønstre av en olje-gassblanding i separatoren. Flerfasemodellen som viste de beste konvergeringsegenskapene og ga de mest realistiske resultatene var den inhomogene *mixture model*. Denne modellen ble derfor videre brukt for simuleringer utført for å kvantifisere separasjonsegenskapene.

Hvordan ulike trykkforskjeller mellom de to utløpene påvirker separasjonsytelsen ble analysert ved å bruke flere forskjellige trykk i gassutløpet. En liten variasjon i utløpstrykket hadde stor effekt på strømningsfordelingen. Optimale driftsforhold med hensyn til trykkforskjellen mellom de to uttakene har blitt funnet. Et studie av ulike volumfraksjoner i innløpet viste liten effekt på gasseparasjonen og ingen effekt på væskeseparasjonen eller strømningsmønsteret.

Hydrodynamisk slug-strømning av to ulike frekvenser ble studert. En høy separasjonsytelse, sammenlignbart med simuleringer med stabile innløpsbetingelser, ble sett for høyfrekvent slugging. Lengre slugger resulterte i en noe redusert separasjonsytelse. Separatoren viste gode slug-håndteringsevner for de studerte strømningsbetingelsene.

Table of Contents

List of Tables

List of Figures

List of Symbols

Abbreviations

CFD	Computational fluid dynamics
GCU	Gas carry under
GVF	Gas volume fraction
LCO	Liquid carry over
MAX	Maximum
OG	Outlet gas
OL	Outlet liquid
RMS	Root mean square

Subscripts

b	Bubble
c	Continuous fluid
d	Droplet
g	Gas
l	Liquid
o	Oil
p	Particle

Symbols

α	Volume fraction

Δy	Distance from wall	m
δ	Boundary layer thickness	m
η	Separation performance	
μ	Dynamic viscosity	Pas
ρ	Density	kg/m^3
τ_w	Wall shear stress	Pa
A	Cross-sectional area	m^2
C_D	Drag coefficient	
C_f	Skin friction coefficient	
D	Diameter	m
F_b	Buoyancy force	N
F_f	Friction force	N
F_g	Gravitational force	N
g	Gravity	m/s^2
m	Mass flow	kg/s
q	Flow rate	m^3/s
Re	Reynolds number	
u	Velocity	m/s
u_*	Wall characteristic velocity, called friction velocity	m/s
u_{mix}	Mixture velocity	m/s
V	Volume	m^3
y^+	Dimensionless wall distance	

Chapter 1

Introduction

Subsea processing has been used for many years in the industry, and have gradually been used in deeper water depths and for increased tieback distances (Kondapi et al., 2017). Utilization of subsea processing provides many benefits; it adds additional energy to the production fluid, making it economically viable to produce from low-energy reservoirs, deep-water fields and fields far away from topside facilities. Subsea separation upstream of boosting equipment enables the use of a compressor and increases the efficiency of a pump. Subsea separation and re-injection of water reduces both liquid loading in the pipelines and necessary topside infrastructure. A subsea separation of fluids is also used to manage flow assurance risks, by giving enhanced control over the flow and mitigate the formation of solids.

There are challenges regarding moving equipment subsea, especially considering deep-water fields with high pressure. Conventional separator vessels with a large diameter require thick walls, hence the equipment is heavy and expensive. Reducing the diameter on separators gives a more compact solution compared to conventional vessels, as they require a thinner wall. Many compact separators exploit the advantages with a small diameter by the use of a pipe-based construction.

The gas-liquid pipe-based separator shown in Fig. 1.1, consists of a downward inclined horizontal pipe with six vertical pipes for gas removal. The liquid will flow down the lower horizontal pipe as this is the heavy phase, while the gas will rise through the vertical pipes and out of the upper horizontal pipe. The vertical pipes will be partially filled with liquid and thus having a spare volume suitable to accomodate for fluctuations in the inlet flows of liquid and gas, e.g. due to slug flow (Sagatun et al., 2008). A small diameter provides short retention time, which makes the separator a compact solution compared to conventional vessels with larger diameters. The pipe-based construction is cost effective and a good solution for the high pressure in deep-water subsea facilities.

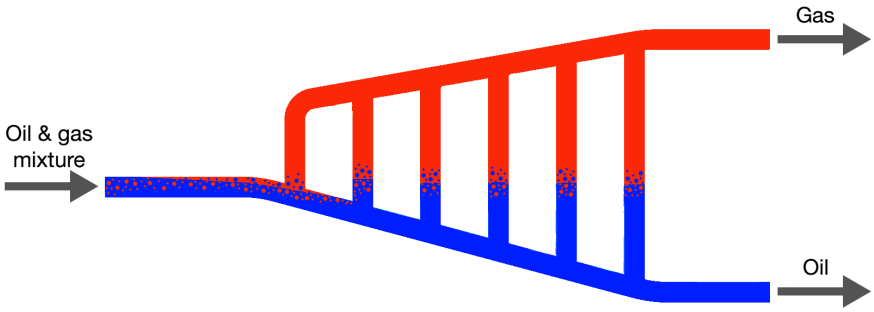

Figure 1.1: Function of the separator

The ultimate goal of this report is to model numerically the multiphase flow dynamics in the multi-branch oil-gas pipe separator and to quantify its efficiency and operational range. This thesis is a continuation of Refsnes (2017), where a mesh validation was carried out for single phase flow conditions in the multi-branch separator presented in this report. This study utilizes the same mesh for multiphase flow conditions.

The objective of this study is to use a numerical setup in ANSYS CFX, a computational fluid dynamics tool, to analyse the flow behaviour and performance of the separator for different boundary conditions. The mesh used for the numerical simulations are validated using a discretization error analysis by Celik et al. (2008). The performance of four different multiphase models in ANSYS CFX are evaluated in terms of their convergence characteristics and observations on the flow distribution, to determine the model providing the most realistic results. The results of steady state and transient simulations are compared to find the most appropriate simulation approach. The effect of various outlet pressures and inlet volume fractions on the flow distribution and separation efficiency are tested to find optimal operating conditions. The flow behaviour and separation performance for two different slug flow conditions are evaluated.

Chapter structure

- The first two paragraphs in the introduction is taken from a specialization project written prior to this thesis (Refsnes, 2017).
- Chapter 2 presents theory which serves as an introduction to concepts related to conducted numerical experiments. This includes information on industry application of the multi-branch separator, gas-liquid separation, CFD, multiphase flow and turbulence. A procedure for discretization error analysis on meshes used for CFD studies is also introduced.
- Chapter 3 presents descriptions of geometry, settings and criteria for accepting results of implemented numerical models. Simulation plans and details on configurations of the numerical experiments are also presented here.
- Chapter 4 presents results of a discretization error analysis on the mesh as well as comparison and analysis of simulation results.
- Chapter 5 lists the main conclusions and recommendations for future work.

Chapter 2

Theory

Parts of the theory presented in this chapter is taken from a report written prior to this thesis (Refsnes, 2017). This includes: a small part of Section 2.1; all of Section 2.2, 2.3 and 2.6; the first part of Section 2.4 (before Section 2.4.1); most of section 2.5 (except 2.5.1).

2.1 Industry application of the multi-pipe separator

The multi-pipe separator studied in this thesis is inspired by the Harp separator, patented by Norsk Hydro (Gramme and Lie, 2011), which is a part of the SSAO Marlim Project (SSAO is short for Separação Submarina Água-Óleo in Portugese, which means Subsea Oil-Water Separation) in the Marlim field in Brazil (Orlowski et al., 2012), (Euphemio et al., 2012). The Harp is placed at a water depth of 876 meters and the fluids travel 2,400 meters from the subsea processing unit to the topside facility (Euphemio et al., 2012). Marlim field is a brownfield producing with a high water cut. Topside processing and disposing of water is expensive, hence a subsea water separation station with a configuration as shown in Fig. 2.1 was implemented to reduce costs. The Harp is placed at the inlet of a pipe separator for oil-water separation, which is designed for a liquid flow rate of 3500 m^3/d (Euphemio et al., 2012). The water is further processed and reinjected into the formation while the oil and gas are mixed and transported to surface facilities. The main intention of the Harp is slug catching and bulk separation of gas to enable the use of a small diameter in the pipe separator downstream of the liquid outlet.

Such a pipe-based separator could be used for different applications, especially upstream of gas or liquid boosters. Gas compression systems, for instance, can be very sensitive of the liquid content in the gas stream, compromising the equipment performance. Liquid boosting, on the other hand, can tolerate very high void fraction in the liquid stream, but at expense of efficiency and boosting capability. Gas-liquid separation may enable better operating conditions and allow higher boosting efficiency in both cases.

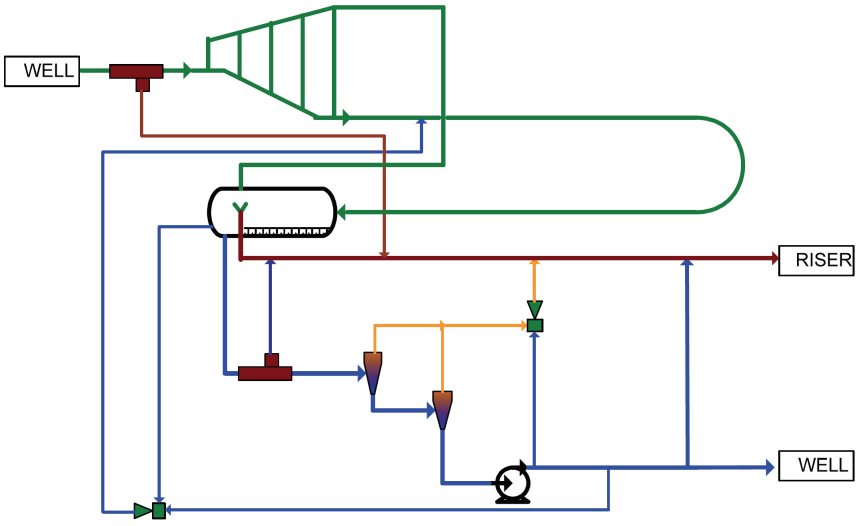

Figure 2.1: System configuration of SSAO Marlim Project (Orlowski et al., 2012)

2.2 Gas-liquid separation

Separation of a mixture of two fluids require enough time spent in a separator for the droplets and bubbles to settle. This section introduces a simplified explanation of particle settling and explains which forces affects the settling time. Compact separation technology which implement solutions to decrease the settling time of a droplet/bubble are also presented.

2.2.1 Droplet/bubble dynamics

A particle entrapped in a continuous fluid will have a gravitational force (F_g) and a buoyancy force (F_b) acting in opposite directions. The particle will rise in the continuous fluid if it consists of a lower density and sink if it consists of a higher density. As the rising/sinking velocity increases, so will the friction force (F_f) acting on the particle until a constant velocity is reached. The same forces act on droplets and bubbles. Thus, the forces acting on a droplet, d, in continuous gas and on a bubble, b, in continuous liquid are showed in Fig. 2.2.

A constant sinking velocity, also called terminal velocity, of a constant volume particle, p, in a continuous static fluid, c, will have equal forces acting in opposite directions. The sinking velocity of a droplet, u_d is expressed as in Eq. 2.4, and is found by putting the gravitational force (Eq. 2.2) equal to the sum of the buoyancy (Eq. 2.3) and the frictional force (Eq. 2.1). The rising speed of a bubble, u_b is expressed in Eq. 2.5.

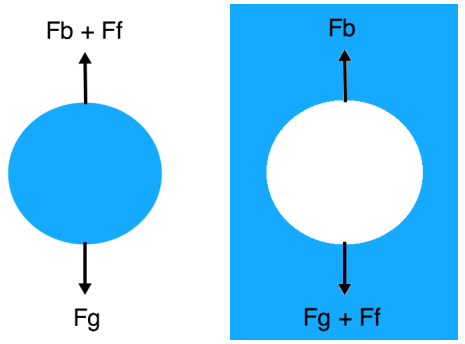

(a) Droplet in continuous gas

(b) Bubble in continuous liquid

Figure 2.2: Forces acting on a sinking/rising droplet/bubble in continuous fluid

$$F_f = 0.5 C_D \rho_c u_p^2 A_p \tag{2.1}$$

$$F_g = \rho_p g V_p \tag{2.2}$$

$$F_b = \rho_c g V_p \tag{2.3}$$

Where:
C_D is a drag coefficient.
ρ is density $[kg/m^3]$.
g is gravitational acceleration $[m/s^2]$.
$A_p = \pi D_p^2/4$ is the cross-sectional area of the particle $[m^2]$.
$V_p = \pi D_p^3/6$ is the volume of the particle $[m^3]$.
D_p is the particle diameter $[m]$.

$$u_d = \sqrt{\frac{4}{3}\frac{g D_d}{C_D}}\sqrt{\frac{\rho_l - \rho_g}{\rho_g}} \tag{2.4}$$

$$u_b = \sqrt{\frac{4}{3}\frac{g D_b}{C_D}}\sqrt{\frac{\rho_l - \rho_g}{\rho_l}} \tag{2.5}$$

The drag coefficient depends, among other factors, on the Reynolds number of the particle (Re_p). The Reynolds number (Eq. 2.6) is based on the relative velocity between the particle and the continuous phase, $u_{p,r}$.

$$Re_p = \frac{\rho_c D_p u_{p,r}}{\mu_c} \tag{2.6}$$

Where μ is the dynamic viscosity [Pas].

The sinking/rising velocity of a droplet/bubble in a continuous phase is affected by multiple variables, such as density, viscosity and droplet size. The flow direction of the continuous phase relative to the direction of the gravity force plays an important role as well.

The maximum droplet/bubble size in a continuous flowing fluid differs from a static fluid due to turbulent velocity fluctuations. Droplets and bubbles will continuously change in size, as surface tension makes them coalesce while turbulent forces break them up. It is complicated to calculate an exact terminal velocity of a droplet/bubble trapped in a flowing fluid, but the terminal velocity of a droplet/bubble in a static fluid provides an idea of the factors affecting the separation of two fluids.

2.2.2 Compact separation

Residence time of each individual fluid is the amount of time the fluid spends in a separator. The required residence time to separate the fluids depends on the terminal velocity of a droplet/bubble and the distance it has to travel. Compact separation technologies address these two factors to decrease the necessary retention time. Some compact solutions use centrifugal force to increase the settling velocity, as the gravitational acceleration, g, can be replaced with centripetal acceleration, rw^2, in Eq. 2.2 and 2.3 for these cases, where r is the radius of the swirling motion and w is the angular velocity. Compact gravity-based separators use a small diameter to shorten the transport distance, hence a shorter residence time is necessary. The pipe-based separator addressed in this report is an example of a compact gravity-based gas-liquid separator with a small diameter.

2.3 CFD

Computational Fluid Dynamics (CFD) is the use of computational methods like numerical analyses and data structures to solve fluid flow problems and how the flow affects and interact with contours it flows past. Computers are used to numerically solve the partial differential equations. The Finite Volume Method is a common approach to solve these equations, and is the method used in the CFD simulation tool ANSYS CFX. The method consists of dividing the fluid domain into small volumes, and numerically solve the equations in each volume.

CFD processing is split into four main steps: pre-processing, solver and post-processing (Versteeg and Malalasekera, 1995), as shown in the flowchart of Fig. 2.3.

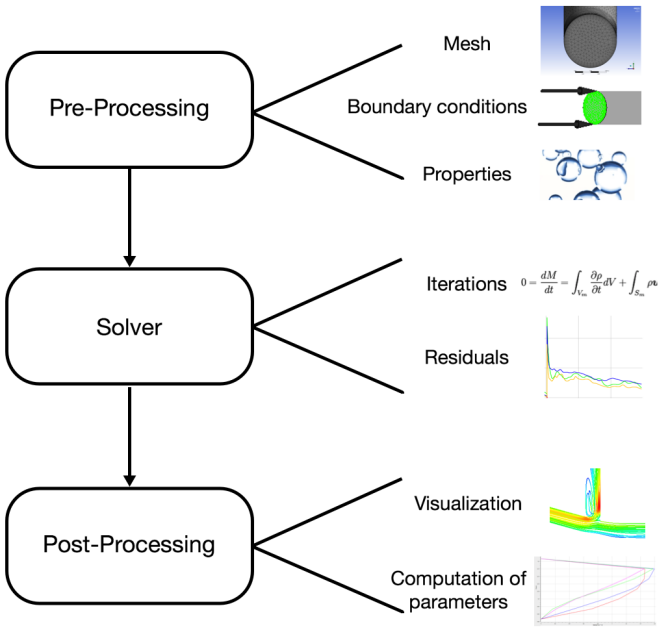

Figure 2.3: CFD flowchart

Pre-processing includes geometry and mesh creation of the system as well as specifications for the fluid flow simulation. Not all physical and chemical processes are of interest for different applications. Thus, it is necessary to select which processes that needs to be modelled and leave out the rest to reduce computational effort. Defining fluid properties and setting boundary conditions needed to solve the problem is also done in this stage.

Solver is the part where the simulation is run, and fluid flow behaviour is approximated by solving equations iteratively using an initial guess. Residuals are a measure of how close the results of the equations are to the exact solution and is used as a measure of convergence of the results. Root Mean Square (RMS) values of all the residuals in the domain are used as a measure of solution convergence as a whole. Max residuals show the value of the highest residuals found in one specific node in the domain.

Post-processing contain information on the fully developed flow in the system which contain multiple graphics capabilities. Creation of plots, surfaces or other graphics is used to get information on the flow behaviour.

CFD has been used in a variety of physical problems and is widely used to get information on the flow behaviour inside a system for design purposes in the petroleum industry. The simulation program allows users to compare the flow behaviour and separation performance of multiple designs before a prototype is made, resulting in a reduced amount of costly experimental testing.

Performing CFD simulations in addition to experimental testing is advantageous as it provides details on internal flow dynamics in addition to visual results from experiments.

2.4 Multiphase flow

This section presents a brief description on multiphase flow, an introduction to multiphase flow models available in ANSYS CFX and examples of models employed in multiphase simulations.

Multiphase flow is a flow at which multiple phases are present. Flows with a mixture of gas and liquid, solid particles and liquid or gas, solids and liquid are examples of multiphase flows. A flow consisting of two liquids with different densities, such as oil and water, is also considered multiphase.

The composition of multiphase flows can be split into two main groups: dispersed or separated flow (Bratland, 2010). A flow where one phase is dispersed into noncontinuous elements in a continuous second phase is called a dispersed flow. Gas bubbles in a continuous liquid or solid particles in a continuous gas are examples of dispersed flows (Fig. 2.4a). In a separated flow, both phases are continuous with one contact surface between them. Stratified flow or annular flow are examples of separated flows (Fig. 2.4b and 2.4c).

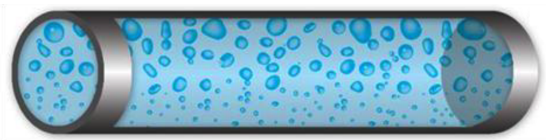

(a) Dispersed bubble flow

(b) Stratified flow

(c) Annular flow

Figure 2.4: Dispersed and separated flows (Bratland, 2010)

2.4.1 Slug flow

Slug flow is a common flow regime in the industry. It is an alternating flow with gas bubbles, also called Taylor bubbles or gas pockets, and liquid slugs as shown in Fig. 2.5. The figure shows a hydrodynamic slug which generally have a length of less than 500 times the pipe diameter (Bratland, 2010).

Figure 2.5: Slug flow (Bratland, 2010)

Liquid slugs contains entrained gas bubbles. Hence, the liquid volume fraction (α_l) is generally less than one. The diameter of a Taylor bubble can be up to the inner diameter of the pipe. Taylor bubbles contains small liquid droplets and a liquid film along the pipe wall, which is placed below the bubble for horizontal pipe flow. The gas volume fraction (α_g) is therefore generally less than one for gas bubbles during slug flow conditions.

2.4.2 ANSYS CFX multiphase models

This chapter presents details on available multiphase models in ANSYS CFX and information on what conditions the models apply for and are recommended for.

It is possible to choose between homogeneous or inhomogeneous flow conditions, include free surface calculations and select an interphase transfer model. Two of the available fluid morphologies are continuous-continuous or continuous-dispersed flows. Examples of momentum transfer terms which can be considered are buoyancy, drag force and different non-drag forces.

The inhomogeneous model

All fluids have their own phase equations, hence possesses their own flow field. Different sub-models are used to model the interaction between the fluids via interphase transfer terms. The available sub-models are; the particle model, the mixture model and the free surface model. Appendix B provides details about when the different models are applicable.

The particle model requires one continuous and one dispersed phase with a diameter to specify beforehand as an input parameter. It is possible to model the dispersed phase by the use of a single bubble size, called mono-dispersion, or multiple bubble sizes, called poly-dispersion. The model is recommended for simple dispersed flow problems like gas-liquid bubbly flows, liquid droplets in a gas or an immiscible liquid or solid particles in a fluid (ANSYS, 2016).

The mixture model requires both phases to be continuous and treats the phases symmetrically. Properties of the fluids are calculated as volume averaged mixtures. It is suitable and possibly a better model than the particle model for flows with complex interfacial boundaries and for gas-liquid flows with flow regime transition (ANSYS, 2016).

The homogeneous model

Each fluid has its own flow field in the inhomogeneous model, while they share a common flow field as a result of a large interphase transfer rate in the homogeneous model. This result in simplified physics as no slip between the fluids are assumed. The phase-specific equations in the inhomogeneous model are reduced to a shared phase equation. Thus, the homogeneous model is the least computationally expensive of the two models. Homogeneous settings exist for velocity, heat transfer and turbulence equations, resulting in the fluids sharing a common phase equation for the variable in question.

The homogeneous model is valid for completely stratified gravity flows where the interphase is clear. Drag dominated flows like dispersed flows with very small particles is also a valid case, as the phase velocities equalize very quickly. Particles in a continuous phase will in other cases reach a slip velocity relative to the continuous phase. The homogeneous model is only recommended for these flows if the slip velocities are very small compared to the mean flow velocity.

An interphase transfer model must be specified when the homogeneous model is selected, even though the model does not account for interphase transfer terms. This setting will only affect heat and mass transfer calculations, as some heat- and mass transfer models may require interphase transfer modelling. The choice of interphase transfer model will therefore not affect simulations performed without heat- or mass transfer.

Free surface flow

Free surface flow modelling is used to capture a well-defined and crisp interphase between the fluids and may be good solution when the mesh is not fine enough to keep the smearing of the interphase small enough. Simulations with free surface enabled requires more time to run and is therefore mostly used when the position of the interphase between fluids are of great interest.

It is recommended to use the homogeneous model together with free surface flow when the flow contain a well-defined interphase. The inhomogeneous model may be a better choice if the flow contain entrainment of one phase in the other (ANSYS, 2016).

Modelling surface tension may increase the accuracy of the fluid interphase and is only possible when the flow is set to free surface, as shown in Appendix B.

2.5 Turbulence

Most flows in engineering practices are turbulent, thus it is of interest to understand the behaviour of this flow regime. Turbulent flows are random and chaotic with swirling flow structures, called eddies, of different sizes. Mass, momentum and heat are more effectively transported by these eddies across streamlines in a turbulent flow compared to a laminar flow regime. Higher values of friction are also seen in turbulent flows (Versteeg and Malalasekera, 1995), (Cimbala and Çengel, 2014).

The velocity profile of a turbulent flow contain a sharp drop in velocity near the wall and is much more complex than it is for laminar flow. The main forces affecting the structure and flow behaviour of a turbulent flow changes when it gets close to a wall. Turbulent effects, also called inertia forces, are dominant far from the wall in what is called the outer layer, while viscous effects gradually get more dominant closer to the wall. Viscous effects are dominant in the layer next to the wall, called the linear sub-layer, where the velocity profile is close to linear. Viscous effects are dominant in the next layer as well, the buffer layer, but turbulent effects are gradually becoming more significant. The log-law layer lies between the buffer layer and the outer layer. Turbulent effects are more dominant in this layer than it is in the buffer layer, but viscous effects are still dominant.

A non-dimensional distance, y^+, which resembles the local Reynolds number is a coordinate used to describe the three layers in the inner region and can be expressed as in Eq. 2.7.

$$y^+ = \frac{\rho u_* \Delta y}{\mu} \tag{2.7}$$

Values of y^+ in the layers close to the wall are (Versteeg and Malalasekera, 1995):

- y^+<5: Linear sub-layer
- 5<y^+<30: Buffer layer
- 30<y^+<500: Log-law layer

Values of y^+ are widely used to describe the coarseness of the mesh in CFD. A value of y^+ around 1 is desirable for modelling of near-boundary stream effects, while a y^+ value in the log-law region is preferable when the near wall effects only need to be accounted for in the calculations (Salim and Cheah, 2009).

2.5.1 Calculation of y^+ for pipe flow

Y^+ values for a fluid flowing in a pipe with inner diameter (ID) is found using Eq. (2.8)-(2.12) (cfd online, 2011).

Reynolds number:

$$Re = \frac{\rho u ID}{\mu} \tag{2.8}$$

Skin friction coefficient for turbulent flow in a smooth pipe (Blasius, 1913):

$$C_f = 0.079Re^{-0.25} \tag{2.9}$$

Wall shear stress:

$$\tau_w = C_f \frac{1}{2}\rho u^2 \tag{2.10}$$

Friction velocity:

$$u_* = \sqrt{\frac{\tau_w}{\rho}} \tag{2.11}$$

Y^+ at the first mesh layer at a distance Δy_1 from the pipe wall:

$$y^+ = \frac{\rho u_* \Delta y_1}{\mu} \tag{2.12}$$

2.5.2 ANSYS CFX turbulence models

ANSYS CFX contains many turbulence models which have different advantages. The k-w and the Spalart-Allmaras are good models for meshes with y^+ values in the linear sub-layer, because they are designed for a mesh that is sufficiently accurate to account for all wall-functions. Other models are coupled with a near-wall treatment that works best for a mesh in the log-law region. Examples of these models are k-ε and RSM (Versteeg and Malalasekera, 1995). It used to be recommended to avoid a mesh that resolves the buffer layer for the models designed for the log-law region (Salim and Cheah, 2009). The use of scalable wall functions has however removed the problems associated with low y^+ values (ANSYS, 2016). Turbulence models that are coupled with near-wall treatment are therefore only limited by an upper y^+ value.

Both RSM and k-ε are good turbulence models for industrial applications such as performance analysis on separators. RSM accounts for all individual Reynolds stresses, the k-ε model assumes an isotropic turbulent viscosity (Versteeg and Malalasekera, 1995). Simulation using the RSM turbulence model gives more accurate results but require a much higher computational effort compared to k-ε as it solves multiple extra PDEs. K-ε is the most widely used turbulence model and provides sufficient results for a variety of applications.

2.6 Some examples of CFD simulations of multiphase flow undergoing separation

Afolabi and Lee (2014) used ANSYS Fluent with the particle model and RSM turbulence model to study air-water flow in a GLCC pipe separator. The air was treated as dispersed phase, characterizes by bubble diameter, in a continuous water phase. It was concluded that the multiphase- and turbulence model were good options for the current simulations.

Phase segregation in a helical pipe was analyzed by da Mota and Pagano (2014), with the use of an experimental study together with simulations in ANSYS CFX. K-ϵ was used as turbulence model, and the particle model was used for phase behaviour. Oil was defined as the continuous phase with water and gas as dispersed phases in the form of droplets and bubbles. Numerical simulations were in agreement with experimental results, which hints that the modelling assumptions are appropriate.

Monesi et al. (2013) conducted numerical simulations to check the performance of a slug catcher. Slugs consist of gas dominated stream altering with liquid waves, both of which can be of large dimensions in relation to the pipe. Two different models were created in ANSYS CFX for the liquid and the gas dominated stream. Simulations of the liquid dominated stream was conducted with the particle model using k-ϵ as turbulence model. The model was concluded to be able to predict the performance of the slug catcher for the corresponding operating conditions.

2.7 Discretization error analysis

This section presents a validation method of the numerical uncertainty of CFD simulations following the procedure produced by Celik et al. (2008). The uncertainty is validated using three meshes with an increasingly number of elements. A global cell size, h_i, is expected for a mesh i consisting of cells that are evenly distributed in the domain. The total volume of the fluid domain, V, may be used to find an average global cell size estimated using Eq. (2.13). The meshes are arranged so that mesh number one is the finest mesh, thus $h_1 < h_2 < h_3$.

$$h_i = \left[\frac{V}{N_i}\right]^{1/3} \tag{2.13}$$

Where N_i is number of elements in mesh i. The representative cell sizes are used to calculate the grid refinement factors, $r_{21} = h_2/h_1$ and $r_{32} = h_3/h_2$.

The apparent order, p, a measure of the local order of accuracy, is estimated using iterations on Eq.(2.14) with $q = 1$ as initial guess.

$$p = \frac{1}{ln(r_{21})}\left|ln\left|\frac{\varepsilon_{32}}{\varepsilon_{21}}\right| + q(p)\right| \tag{2.14a}$$

$$q = ln\left(\frac{r_{21}^p - s}{r_{32}^p - s}\right) \tag{2.14b}$$

$$s = 1 * sgn\left(\frac{\varepsilon_{32}}{\varepsilon_{21}}\right) \tag{2.14c}$$

Where ϕ_i is the solution of a variable of interest in mesh i, $\varepsilon_{32} = \phi_3 - \phi_2$ and $\varepsilon_{21} = \phi_2 - \phi_1$.

Fine grid convergense index, GCI, is a measure of the local order of accuracy and is obtained by solving Eq. (2.15),

$$GCI_{fine}^{21} = \frac{1.25 e_a^{21}}{r_{21}^p - 1} \tag{2.15}$$

where e_a^{21} is an approximate relative error defined as in Eq. (2.16).

$$e_a^{21} = \left| \frac{\phi_1 - \phi_2}{\phi_1} \right| \tag{2.16}$$

A global order of accuracy can be found by using the average value of p in Eq. (2.15). This value is recommended for calculation of error bars in computed results. An average value of the numerical uncertainty (GCI_{avg}) is found by taking the average of calculated global order of accuracy. A maximum discretization error (GCI_{max}) is the maximum of calculated global order of accuracy.

Chapter 3

Description of numerical simulations

3.1 Geometry

The geometry of the multi-pipe separator used for numerical simulations in this report is based on the Harp separator used for experiments performed at facilities in Porsgrunn, Norway (Moraes et al., 2012). This is a reduced scale separator compared to the Harp used in the Marlim field. The author didn't have access to the actual geometry of the separator, but reconstructed the geometry by studying the photos provided in the paper and making some assumptions. The modeled geometry of the separator showed in Fig. 3.1 is 4.9 m long and 2 m high, with a pipe diameter of 0.1524 m (6 inches). The boundaries of the separator are shown in Fig. 3.2.

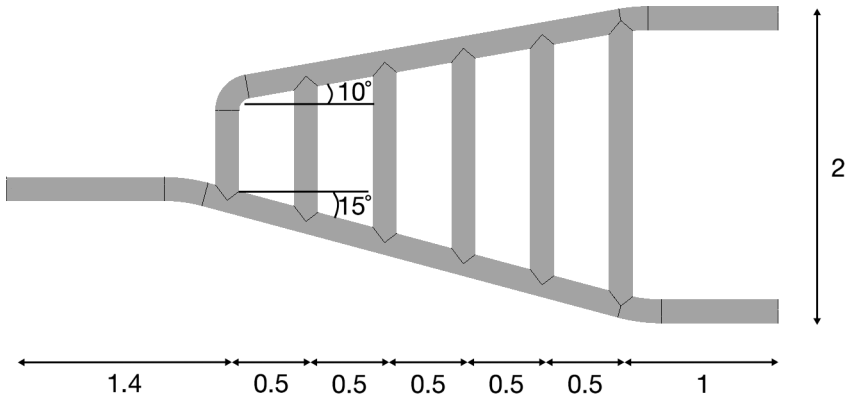

Figure 3.1: Separator design with units in meters (Refsnes, 2017)

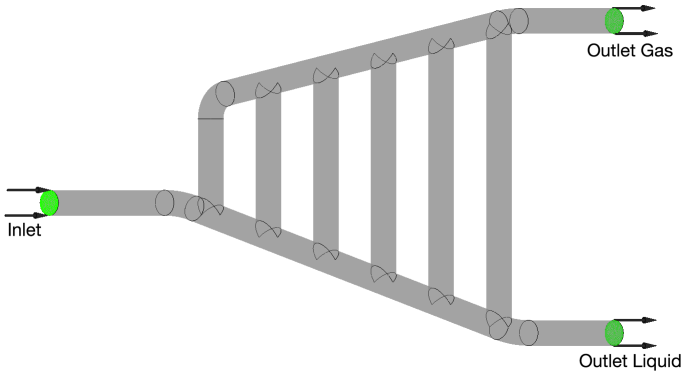

Figure 3.2: Inlet and outlets of the separator (Refsnes, 2017)

3.2 General settings of CFD simulations

Two fluids resembling oil and gas with density and viscosity as shown in Table 3.1 are used for all simulations. The properties are supposed to resemble in-situ fluid properties in the Marlim field Harp separator. A pressure of 85 $bara$, temperature equal 55 $°C$ and a 22° API oil is assumed to be the separator conditions (Euphemio et al., 2007), (Euphemio et al., 2012). The oil and gas properties have been obtained by using black oil correlations as described in the specialization project of Refsnes (2017).

Table 3.1: Oil and gas properties for multiphase simulation

Properties	
ρ_o $[kg/m^3]$	814
μ_o $[Pas]$	0.0095
ρ_g $[kg/m^3]$	128
μ_g $[Pas]$	1.6E-5

Boundary conditions are arranged in the following configuration as this is the most robust (ANSYS, 2016): mixture velocity, assumed to be uniform, and gas volume fraction (GVF) are specified in the inlet, while average static pressures are specified at both outlets. These outlet conditions are realistic as outlet pressures in standard separators may be controlled by valves, or by outlets connected to further separation stages with pressure regulations. The wall roughness of the pipes is set to a smooth wall with a non-slip boundary condition.

Gravity effects are accounted for by adding a gravity acceleration of -9.81 m/s^2 in the vertical direction. Buoyancy is the only interfacial transfer term which is common for all simulations. Fluids are assumed to be incompressible and no heat transfer is considered, as the fluids in a gas-oil separation process are assumed to flow from a reservoir and have

the same temperature. The turbulence is treated as homogeneous, using the k-ϵ model with scalable wall function.

The mesh used for all the simulations was selected after performing a mesh independence study under single phase flow conditions, conducted in the specialization project of Refsnes (2017). The mesh, shown in Fig. 3.3, is formed by tetrahedrons and consist of 1 226k nodes. An inflation layer close to the wall has a first layer thickness (Δy_1) of 4.8E-4 m. Expected y^+ values of both phases are calculated using Eq. (2.8)-(2.12) for a velocity of 2 m/s, resulting in y_g^+=240 and y_o^+=5. Lower values for the gas stream may produce better results. However, the value is within the log-law layer and is very low compared to the y_g^+ value in the pipe centre, which is 38,550. Thus, the mesh is assumed to provide sufficiently low y^+ values for the k-ϵ turbulence model for reliable results.

A more advanced mesh independence study, for validation of the discretization error of the mesh, is performed following the procedure by Celik et al. (2008). The three finest meshes from the mesh independence study are used for this study.

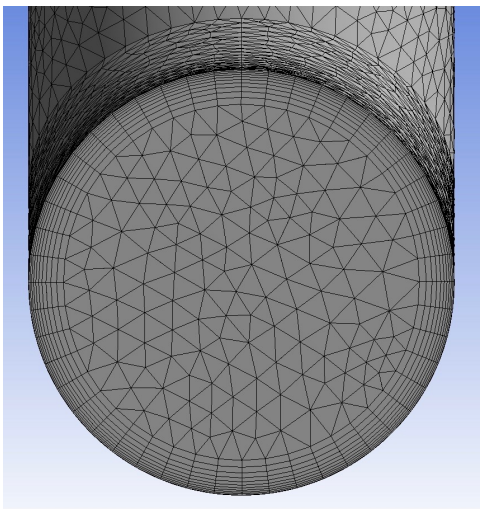

Figure 3.3: Cross section of the mesh (Refsnes, 2017)

Convergence criteria for the simulations are:

- Root mean square (RMS) residuals below a value of 5E-5
- Maximum (MAX) residuals below a value of 1E-3
- Imbalances below 1%

3.3 Description of all simulations

This section presents details on performed simulations of gas-oil separation in the multi-branch separator. Evaluation of the ability of four models to represent a realistic flow behaviour in the domain, is conducted to find the most suitable model for studies on the separation process. The selected model is employed in simulations for performance evaluation of different operational conditions. This includes studies on the effect of outlet pressures, inlet volume fractions and slug flow conditions. An overview of the simulation process is shown in Fig. 3.4.

3.3.1 CFD simulations for model selection

This chapter presents details on the models in Fig. 3.4, which are performed to find the most suitable model for further simulations. Evaluation of the models are based on convergence characteristics and observations on the flow distribution. Details on case 1 to 4 are shown in Table 3.2, and corresponds to model 1,2,3 and 7 in Appendix B. All simulations are performed in steady-state conditions with the following boundary conditions unless specified otherwise:

- Inlet mixture velocity, u_{inlet}^{mix} = 2 m/s and GVF = 0.3
- Outlet gas (OG) average static pressure, P_{OG} = 84.906 $bara$
- Outlet liquid (OL) average static pressure, P_{OL} = 85 $bara$

Table 3.2: Details on simulations for model selection

Case	Morphology	Homogeneous/ inhomogeneous	Free surface	Interphase transfer model
1	Continuous - Continuous	Homogeneous	No	-
2	Continuous - Continuous	Homogeneous	Yes	-
3	Continuous - Continuous	Inhomogeneous	No	Mixture model
4	Continuous - Dispersed	Inhomogeneous	No	Particle Model

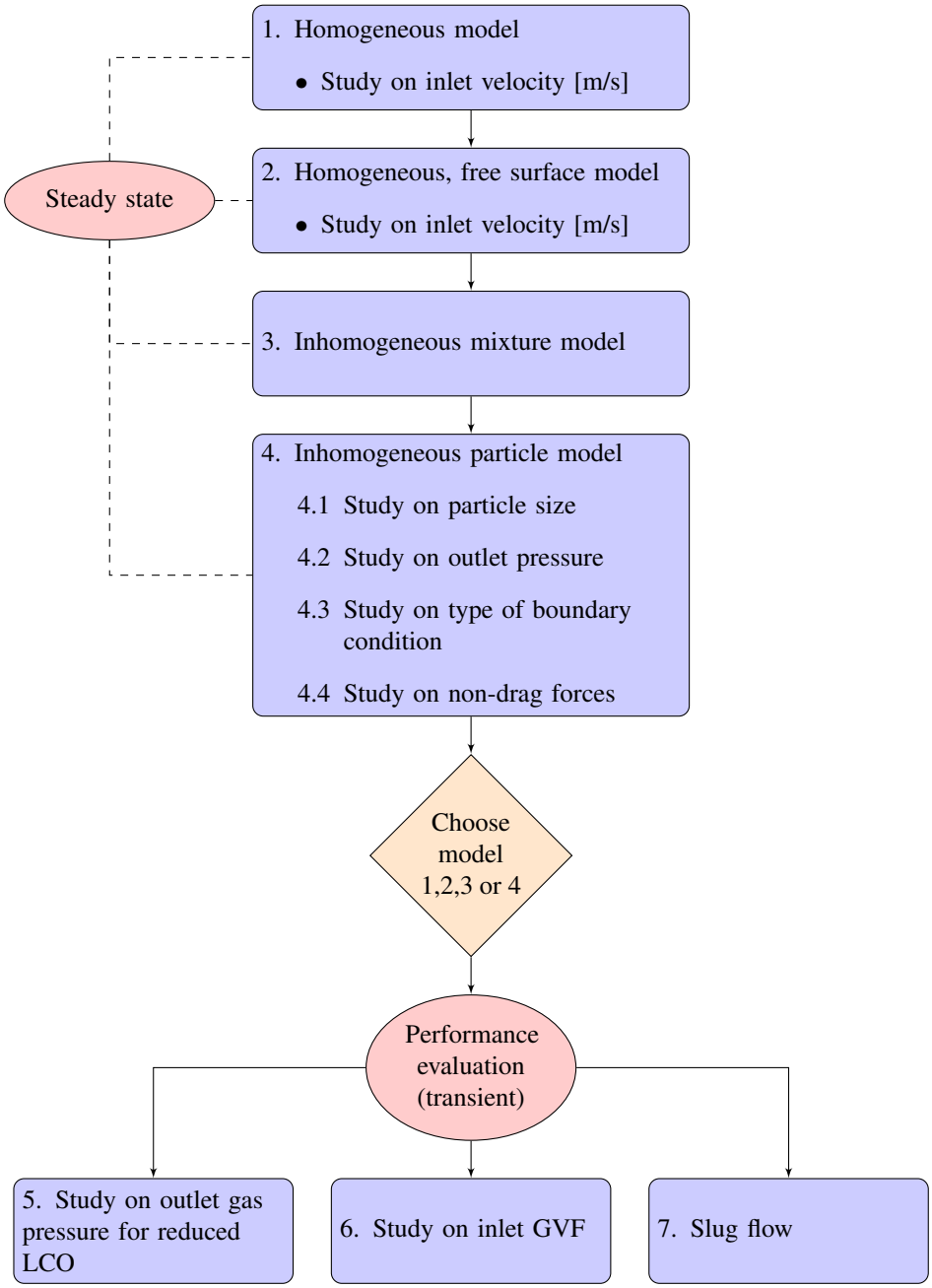

Figure 3.4: Flowchart of simulations

Case 1 & 2 - homogeneous multiphase flow

Homogeneous flow conditions are valid for flows with close to no slip between the phases. Thus, the homogeneous models are assumed to be valid for the current conditions if similar results as the inhomogeneous model are produced.

As homogeneous simulations are less computationally expensive than inhomogeneous simulations, these models are conducted with two different inlet mixture velocities to find which velocity to use for further simulations. The Harp used in the Marlim field is designed for a liquid flow rate of 3500 m^3/d, which corresponds to a velocity through the liquid outlet of approximately 2 m/s with a pipe diameter of 6 inches, thus an inlet velocity of 4 m/s for equal flow rates of the two fluids. Inlet velocities of 1 and 2 m/s are tested as the separator studied in this report is smaller than the Harp separator. Properties of performed homogeneous simulations are given in Table 3.3.

Table 3.3: Simulation plan for homogeneous models

Case		Fluid Morphology	Free Surface	u_{inlet}^{mix} [m/s]
1	1.1	Continuous - Continuous	No	2
	1.2			1
2	2.1	Continuous - Continuous	Yes	2
	2.2			1

Case 3 & 4 - inhomogeneous multiphase flow

This section presents inhomogeneous simulations case 3 and 4 presented in Table 3.2.

The interphase momentum transfer terms considered for case 3, the inhomogeneous mixture model, are buoyancy and drag force, using a drag coefficient of 0.44. Further details on settings used for case 3 can be found in Appendix F.2. Non-drag forces can also be accounted for in the particle model as shown in model 7 in Appendix B. The interphase momentum transfer terms considered for case 4 are:

- Buoyancy
- Drag force
- Lift Force
- Wall lubrication force
- Turbulent dispersion force

Simulations with continuous-dispersed phase flow require a bubble diameter as an input parameter, which can be modelled as mono-dispersed or polydispersed particles. The simulations are not made to replicate a real case with specific droplet distributions, but to show the flow distribution and performance of the separator for multiple conditions. The

simplest case, mono-dispersion, is therefore assumed to be sufficient for the current analysis. Further details on settings used for the particle model can be found in Appendix F.3. Sensitivity studies of the particle model are shown in table 3.4.

Table 3.4: Sensitivity studies on inhomogeneous particle model

Case	Description	Value
	Study on particle size	
4.1	Bubble size $[mm]$	0.01 0.1 1 10
4.2	**Study on outlet pressure**	
	P_{OG} $[bara]$	85
4.3	**Study on type of boundary condition**	
	Outlet liquid: mass flow rate $[kg/s]$	20.2
4.4	**Study on non-drag forces** Deactivated: - Wall lubrication force - Turbulent dispersion force	

Case 4.2 is conducted on 0.1 mm and 1 mm particle diameters, while both case 4.3 and 4.4 are run with a diameter of 0.1 mm. Details of performed simulations using particle model are given in Table 3.5.

Table 3.5: Simulation plan for inhomogeneous particle model

Case	Bubble diameter $[mm]$	Pressure $[bara]$	Mass flow $[kg/s]$	Case 4.4
4.1.1 4.1.2 4.1.3 4.1.4	0.01 0.1 1 10			
4.2.1 4.2.2	0.1 1	85		
4.3	0.1		20.2	
4.4	0.1			X

3.3.2 CFD simulations for performance mapping and evaluation

This section presents the simulations for performance mapping and evaluation shown in Table 3.6. Steady state and transient simulation are conducted on two of the cases, to evaluate if transient simulations are needed. The inhomogeneous mixture model (case 3) is the multiphase model selected to continue the study for case 5,6 and 7. Thus, the interphase momentum transfer terms considered are buoyancy and drag force. Details of performed simulations are given in Table. 3.7, with the following boundary conditions applying to all simulations:

- $u_{inlet}^{mix} = 2\ m/s$
- $P_{OL} = 85\ bara$

Table 3.6: Studies for performance evaluation

Case	Explanation	Value
	Study on OG pressure	
5	$P_{OG}\ [bara]$	84.90-84.99
	Study on inlet GVF	
6	α_{inlet}^{g}	0.5 0.7

Table 3.7: Simulation plan for performance evaluation

Case		α_{inlet}^{g}	P_{OG} $[bara]$
5	5.1	0.3	84.90
	5.2		84.91
	5.3		84.92
	5.4		84.93
	5.5		84.94
	5.6		84.95
	5.7		84.96
	5.8		84.97
	5.9		84.99
6	6.1.1	0.5	84.94
	6.1.2	0.7	
	6.2.1	0.5	84.95
	6.2.2	0.7	

Case 5 is a sensitivity study on outlet gas pressure, studied on nine different pressures. The close range between the tested values are used to ensure consistency of a trend to provide reliable results. Both fluids have constant properties which are unaffected by the pressure.

The study is therefore made to see the effect of the pressure difference between the two outlets ($\Delta P_{outlets}$).

The effects of three different volume fractions are studied. Case 5 consist of an inlet GVF of 0.3, while case 6 employ volume fractions of 0.5 and 0.7. All volume fractions are performed on two different OG pressures to see if the same trend is seen for both cases for increased result reliability. Inlet boundary conditions and corresponding in-situ flow rates shown in table 3.8 are found using Eq. 3.1 and 3.2,

$$q_o = u_{mix} A \alpha_o \tag{3.1}$$

$$q_g = u_{mix} A \alpha_g \tag{3.2}$$

where A is the cross-sectional area of the inlet, α_g is the GVF and α_o = $1 - \alpha_g$.

Table 3.8: Inlet boundary conditions

α_g	u $[m/s]$	q_o $[m^3/d]$	q_g $[m^3/d]$
0.3	2	2,200	950
0.5		1,600	1,600
0.7		950	2,200

Gas carry under (GCU) and liquid carry over (LCO) are measures of the amount of gas escaping through the liquid outlet and liquid escaping through the gas outlet respectively, which are calculated using Eq. (3.3) and (3.4). Oil and gas separation performance can be found using Eq. (3.5) and (3.6). This is equal to 1-GCU and 1-LCO, hence liquid carry over and gas carry under are important values for performance evaluation.

$$LCO = \frac{m^o_{OG}}{m^o_{OG} + m^o_{OL}} \tag{3.3}$$

$$GCU = \frac{m^g_{OL}}{m^g_{OG} + m^g_{OL}} \tag{3.4}$$

$$\eta_o = \frac{m^o_{OL}}{m^o_{OG} + m^o_{OL}} \tag{3.5}$$

$$\eta_g = \frac{m^g_{OG}}{m^g_{OG} + m^g_{OL}} \tag{3.6}$$

Where m^g_{OG}, m^g_{OL} are the mass flow rates of gas through outlet gas and outlet liquid and m^o_{OG}, m^o_{OL} are the mass flow rates of oil through outlet gas and outlet liquid.

Optimal separation conditions must allow for flow fluctuations upstream of the separator, as this is the case for most industry applications. A liquid level placed just below the middle part of the vertical pipes will allow for some variations in inlet conditions without a large drop in separation performance. Optimal configurations are therefore based on both performance calculations and flow distribution for the various conditions tested in case 5 and 6.

Transient simulations are used for all further simulations as this provides significantly reduced residuals. Some flow variations are expected per time for transient simulations. All calculated values on transient simulations are therefore based on average values within a time period which shows a stabilized trend. Standard deviation is used as error estimates of the results within the same time period.

Transient simulation lengths of 10 times the longest residence time of the two fluids are assumed to be sufficient for the results to stabilize. Approximate residence times are found by Eq. (3.7).

$$Residence\ time = \frac{Distance}{Velocity} \tag{3.7}$$

Fig. 3.5 shows the assumed travel path through the separator in colors. The green line applies for both fluids, the red line is gas and the blue line is the travel path of the oil. The velocity is assumed to be equal to the inlet velocity of 2 m/s at the green line and 1 m/s at the red and blue line, after the flow is split in two. A gas particle travels 5.6 meters and an oil particle travels 5 meters from inlet to outlet. Thus, the gas and oil residence times are 4.5 and 3.9 seconds. All transient simulations are run for 45 seconds, which is long enough for a bubble to flow from inlet to outlet 10 times.

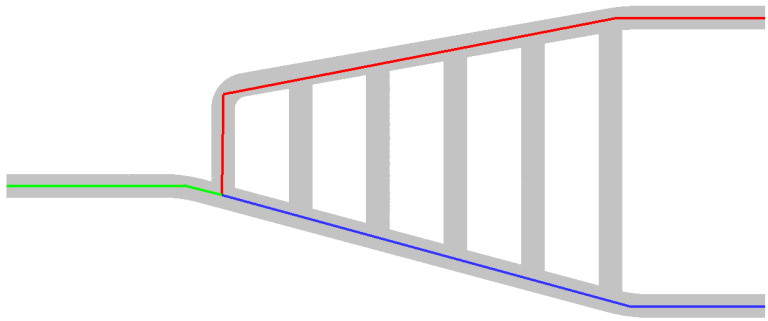

Figure 3.5: Distance travelled for residence time calculations

3.3.3 CFD simulations for evaluation of slug handling

A study on the ability to handle upstream slug flow conditions of various frequencies is conducted. Two numerical models are made to replicate slug flow by using a time-dependent inlet condition. Liquid and gas dominated feeds during a slug flow usually contains entrained particles of the other phase. Thus, inlet volume fractions are set to alternate between 0.1 and 0.9. Boundary conditions are similar to case 6.2.1 with an inlet velocity of 2 m/s and outlet gas pressure set to 84.95 $bara$. These inlet conditions create the same average flow rates as the base case with oil and gas flow rates of 1,600 m^3/d.

The simulation plan for case 7 is shown in Table 3.9. Case 7.1 contains 1 second long slugs which corresponds to 2 meter lengths, while case 7.2 contain 4 second long slugs which corresponds to 8 meter lengths. Fig. 3.6 displays how the gas volume fraction varies with time for the first seconds of the transient simulations.

Table 3.9: Simulation plan for evaluation of slug handling

Case		Inlet GVF	Slug length [$seconds$]
7	7.1	0.1/0.9	1
	7.2		4

The simulations are run for 45 and 48 seconds, which is assumed to be long enough for the flow behaviour in the separator to stabilize and to capture possible fluctuations in the simulations. This may be extended if stabilization is not reached within this time.

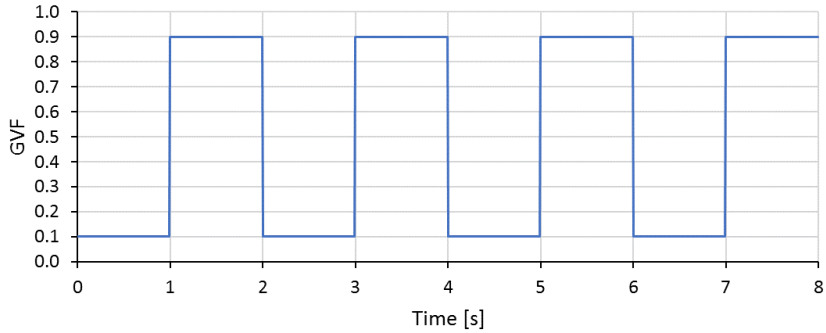

(a) Case 7.1 (2 meter slugs)

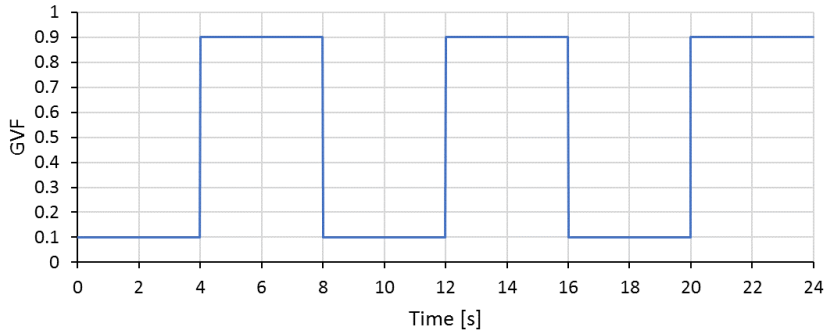

(b) Case 7.2 (8 meter slugs)

Figure 3.6: Inlet conditions for case 7, showing α_g versus time

Chapter 4

Results and discussion

4.1 Discretization error analysis

This section presents results of the numerical uncertainty validation performed by the procedure described in section 2.7.

The three meshes used in the validation contain cells that are evenly distributed in the domain. Thus, a global cell size can be found using Eq. (2.13), with the total volume of the fluid domain being 0.277 m^3. Number of elements and calculated representative cell sizes are shown in Table 4.1. The representative cell sizes are used to calculate the grid refinement factors, resulting in $r_{21} = 1.622$ and $r_{32} = 2.445$.

Table 4.1: Number of elements in mesh i

i	3	2	1
N	1,460,623	3,571,611	5,793,738
h	1.90E-07	7.76E-08	4.78E-08

Table 4.2 summarizes the discretization error study, where delta P is the pressure difference between the inlet and the two outlets. Pressure, delta pressure and velocity values have maximum discretization errors below 2.7% and average discretization errors below 1.6%. Mass flow values are higher, with an average discretization error of 5.66%. Velocity values are found in single points, while cross-sectional planes are used to extract pressure and mass flow values from the simulations. Figures showing the location of the points and planes used in the study can be found in Appendix A.1, where calculated delta pressure and mass flow are at the boundaries.

Table 4.2: Error estimates

	Pressure	Delta P	Mass Flow	Velocity
Number of points	11	2	3	5
P_{min}	1.01	2.60	0.22	0.43
P_{max}	9.48	3.33	0.76	4.03
P_{avg}	3.39	2.96	0.44	1.9
GCI_{max}	0.00	0.72	8.87	2.69
GCI_{avg}	0.01	0.53	5.66	1.52

4.2 CFD simulations for model selection

4.2.1 Case 1 & 2 - homogeneous model

Convergence details on residuals and imbalances are given in Appendix C.

Both case 1 simulations converged below the criteria, but shows close to no separation of the fluids, as the gas volume fraction in Fig. 4.1a and 4.1b stays close to 0.3 throughout the domain.

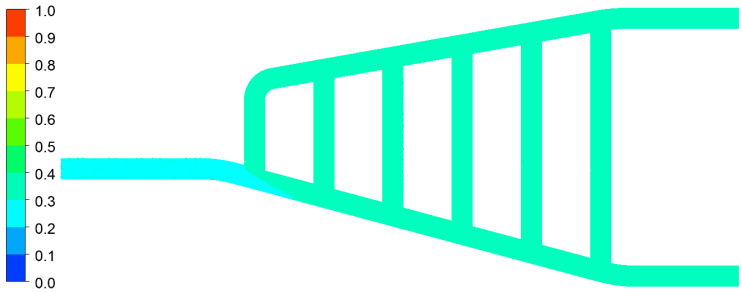

(a) case 1.1 (u_{inlet}^{mix} = 2 m/s)

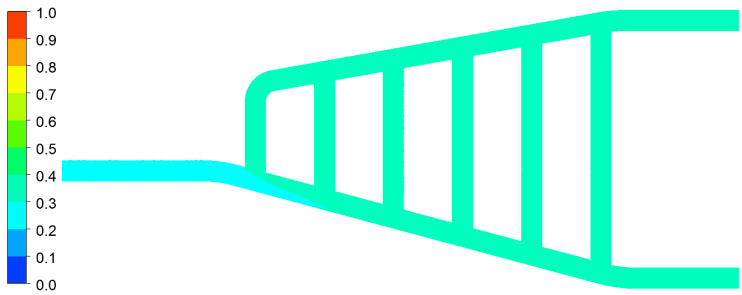

(b) case 1.2 (u_{inlet}^{mix} = 1 m/s)

Figure 4.1: GVF plot of case 1 (homogeneous model)

Convergence in a residual sense was difficult to achieve for free surface flows, but Fig. 4.2a and 4.2b shows a better separation for case 2 compared to case 1.

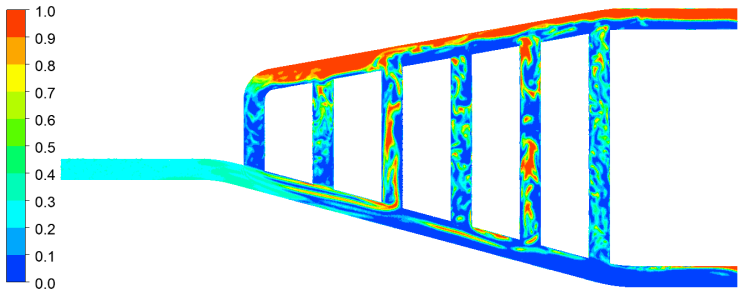

(a) case 2.1 (u_{inlet}^{mix} = 2 m/s)

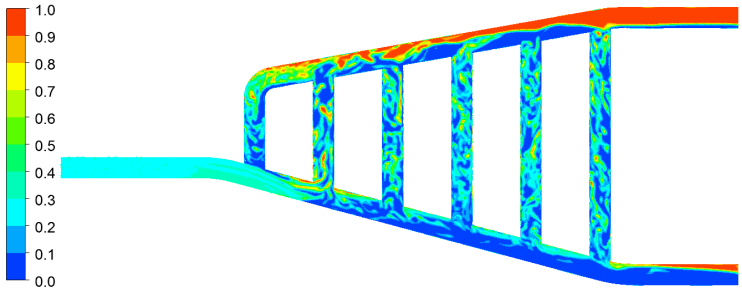

(b) case 2.2 (u_{inlet}^{mix} = 1 m/s)

Figure 4.2: GVF plot of case 2 (homogeneous model with free surface)

The two inlet velocities shows the same convergence and separation behaviour for case 1 and 2. An inlet velocity of 2 m/s is used for further simulations.

4.2.2 Case 3 & 4 - inhomogeneous model

Convergence details on residuals and imbalances can be found in Appendix C, together with streamline velocity plots of both fluids showing the flow distribution. GVF plots which are not displayed in this section can also be found in the same appendix.

The mixture model in case 3 showed quick convergence and most RMS values reached below 5E-6. All imbalances are below 0.05% which is far below the criteria of 1%. The plot of the GVF displayed in Fig. 4.3 shows an early separation of the two fluids.

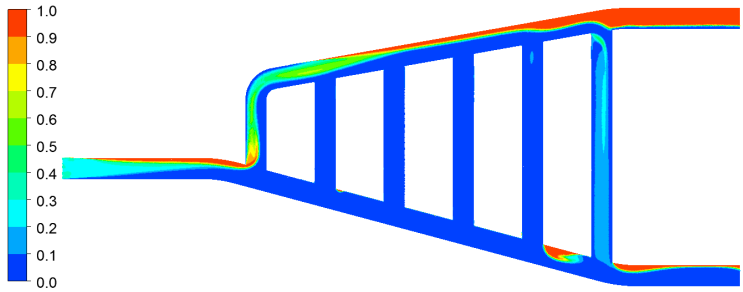

Figure 4.3: GVF plot of case 3 (inhomogeneous mixture model)

Case 4: None of the case 4 simulations are close to converged in a residual or imbalance sense. The gas imbalances are close to 100%, far more than the acceptable value of 1%. The results also show a very different flow pattern than the previous three cases for the same boundary conditions (case 4.1). It is only flow through the gas outlet and a wall is placed at OL covering 100% of the area. The GVF of simulations with particle diameters of 0.1 and 1 mm (case 4.1.2 and 4.1.3 respectively) is approximately 0.3 close to the inlet and 0 everywhere else in the separator, as shown in Fig. 4.4. Similar results are seen for simulations with particle diameters of 0.01 and 10 mm (case 4.1.1 and 4.1.4 respectively).

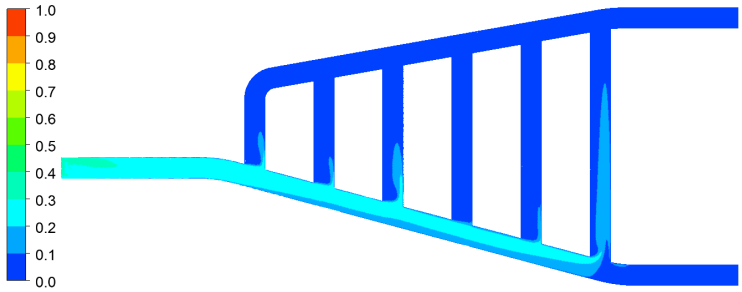

(a) Case 4.1.2 (particle diameter = 0.1 mm)

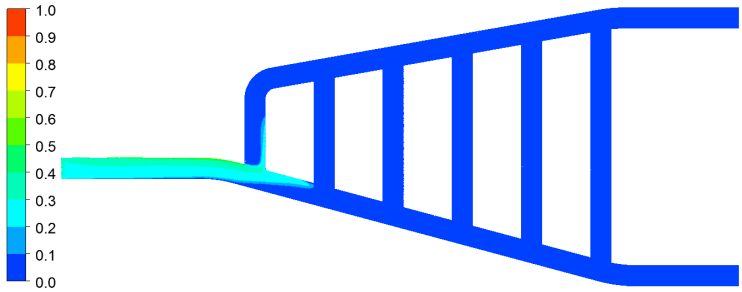

(b) Case 4.1.3 (particle diameter = 1 mm)

Figure 4.4: GVF plot of case 4.1 (inhomogeneous particle model with different particle sizes)

The study on outlet pressure, case 4.2, and the study on type of boundary condition, case 4.3, results in flow through both outlets, but shows little improvements of residuals or imbalances. GVF plots are similar to case 4.1 (Fig 4.4) with a GVF of 0.3 close to the inlet and approximately zero everywhere else.

Case 4.4, with deactivated wall lubrication force and turbulent dispersion force, is the case with the most improvements of imbalances with a gas imbalance close to 15%. This is still far more than the criteria of 1%. Little separation is also seen in the GVF plot showed in Fig. 4.5, with a gas volume fraction close to 0.3 throughout the separator.

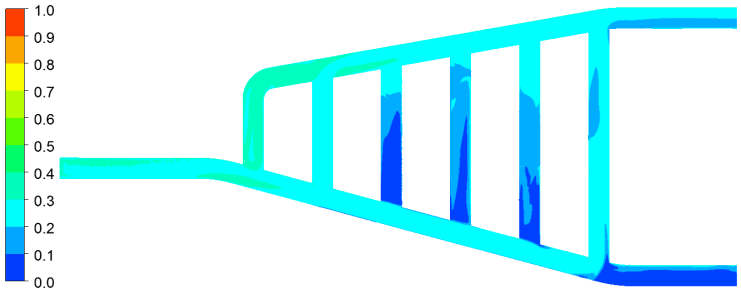

Figure 4.5: GVF plot of case 4.4 (inhomogeneous particle model without wall lubrication force and turbulent dispersion force)

4.2.3 Concluding remarks

- The simple homogeneous model (case 1) and the inhomogeneous-mixture model (case 3) are the only cases to reach below the convergence criteria for RMS and MAX residuals as well as imbalances.
- The simple homogeneous model (case 1) do not present a realistic flow distribution as close to no separation is achieved. It is therefore not used for further simulations.
- The homogeneous model with free surface (case 2) did not reach below the convergence criteria, but shows a more realistic flow distribution than the simple homogeneous model (case 1) and the inhomogeneous particle model (case 4), as separation of the two fluids is seen.
- All the sub-cases studied using the inhomogeneous-particle model did not reach below the convergence criteria and shows an unrealistic flow distribution as close to no separation was achieved. The model is therefore not used for further simulations.
- The homogeneous free surface model (case 2) results shows a slower separation compared to the inhomogeneous mixture model (case 3). Case 3 is assumed to show the better results as the homogeneous model simplifies the physics by assuming no slip between the fluids.

4.3 CFD simulations for performance mapping and evaluation

Transient simulations provides a large improvement on residuals compared to steady state simulations. A significant decrease in the amount of residuals with a value above 1E-3 is seen for transient results, as shown in Fig. 4.6. The same residual improvement is shown for case 5.4 (with $P_{OG} = 84.93\ bara$) in Appendix D. These transient results are with a convergence criteria of RMS values below 5E-5, which is why some MAX residuals are above the criteria of 1E-3. Using the criteria of MAX residuals below a value of 1E-3 was tested for one transient simulation, which required more than double the computational effort. Thus, all transient simulations are set to allow for some maximum residuals with a larger value than the convergence criteria to save computational effort. The location and the amount of the residuals with a value above 1E-3 are for all simulations shown in Appendix D, and are assumed to be of sufficiently small amounts to accept the results.

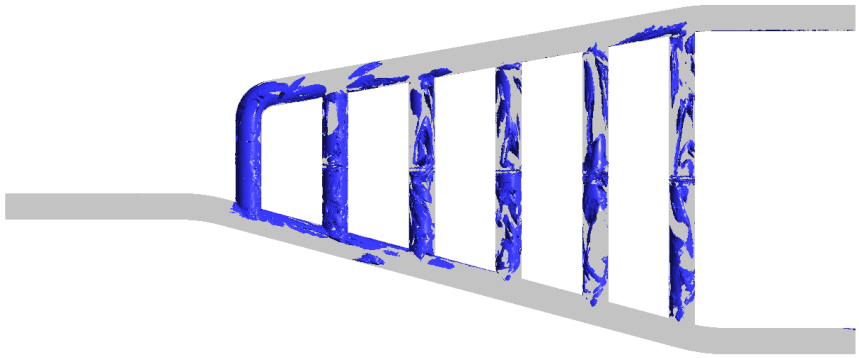

(a) Steady state

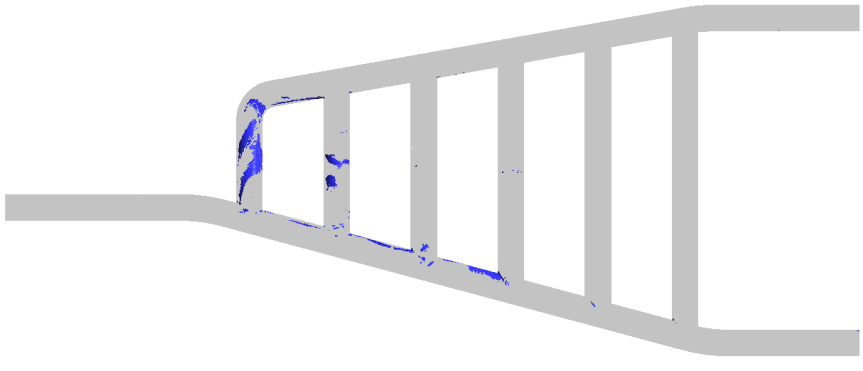

(b) Transient

Figure 4.6: Location of residuals $>$ 0.001 for case 5.5 (α^g_{inlet}=0.3 & P_{OG}=84.94 $bara$)

LCO and GCU are important results for performance evaluation. They are calculated by Eq. (3.3) and (3.4) using mass flow values which are monitored at every time step during the transient simulations. Calculated values are displayed in Appendix D. The values showed in the report is an average of the results from 30 to 45 seconds, which is used because most results show a stabilized tendency after the first 30 seconds. Fig. 4.7 shows an example of a transient behaviour of the LCO, with stabilized results after approximately 25 seconds of simulation time. The error bars in the plots are the standard deviations of these transient results. Exact values mentioned in the following sections may deviate from possible real experimental results, but are provided to show approximate separation performances and to show the tendencies of when the separation performance increases or decreases. Oil and gas separation performances are found by calculating 1-LCO and 1-GCU.

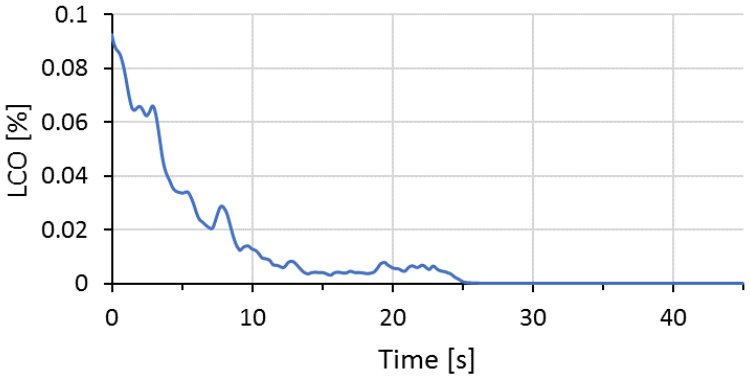

Figure 4.7: Chart showing the transient behaviour of the LCO for case 5.4 (α^{g}_{inlet}=0.3 & P_{OG}=84.93 $bara$)

Other information found in Appendix D are convergence details on residuals and imbalances and streamline velocity plots of both fluids showing the flow distribution. Details on the inlet pressures are displayed in plots in Appendix D.1 and D.2.

4.3.1 Case 5 - effect of the outlet pressure on separation performance

The LCO for case 5.3 was stabilized between 40 and 45 seconds of transient simulation time and was therefore run for another 10 seconds. Thus, the average LCO is calculated from results between 40 and 55 seconds for this case.

Small variations in outlet gas pressure has a big effect on the liquid level in the vertical pipes as shown in Fig. 4.9 and 4.10, where $\Delta P_{outlets} = P_{OL} - P_{OG}$. The results show a liquid level which decreases with a decreasing $\Delta P_{outlets}$.

The different outlet pressures have a large effect on the flow distributions in the branches (vertical pipes). All gas flows up the first branch, while the oil flows in the lower part of the separator for an OG pressure between 84.93 and 84.95 $bara$, as shown in Fig. 4.8b. Lower pressures causes some oil to flow with the gas up the first branch and down one of the next pipes, where: $P_{OG} = 84.92\ bara$ result in oil flowing down branch 2-4, $P_{OG} = 84.91\ bara$ result in most down-flow through pipe 5 and $P_{OG} = 84.90\ bara$ result in most down-flow through the last pipe (Fig. 4.8a).

An increase in OG pressure above 84.95 $bara$ leads to gas flowing up one of the next pipes, where: $P_{OG} = 84.96\ bara$ result in up-flow through branch 3, $P_{OG} = 84.97\ bara$ cause up-flow through branch 5 while up-flow through the last branch is seen for $P_{OG} = 84.99\ bara$ (Fig. 4.8c). A circular movement similar to those shown in Fig. 4.8c is seen for all cases with gas flowing up pipe 2-6. Streamline plots which also shows the magnitude of the velocity can be found in Appendix D for all cases.

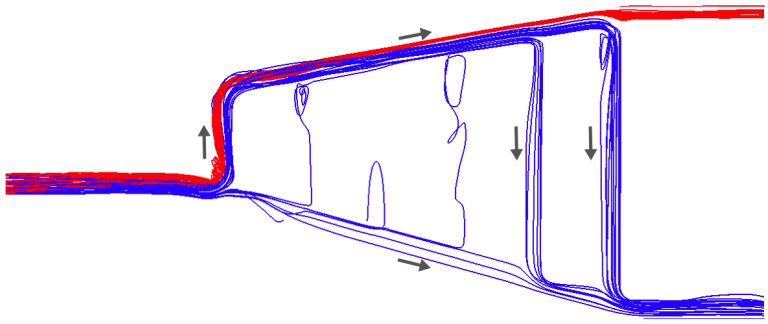

(a) Case 5.1: P_{OG} = 84.90 $bara$ ($\Delta P_{outlets}$ = 0.10 bar)

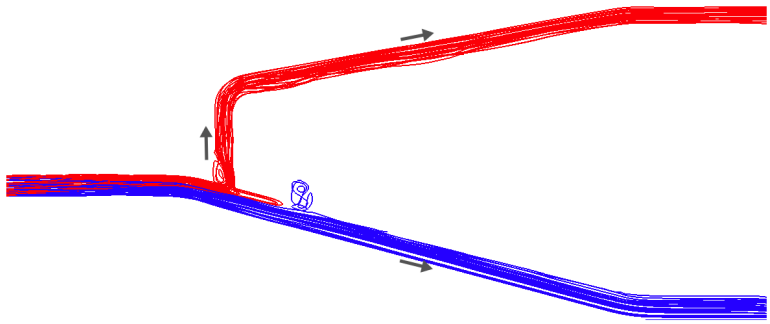

(b) Case 5.6: P_{OG} = 84.95 $bara$ ($\Delta P_{outlets}$ = 0.05 bar)

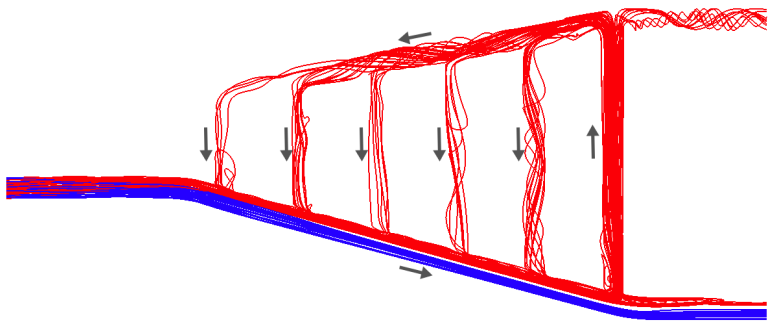

(c) Case 5.9: P_{OG} = 84.99 $bara$ ($\Delta P_{outlets}$ = 0.01 bar)

Figure 4.8: Oil (blue) and gas (red) streamline plot, with arrows indicating the main flow direction

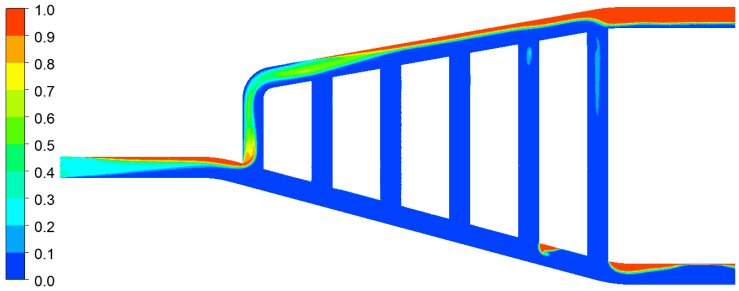

(a) Case 5.1: P_{OG} = 84.90 $bara$ ($\Delta P_{outlets}$ = 0.1 bar)

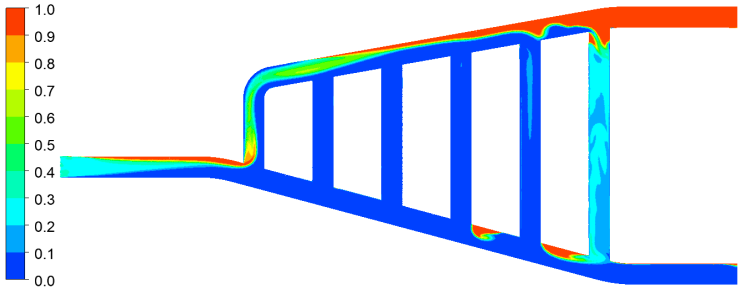

(b) Case 5.2: P_{OG} = 84.91 $bara$ ($\Delta P_{outlets}$ = 0.09 bar)

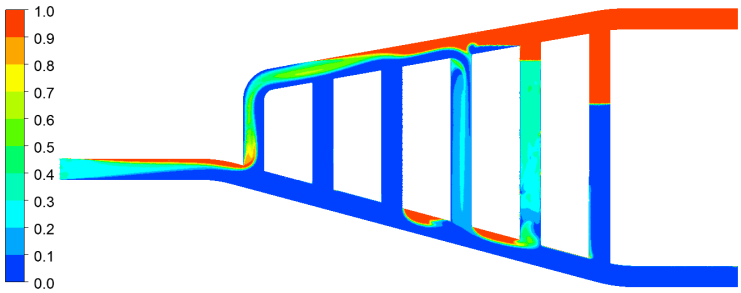

(c) Case 5.3: P_{OG} = 84.92 $bara$ ($\Delta P_{outlets}$ = 0.08 bar)

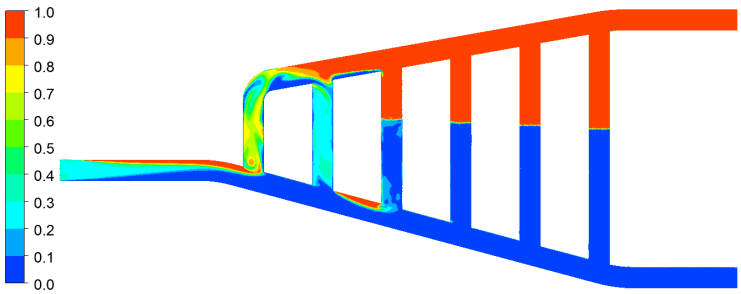

(d) Case 5.4: P_{OG} = 84.93 $bara$ ($\Delta P_{outlets}$ = 0.07 bar)

Figure 4.9: GVF plots with different P_{OG}

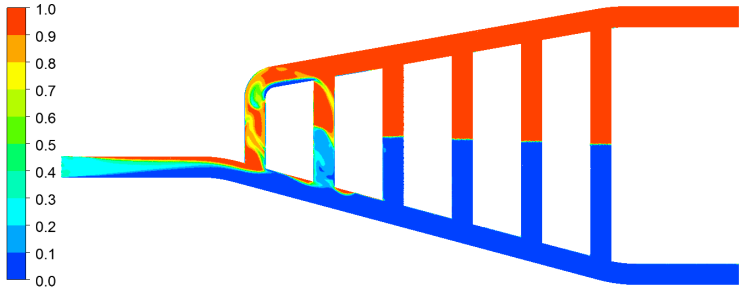

(a) Case 5.5: P_{OG} = 84.94 $bara$ ($\Delta P_{outlets}$ = 0.06 bar)

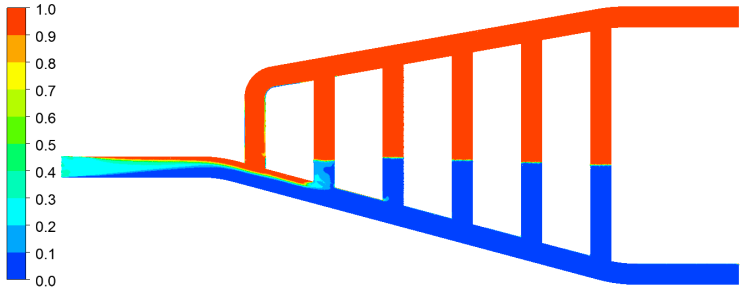

(b) Case 5.6: P_{OG} = 84.95 $bara$ ($\Delta P_{outlets}$ = 0.05 bar)

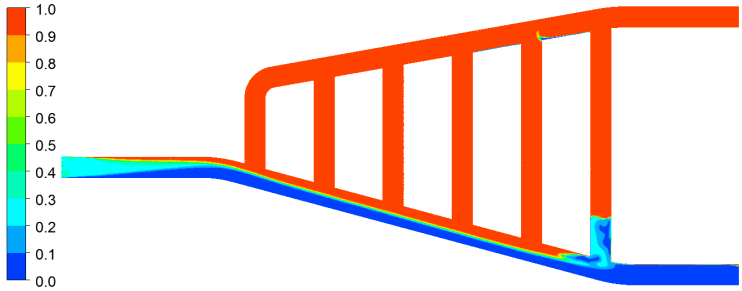

(c) Case 5.8: P_{OG} = 84.97 $bara$ ($\Delta P_{outlets}$ = 0.03 bar)

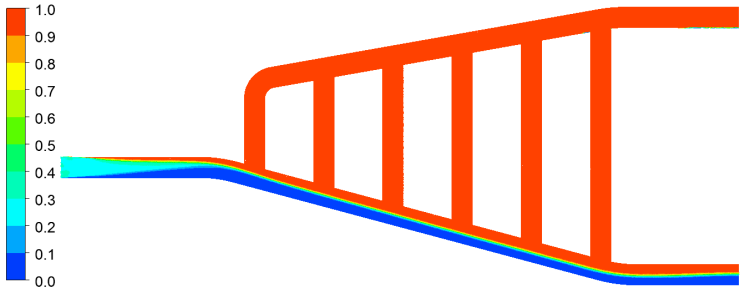

(d) Case 5.9: P_{OG} = 84.99 $bara$ ($\Delta P_{outlets}$ = 0.01 bar)

Figure 4.10: GVF plots with different P_{OG} (P_{OG} = 84.96 $bara$ (Case 5.7) is shown in Appendix D.1)

The effect of outlet gas pressure on LCO and GCU are displayed in the chart in Fig. 4.11. Error bars are too small to see in the plot. Values up to 10% are displayed to show details of the lower values. A chart showing all values can be found in Appendix D.1. Outlet pressure conditions with $\Delta P_{outlets}$ between 0.03 and 0.09 bar result in gas and oil separation performances higher than 98.31% and 99.995% respectively. An improved gas separation performance equal to 99.84% is provided if $\Delta P_{outlets}$ is kept between 0.04 and 0.08 bar.

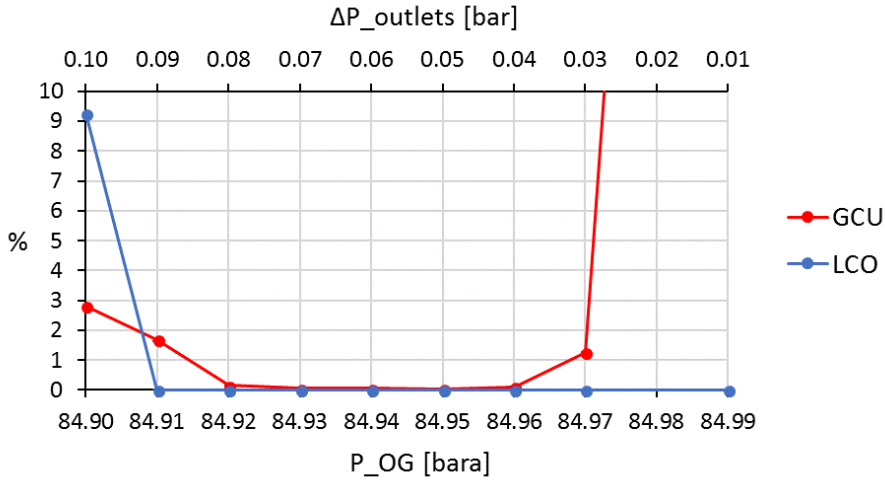

Figure 4.11: Charts of LCO and GCU versus P_{OG}

A low LCO is seen for all OG pressures except 84.90 $bara$ which result in an LCO of 9.26%. This increased LCO is due to a higher liquid level, which is at the bottom of the gas outlet for an OG pressure of 84.90 $bara$ (Fig. 4.9a). Further decreasing of the OG pressure will lead to an increasing LCO.

The increased GCU for OG pressures below 84.92 $bara$ are due to the change in the flow distribution. The oil moves up with the gas through the first branch and down the last two vertical pipes for these pressures, as shown in the streamline plots of the oil velocity in Fig. 4.12. A velocity close to zero is seen in the middle part of the lower horizontal pipe, thus most of the oil flows up and around this part. This result in gas being carried with the oil down the last branches and out of the liquid outlet.

A decreased performance is seen for OG pressures above 84.96 $bara$, in which P_{OG}=84.97 $bara$ result in a GCU of 1.27%, while P_{OG}=84.99 $bara$ result in a GCU of 67.39%. This is due to a liquid level at the very bottom of the last vertical pipe for an OG pressure of 84.97 $bara$ and at the middle of the OL for an OG pressure of 84.99 $bara$, shown in Fig. 4.10c and 4.10d respectively.

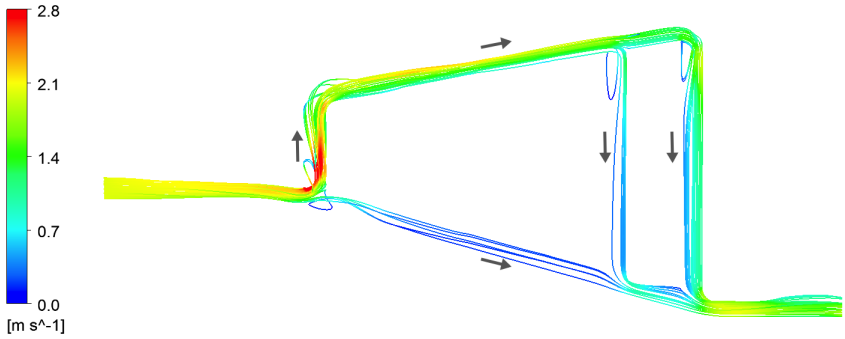

(a) Case 5.1: P_{OG} = 84.90 $bara$ ($\Delta P_{outlets}$ = 0.10 bar)

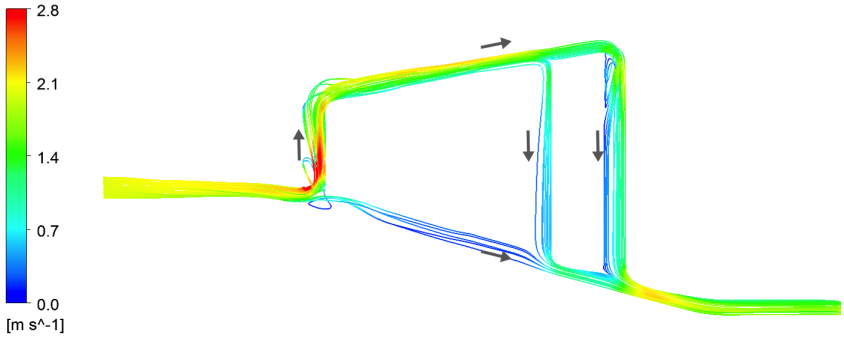

(b) Case 5.2: P_{OG} = 84.91 $bara$ ($\Delta P_{outlets}$ = 0.09 bar)

Figure 4.12: Streamline plots showing the magnitude of the oil velocity, with arrows indicating the main flow direction

The normal liquid level in the pipes must allow for some flow variations as the separator should be able to handle fluctuating inlet conditions and slug flow. The fluid interphase in the results with $\Delta P_{outlets}$ of 0.05 and 0.06 bar are the best because the LCO and GCU are low and the level is low enough such that if a sudden liquid slug ingress the separator there is spare volume to receive it. These two outlet pressures are used for simulations of case 6.

4.3.2 Case 6 - impact of the inlet GVF on separation performance

Case 6.1, which have an outlet gas pressure of 84.95 $bara$, was only run for 3 seconds of transient simulation time to give an indication of the flow distribution due to time limits. Exact values cannot be extracted from these results.

Varying inlet volume fractions do not affect the liquid height in the separator as shown in Fig. 4.13 and 4.14. The flow distribution is also unaffected and are therefore equal to Fig. 4.8b for all three inlet volume fractions. Thus, a larger inlet GVF result in a higher gas

velocity and lower oil velocity through the separator, which gives the bubbles less time to settle. The same applies for droplets for a case with low inlet GVF. All three cases are well separated with a liquid separation performance higher than 99.99% and a gas separation performance higher than 99.95% as shown in Fig. 4.15.

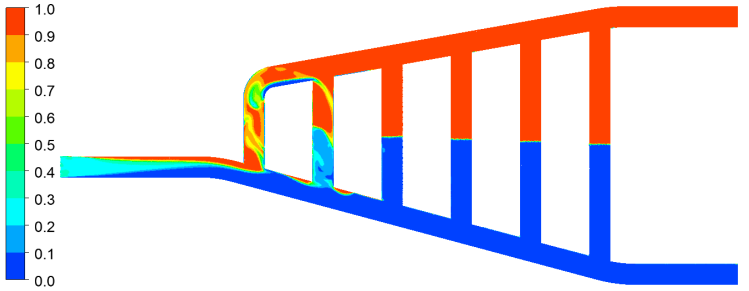

(a) Case 5.2 (α^g_{inlet} = 0.3)

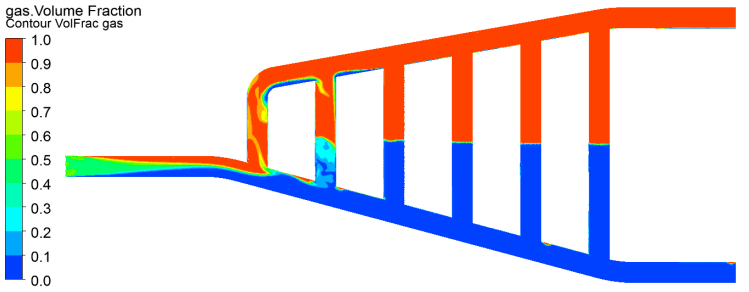

(b) Case 6.1.1 (α^g_{inlet} = 0.5)

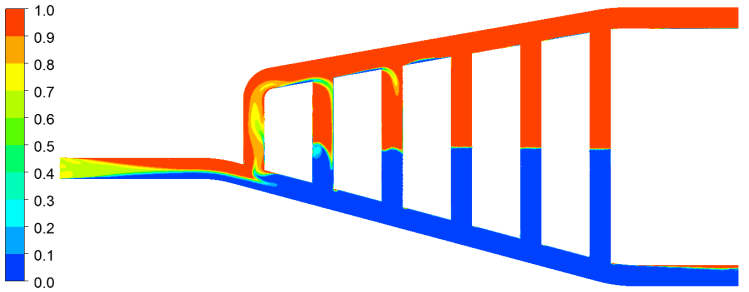

(c) Case 6.1.2 (α^g_{inlet} = 0.7)

Figure 4.13: GVF plots with $\Delta P_{outlets}$=0.06 bar and different α^g_{inlet}

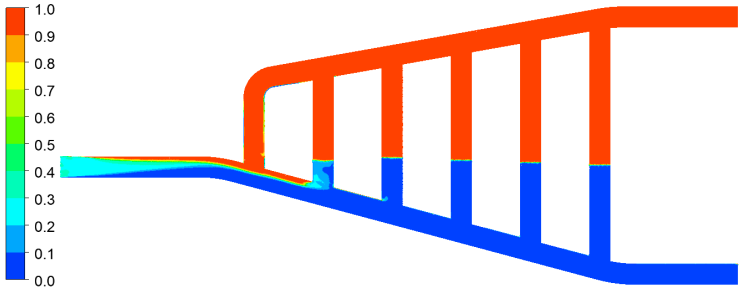

(a) Case 5.3 (α^g_{inlet} = 0.3)

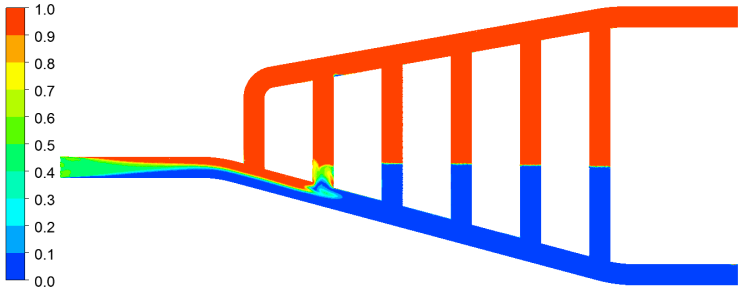

(b) Case 6.2.1 (α^g_{inlet} = 0.5)

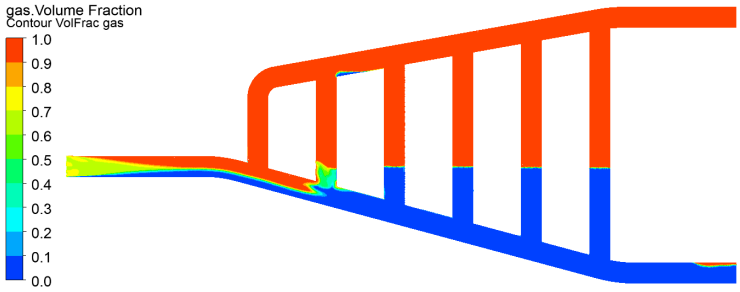

(c) Case 6.2.2 (α^g_{inlet} = 0.7)

Figure 4.14: GVF plots with $\Delta P_{outlets}$=0.05 bar and different α^g_{inlet}

Varying inlet GVFs between 0.3 and 0.7 do not have an effect on the LCO, as shown in Fig. 4.15a. The retention time is therefore high enough in all cases for the droplets to settle. The error bars of inlet GVFs of 0.3 and 0.5 are larger than the average number itself. However, all three inlet gas volume fractions have an LCO below 1.7E-5%, which is very small. The errors are therefore also not of any significance as the highest error is 1.6E-5%.

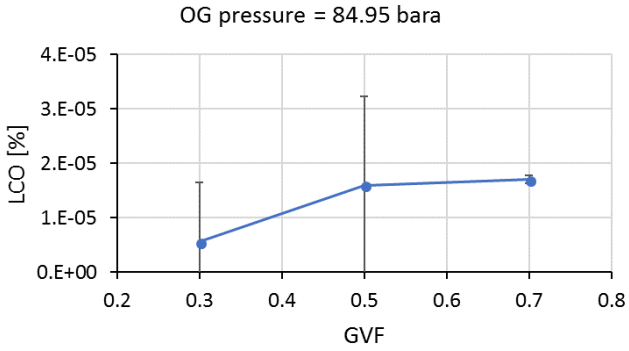

(a) LCO vs α^g_{inlet}

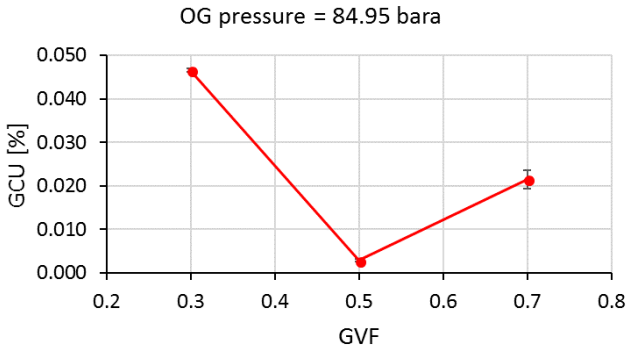

(b) GCU vs α^g_{inlet}

Figure 4.15: Charts of LCO and GCU versus α^g_{inlet}

The GCU for transient results of an inlet gas volume fraction of 0.7 did not stabilize but showed a slowly decreasing trend. The GCU was still not stabilized after another 20 seconds of simulation time. Further simulations are therefore necessary to make any conclusions of this value but are not conducted in this study due to time limits. The GCU with an inlet GVF of 0.5 is only 6% of the carry under with an inlet GVF of 0.3. A decreasing GCU for increasing inlet GVFs may be explained by the reduced liquid velocity through the separator which provides more time for the gas bubbles to settle.

4.4 CFD simulations for evaluation of slug handling

This section presents results and discussion of simulations with slug flow inlet conditions. Estimations of slug flow handling are based on an assumption in which the gas filled part of the separator is the buffer volume for an oil slug. Case 6.2.1 (Fig. 4.14b) is the base case for the slug flow simulations and is used to estimate this buffer volume. The base case is 60% filled with gas which equals a buffer volume of 0.166 m^3. 2 and 8 meter long slugs contain slug volumes of 0.036 and 0.146 m^3 respectively, which is 22 and 88% of the buffer volume. Thus, the separator is assumed to handle case 7.1 and 7.2 without a significantly reduced separation performance.

4.4.1 Case 7.1 - 2 meter slugs

An inlet condition with 2 meter long slug flows creates a wave-like behaviour in the vertical pipes, shown in Fig. 4.19. More GVF plots which shows the transient behaviour can be found in Appendix E. This transient behaviour result in a fluctuating inlet pressure, as the two outlet pressures are set to be constant. Boundary pressures are plotted versus time in Fig. 4.16, which shows a stabilized trend after about 14 seconds.

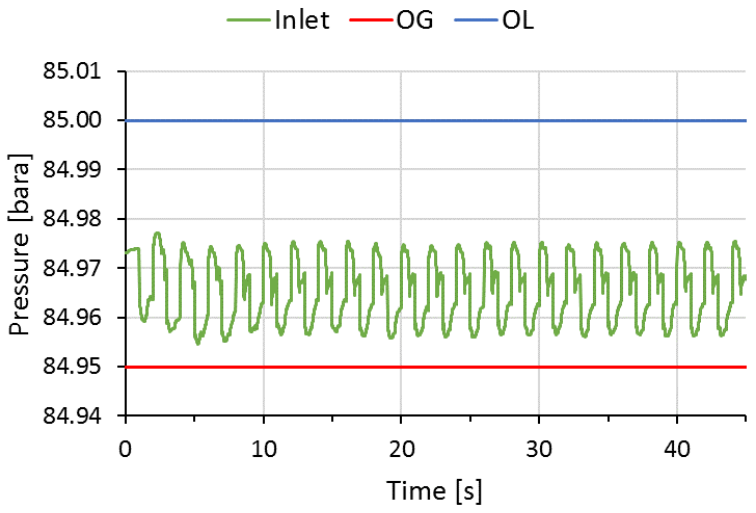

Figure 4.16: Chart of boundary pressures versus time

Fig. 4.21 shows the constant inlet mixture velocity and how the fluid velocities through the outlets vary between 0.8 and 1.2 m/s as a result of the alternating inlet gas volume fractions. A gas pocket increases the velocity through the gas outlet and an oil slug increase the velocity through the liquid outlet.

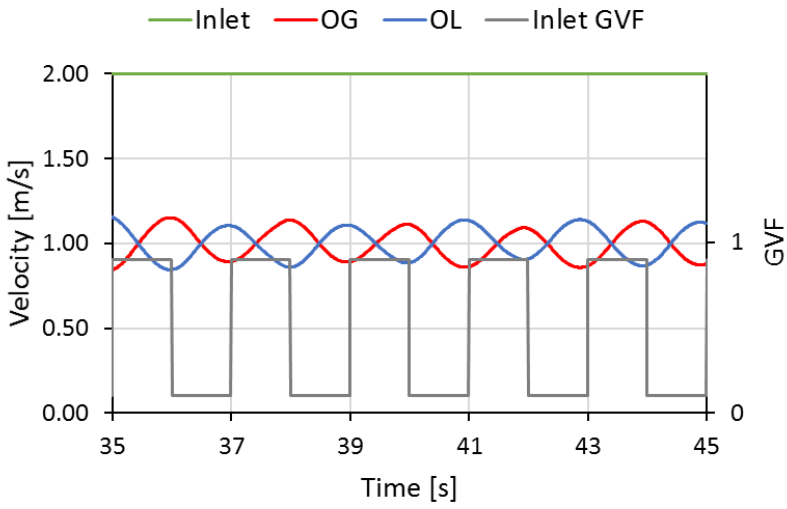

Figure 4.17: Chart of boundary velocities and α^g_{inlet} versus time for the last 10 seconds of the simulation

A high performance is maintained with average LCO and GCU of 5.8E-4±4.0E-4% and 0.040±0.053% respectively. Mass flow values used for the calculations are displayed in Appendix E. The charts in Fig. 4.18 shows the transient behaviour of the LCO and GCU after 14 seconds, which are used to calculate the average values.

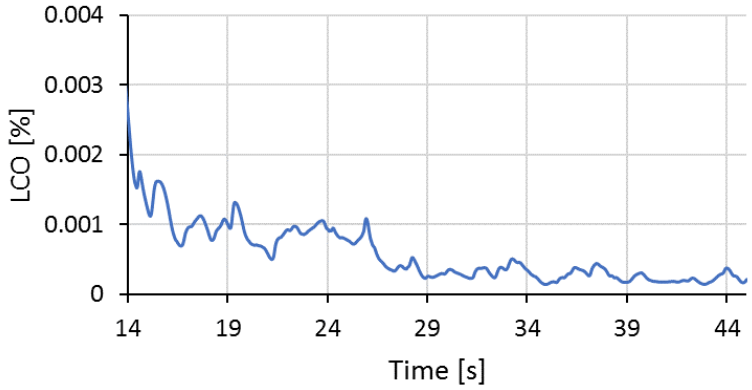

(a) LCO vs time

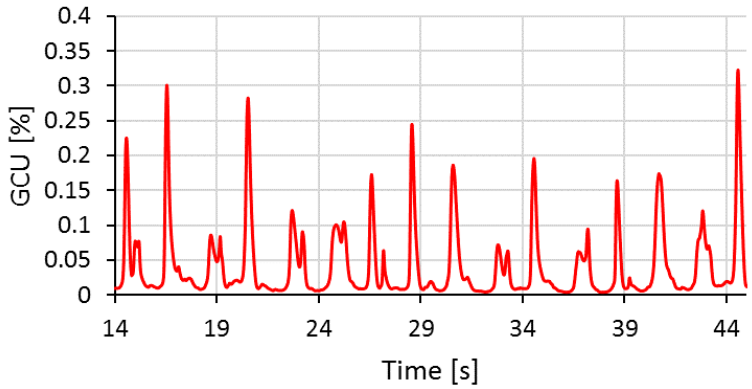

(b) GCU vs time

Figure 4.18: Charts showing the transient behaviour of LCO and GCU

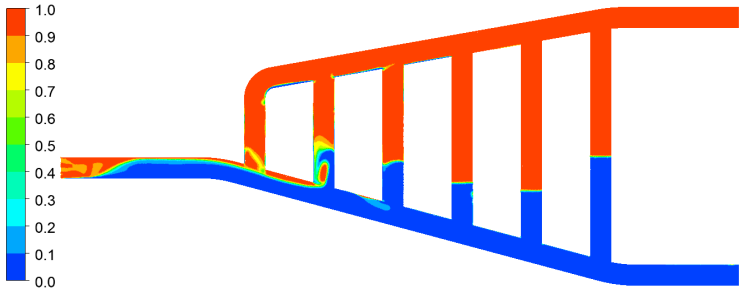

(a) At time = 43.2 s - 0.2 seconds after an oil slug arrives

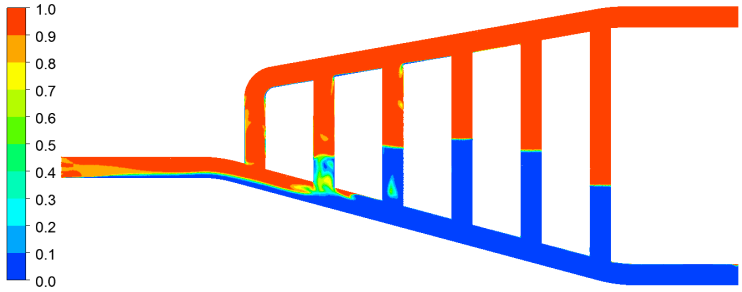

(b) At time = 44 s - end of an oil slug and start of a gas pocket

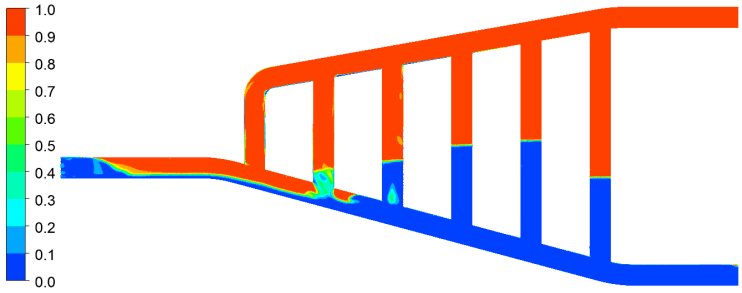

(c) At time = 44.2 s - 0.2 seconds after a gas pocket arrives

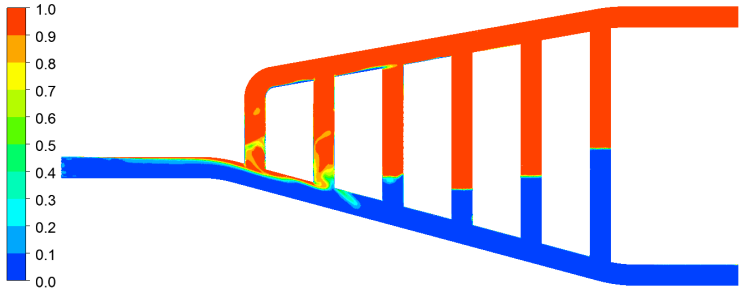

(d) At time = 45 s - end of a gas pocket

Figure 4.19: GVF plots showing the flow distribution

4.4.2 Case 7.2 - 8 meter slugs

A similar wave-like behaviour as for 2 meter long slugs is seen for 8 meter long slugs in case 7.2, as shown in Fig. 4.24 and 4.25. The highest change in liquid height occur during the first seconds of the arrival of a slug and a gas bubble, while it stays more constant during the last seconds. The low change in liquid height at the end of a slug can be explained by one of the outlets almost or completely closing in, letting close to no flow through the outlet.

The inlet pressures fluctuates, but stays between 84.95 and 85 $bara$ as shown in Fig. 4.20 as a result of constant outlet pressures and varying inlet conditions. Keeping the pressure between the outlets constant results in back flow at the liquid outlet for the low liquid level during gas dominated feeds. It also results in back flow at the gas outlet for the high liquid level during oil slugs. No back flow is allowed through the outlets which is why a wall is placed at the cross-sectional area instead. This did not happen in the previous case with 2 meter slugs.

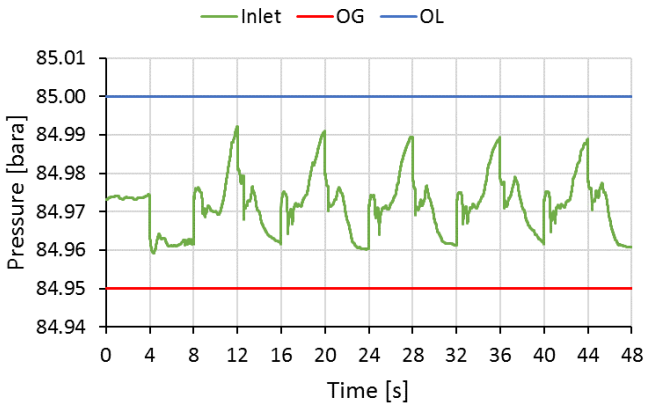

Figure 4.20: Chart of boundary pressures versus time

Fig. 4.21 shows the constant inlet velocity and how the fluid velocities through the outlets vary between 0 and 2 m/s as a result of the alternating inlet gas volume fractions. The liquid outlet is close to 100% shut in at the end of a gas pocket, and the gas outlet is completely shut in at the end of a liquid slug, creating an outlet velocity close to or equal zero.

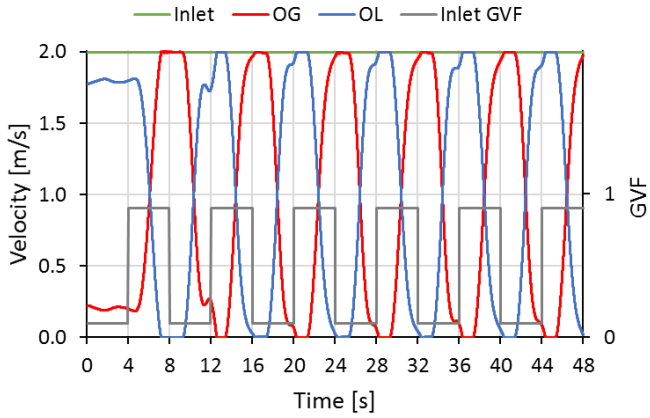

Figure 4.21: Chart of boundary velocities and α^g_{inlet} versus time

All performance evaluations are based on mass flow results between 12 and 48 seconds of transient simulation time (displayed in Appendix E), as these results shows a stabilized trend. Fig. 4.22a displays the transient behaviour of calculated LCO (by Eq. (3.3)) which contains an average value of 0.19±0.74%. The large standard deviation is expected as the LCO varies due to the fluctuating flow conditions.

No fluid flows through the gas outlet when this is closed in, resulting in m^g_{OG}=0 in Eq. (3.4). Thus, the GCU is equal to m^g_{OL}/m^g_{OL}=1=100% for this case. This is seen at the end of every liquid slug in Fig. 4.22b, which result in an average GCU as high as 13.8±33.8%. Thus, the GCU is not a good representation of how well the gas is separated.

The mass% of gas flowing through OL is compared with the 2 meter slugs case (case 7.1) in Fig. 4.23. Where the mass% is the gas mass flow per total mass flow through OL. The average mass% of the 2 and 8 meter long slugs are 0.0055±0.0068% and 0.0045±0.0096% respectively. Thus, the separation efficiencies for the two slug flow conditions are similar, as they result in an equally low mass% of gas exiting through the liquid outlet.

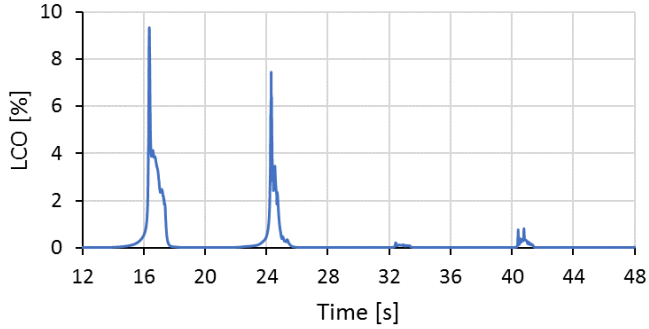

(a) LCO vs time

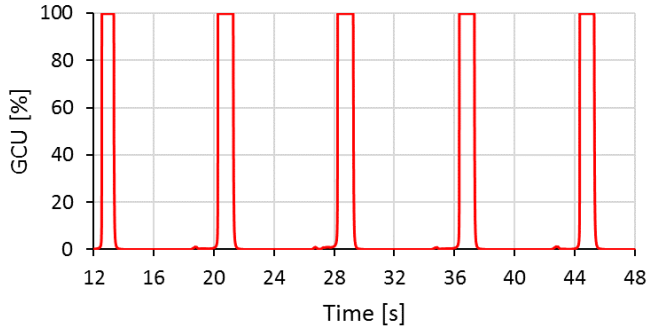

(b) GCU vs time

Figure 4.22: Transient behaviour of LCO and GCU

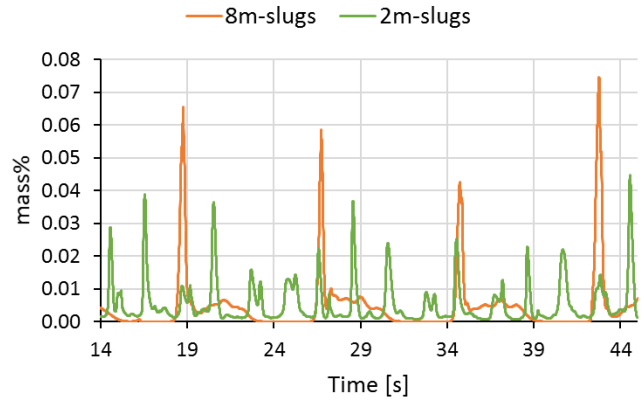

Figure 4.23: Chart of mass% gas flowing through OL for 8 and 2 meter slugs (case 7.1 and 7.2)

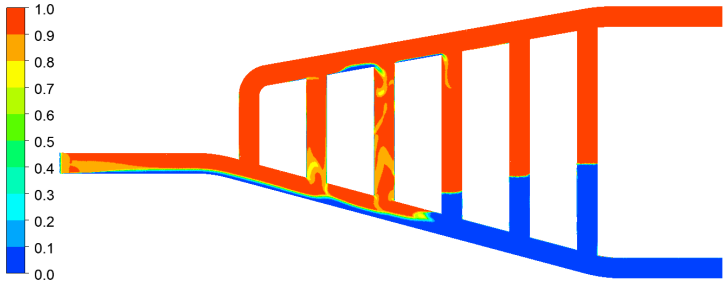

(a) At time = 40 s - an oil slug arrives at inlet

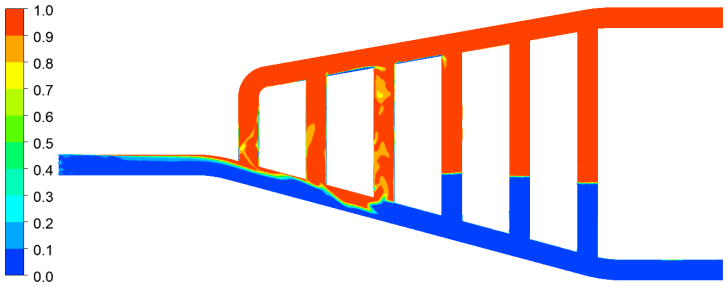

(b) At time = 41 s

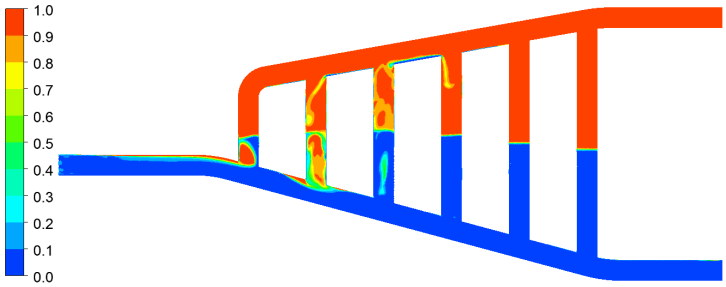

(c) At time = 42 s

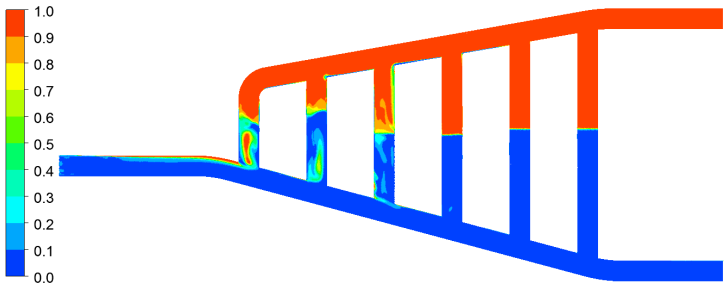

(d) At time = 43 s

Figure 4.24: GVF plots showing the transient behaviour during an oil slug

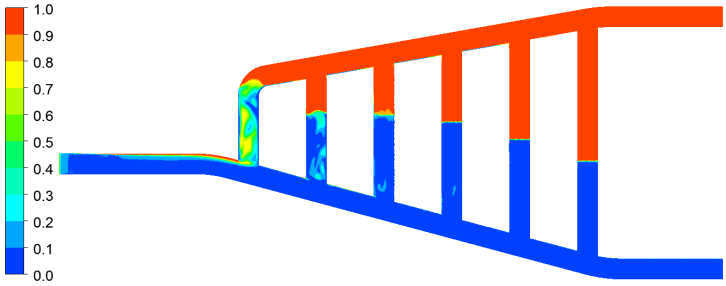

(a) At time = 44 s - a gas pocket arrives at inlet

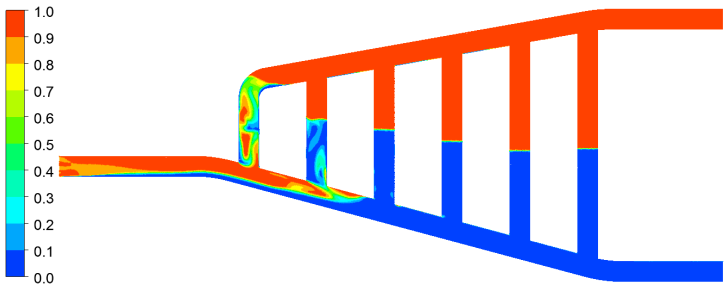

(b) At time = 45 s

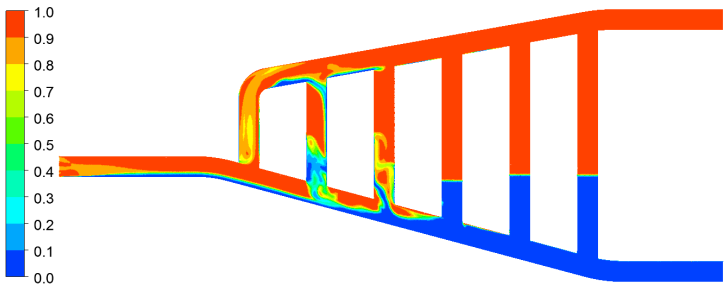

(c) At time = 46 s

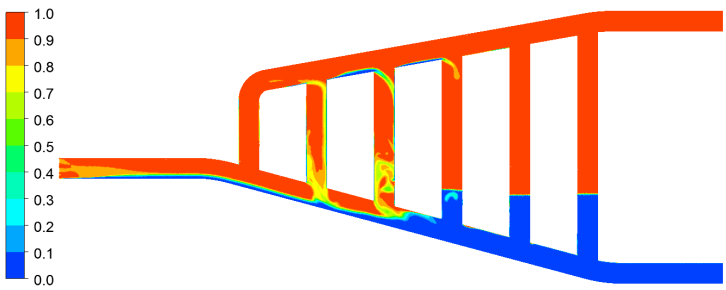

(d) At time = 47 s

Figure 4.25: GVF plots showing the transient behaviour during a gas pocket

4.5 Limitations and uncertainties

Wall y^+ values are high in the gas flow with most values around 200-300. Lower values may improve the results. The values are however below 500 which is within the log-law layer. A high gas velocity is seen for cases with a low OG pressure, which contain y^+ values up to 600 for a small section along the pipe wall. This may reduce the accuracy of the results.

Due to the lack of experimental and test data, the numerical results shown previously could not be validated. Different flow characteristics are seen through the separator. Thus, it is unclear how well one model is able to represent the different parts of the domain. The particle model may be a better model for the leftmost part of the separator with low GVF, as a continuous-dispersed morphology is likely in this case. The mixture model is possibly the best solution for higher inlet GVFs as a continuous-continuous morphology is more likely in this case. A free surface model may be the best solution for the part after separation have taken place, as a clear surface is seen for this part.

Chapter 5

Conclusions and recommendations

The results obtained from numerical experiments on an oil-gas pipe-separator show the following:

- No separation was achieved when using a homogeneous model without free surface.
- Separation was achieved when using a homogeneous model with free surface, but the model did not converge below the criteria.
- An inhomogeneous model with a continuous and a dispersed phase using the particle model was studied and did not converge below the criteria or show any separation of the two phases.
- An inhomogeneous model with continuous-continuous phases using the mixture model was studied and showed fast convergence and separation of the two fluids. This model was used for simulations on separation performance.
- Simulations with an increasing pressure difference between the two outlets ($\Delta P_{outlets}$) showed a responding increasing liquid height in the vertical pipes.
- Outlet pressure conditions with $\Delta P_{outlets}$ between 0.03 and 0.09 bar resulted in gas and liquid separation performances higher than 98.31% and 99.995% respectively. An improved gas separation performance equal to 99.84% was provided for $\Delta P_{outlets}$ kept between 0.04 and 0.08 bar.
- The liquid level in the separator was not affected by different inlet volume fractions with stable inlet flow conditions. The study with three inlet volume fractions also showed no significant effect on the oil separation performance. An increased gas separation performance was seen for increasing inlet gas volume fractions in the first two cases - from 99.95 to 99.98%. Longer simulation times are required to draw conclusions on the last case.

- Slug flow inlet conditions with 2 meter long slugs was well separated with an average oil and gas separation performance higher than 99.99% and $99.96 \pm 0.05\%$ respectively.
- The separation performance was reduced slightly with the longer slugs of 8 meters, resulting in an oil separation performance of $99.81 \pm 0.74\%$.
- No realistic calculation of gas separation performance was extracted from the study on 8 meter slugs. The gas mass flow per total mass flow through the liquid outlet was therefore compared for the two slug flow cases, which showed similar low amounts of gas exiting through OL.
- The multi-branch separator showed well slug-handling abilities and high separation performances for the studied slug flow conditions.
- Recommendations for improvements of results:
  - Run longer transient simulations for case 6.1 to check coherence with the effects of varying inlet GVFs for case 6.2.
  - Run all simulations for 20 times the retention time to ensure stabilized results for all cases.
  - Change the inflation layer on the mesh to get a first-layer thickness closer to the wall.
- Suggestions for future investigations include:
  - Experimental studies can be performed to compare experimental data with simulation results.
  - Investigate the effect of different inlet velocities on the separation performance.
  - Study slug handling abilities for slugs with a varying velocity and a wider range of slug frequencies.
  - Create different flow patterns upstream of the separator to study the separation performance and flow behaviour for different flow regimes.
  - Perform a design study on the number of vertical pipes and how it affects the separation performance.
  - Conduct 3-phase multiphase flow simulations with gas, oil and water.

Bibliography

Afolabi, E., Lee, J., 2014. An eulerian-eulerian cfd simulation of air-water flow in a pipe separator. The Journal of Computational Multiphase Flows 6 (2), 133–149.

ANSYS, 2016. Ansys cfx help 17.2. S.l.:s.n.

Blasius, H., 1913. Das ähnlichkeitsgesetz bei reibungsvorgängen in flüssigkeiten. In: Mitteilungen über Forschungsarbeiten auf dem Gebiete des Ingenieurwesens. Springer, pp. 1–41.

Bratland, O., 2010. Pipe flow 2: Multi-phase flow assurance. Ove Bratland.

Celik, I. B., Ghia, U., Roache, P. J., et al., 2008. Procedure for estimation and reporting of uncertainty due to discretization in {CFD} applications. Journal of fluids {Engineering-Transactions} of the {ASME} 130 (7).

cfd online, Jun 2011. Y plus wall distance estimation. `https://www.cfd-online.com/Wiki/Y_plus_wall_distance_estimation`, Accessed: 10 May 2018.

Cimbala, J. M., Çengel, Y. A., 2014. Fluid mechanics: fundamentals and applications.

da Mota, F. R., Pagano, D. J., 2014. Simulation and experimental study of phase segregation in helical pipes: A new method for flow conditioning. Flow Measurement and Instrumentation 35, 99–108.

Euphemio, M., Oliveira, R., Nunes, G., Capela, C., Ferreira, L., et al., 2007. Subsea oil/water separation of heavy oil: Overview of the main challenges for the marlim field-campos basin. In: Offshore Technology Conference. Offshore Technology Conference.

Euphemio, M. L., Lima, I. F., Orlowski, R., Ribeiro, L. S., Lourenco, I., Pereira, R. d. S., Inacio, F., Gontijo, F., et al., 2012. Marlim ssao 3-phase subsea separation system: Project overview and execution stragegy. In: Offshore Technology Conference. Offshore Technology Conference.

Gramme, P. E., Lie, G. H., Mar. 8 2011. Pipe separator inlet. US Patent 7,901,492.

Kondapi, P., Chin, Y. D., Srivastava, A., Yang, Z. F., et al., 2017. How will subsea processing and pumping technologies enable future deepwater field developments? In: Offshore Technology Conference. Offshore Technology Conference.

Monesi, A., Pinelli, M., Verga, C., et al., 2013. Slug catcher two-phase flow modeling and numerical simulations. In: OTC Brasil. Offshore Technology Conference.

Moraes, C. A. C., da Silva, F. S., Marins, L. P. M., Monteiro, A. S., de Oliveira, D. A., Orlowski, P., Folhadela, H., Mikkelsen, R., Kolbu, J., McKenzie, L., et al., 2012. Marlim 3 phase subsea separation system: Subsea process design and technology qualification program. In: Offshore Technology Conference, Houston. Vol. 30.

Orlowski, R., Euphemio, M. L. L., Euphemio, M. L., Andrade, C. A., Guedes, F., Tosta da Silva, L. C., Pestana, R. G., de Cerqueira, G., Lourenço, I., Pivari, A., et al., 2012. Marlim 3 phase subsea separation system-challenges and solutions for the subsea separation station to cope with process requirements. In: Offshore Technology Conference. Offshore Technology Conference.

Refsnes, H. S., 2017. Computational fluid dynamics (cfd) simulation of the harp separator.

Sagatun, S. I., Gramme, P., Horgen, O. J., Ruud, T., Storvik, M., et al., 2008. The pipe separator-simulations and experimental results. In: Offshore Technology Conference. Offshore Technology Conference.

Salim, S. M., Cheah, S., 2009. Wall y strategy for dealing with wall-bounded turbulent flows. In: Proceedings of the international multiconference of engineers and computer scientists. Vol. 2. Hong Kong.

Versteeg, H. K., Malalasekera, W., 1995. An introduction to computational fluid dynamics: the finite volume method. Longman Scientific & Technical.

Appendix A

Theory

A.1 Discretization Error Calculations

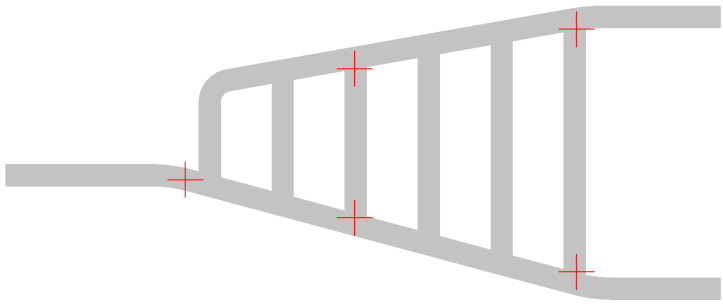

Figure A.1: Location of points for velocity calculation (Refsnes, 2017)

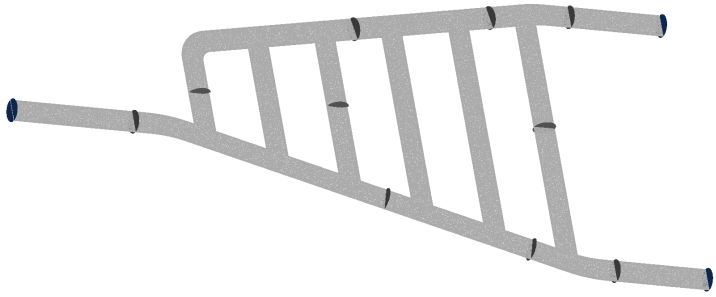

Figure A.2: Location of planes for pressure calculation (Refsnes, 2017)

Appendix B

Multiphase settings in ANSYS CFX

Basic Settings	Fluid Models		Fluid Pair Models		
			Model		
Continuous Fluid - Continuous Fluid	Homogeneous	No free surface	1	**Interphase Transfer**	Mixture Model None
				Surface Tension Model	
				Drag Force	
				Non-drag forces	
		Free Surface	2	**Interphase Transfer**	Mixture Model Free Surface None
				Surface Tension Model	Continuum Surface Force None
				Drag Force	
				Non-drag forces	
	Inhomogeneous	No free surface	3	**Interphase Transfer**	Mixture Model
				Surface Tension Model	
				Drag Force	Drag Coefficient
				Non-drag forces	
		Free Surface	4	**Interphase Transfer**	Mixture Model Free Surface
				Surface Tension Model	Continuum Surface Force None
				Drag Force	Drag Coefficient
				Non-drag forces	
Continuous Fluid - Dipspersed Fluid/ Polydispersed Fluid	Homogeneous	No free surface	5	**Interphase Transfer**	Particle Model None
				Surface Tension Model	
				Drag Force	
				Non-drag forces	
		Free Surface	6	**Interphase Transfer**	Particle Model Free Surface None
				Surface Tension Model	Continuum Surface Force None
				Drag Force	
				Non-drag forces	
	Inhomogeneous	No free surface	7	**Interphase Transfer**	Particle Model
				Surface Tension Model	
				Drag Force	Schiller Naumann Ishii Zuber Grace Drag Coefficient
				Non-drag forces	Lift Force Virtual Mass Force Wall Lubrication Force Turbulent Dispersion Force
		Free Surface	8	**Interphase Transfer**	Particle Model Free Surface
				Surface Tension Model	Continuum Surface Force None
				Drag Force	Schiller Naumann Ishii Zuber Grace Drag Coefficient
				Non-drag forces	Lift Force Vitrual Mass Force * Wall Lubrication Force Turbulent Dispersion Force

*Only possible when the "Particle Model" is used for Interphase transfer

Figure B.1: Multiphase models map

Appendix C

Details on CFD simulations for model selection

C.1 Case 1

Case 1.1

Table C.1: Residuals and imbalances for case 1.1

Equation	RMS	MAX	Location MAX - Node number	Imbalance [%]
U-Mom	2.2E-5	5.2E-4	102586	0.0000
V-Mom	3.0E-5	7.2E-4	1116240	-0.0001
W-Mom	2.0E-5	6.0E-4	1118311	-0.0000
P-Vol	1.5E-10	1.2E-8	1094218	0.3049
Mass-oil	1.4E-4	3.0E-3	1185794	0.3859
K-TurbKE	2.2E-5	1.1E-3	440	
E-Diss.K	6.2E-6	7.8E-4	1167086	

Case 1.2

Table C.2: Residuals and imbalances for case 1.2

Equation	RMS	MAX	Location MAX - Node number	Imbalance [%]
U-Mom	1.4E-5	4.8E-4	11547	0.0000
V-Mom	1.3E-5	3.0E-4	27949	-0.0000
W-Mom	8.5E-6	3.2E-4	6310	-0.0000
P-Vol	1.9E-11	2.9E-9	1147623	0.0191
Mass-oil	1.2E-5	5.8E-4	96265	0.0207
K-TurbKE	9.1E-6	3.2E-4	70449	
E-Diss.K	3.4E-6	2.6E-4	1148976	

C.2 Case 2

Case 2.1

Table C.3: Residuals and imbalances for case 2.1

Equation	RMS	MAX	Location MAX - Node number	Imbalance [%]
U-Mom	4.4E-4	1.2E-2	29823	-0.0015
V-Mom	7.1E-4	1.7E-2	1096798	0.0026
W-Mom	3.4E-4	1.3E-2	79291	0.0011
P-Vol	7.0E-9	4.0E-7	29800	3.7807
Mass-oil	3.3E-2	4.0E-1	11113	4.7914
K-TurbKE	1.2E-3	6.4E-2	198295	
E-Diss.K	3.2E-4	4.5E-2	1171388	

Case 2.2

Table C.4: Residuals and imbalances for case 2

Equation	RMS	MAX	Location MAX - Node number	Imbalance [%]
U-Mom	4.9E-4	1.3E-2	104531	0.0004
V-Mom	7.7E-4	1.6E-2	60712	0.0005
W-Mom	4.0E-4	1.2E-2	1035890	0.0006
P-Vol	5.2E-9	4.2E-7	1160684	16.0391
Mass-oil	3.4E-2	3.6E-1	326451	20.3114
K-TurbKE	1.2E-3	4.9E-2	95467	
E-Diss.K	3.2E-4	9.8E-2	1215778	

C.3 Case 3

Table C.5: Residuals and imbalances for case 3

Equation	RMS	MAX	Location MAX - Node number	Imbalance [%]
U-Mom-oil	1.5E-6	1.1E-4	1218080	0.0000
V-Mom-oil	2.4E-6	2.4E-4	1167800	-0.0000
W-Mom-oil	9.6E-7	4.7E-5	38857	-0.0000
U-Mom-gas	5.7E-7	4.8E-5	1218027	-0.0000
V-Mom-gas	2.9E-7	1.7E-4	1167800	0.0000
W-Mom-gas	1.9E-7	3.5E-5	1213965	-0.0000
P-Vol	6.9E-11	2.5E-8	1160885	-0.0117
Mass-oil	6.8E-4	3.8E-1	983015	0.0479
Mass-gas	5.1E-4	2.3E-1	983015	0.0403
K-TurbKE	1.9E-6	2.4E-4	1167800	
E-Diss.K	3.4E-8	1.9E-5	1167800	

(a) Gas velocity

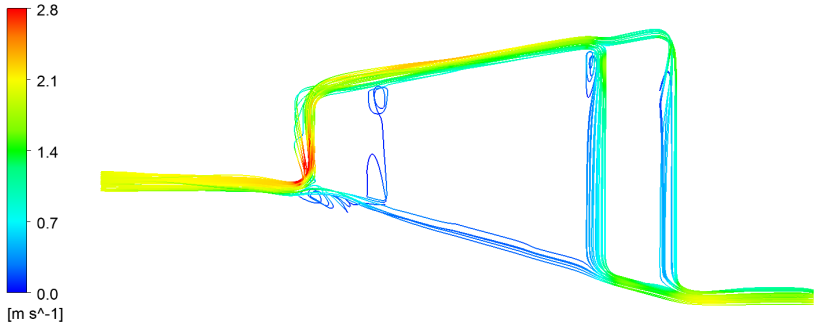

(b) Oil velocity

Figure C.1: Streamline plot of gas and oil velocity from case 3

C.4 Case 4

Case 4.1.1

Table C.6: Residuals and imbalances for case 4.1.1

Equation	RMS	MAX	Location MAX - Node number	Imbalance [%]
U-Mom-oil	8.8E-1	3.8E+1	1090674	-7.3662
V-Mom-oil	9.2E-1	1.7E+1	458384	1.2575
W-Mom-oil	1.3E+0	2.6E+1	1129631	-0.0117
U-Mom-gas	8.0E-1	3.4E+1	1090674	7.3660
V-Mom-gas	8.4E-1	1.5E+1	458384	-1.2578
W-Mom-gas	1.1E+0	2.3E+1	1129631	0.0117
P-Vol	5.5E-7	1.5E-5	658479	-23.9167
Mass-oil	3.1E-2	1.6E+0	739239	-1.1995
Mass-gas	1.5E-1	9.3E+1	492912	94.7920
K-TurbKE	6.0E-5	2.0E-3	569398	
E-Diss.K	1.2E-4	1.0E-2	1191151	

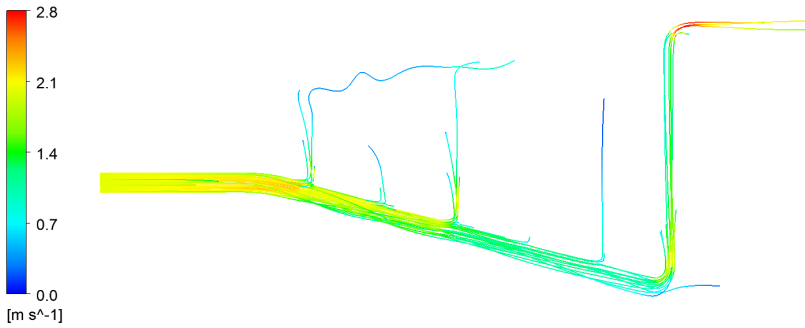

(a) Gas velocity

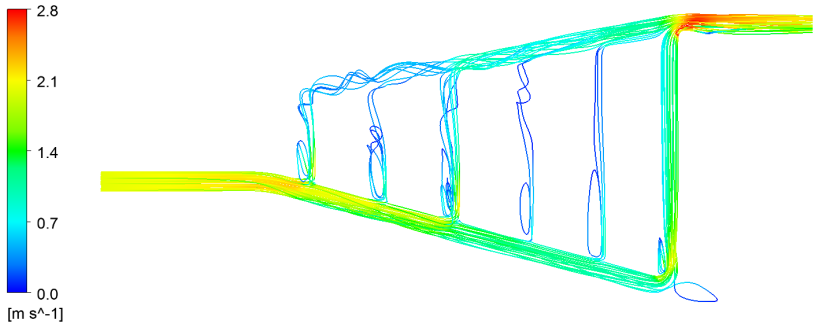

(b) Oil velocity

Figure C.2: Streamline plot of gas and oil velocity from case 4.1.1

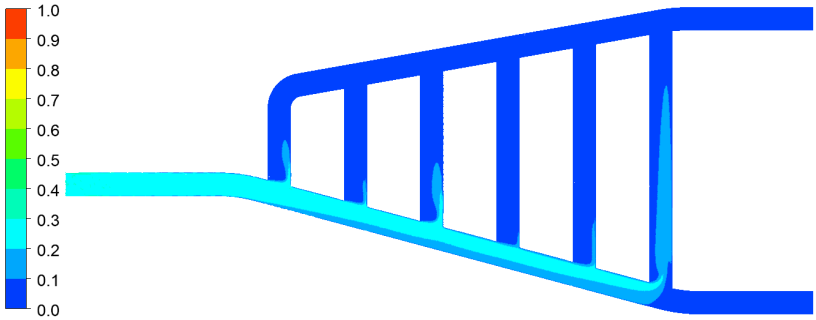

Figure C.3: GVF plot of case 4.1.1

Case 4.1.2

Table C.7: Residuals and imbalances for case 4.1.2

Equation	RMS	MAX	Location MAX - Node number	Imbalance [%]
U-Mom-oil	1.0E-2	4.4E-1	1090674	-0.0773
V-Mom-oil	9.8E-3	1.7E-1	539048	-0.0157
W-Mom-oil	1.4E-2	2.9E-1	1129631	-0.0024
U-Mom-gas	9.7E-3	4.2E-1	1090674	0.0772
V-Mom-gas	9.3E-3	1.7E-1	539048	-0.0160
W-Mom-gas	1.3E-2	2.8E-1	1129631	0.0024
P-Vol	5.7E-7	1.5E-5	737932	-23.8863
Mass-oil	3.0E-2	2.2E+0	821992	0.2479
Mass-gas	2.5E-1	1.3E+2	571526	94.7630
K-TurbKE	6.4E-5	2.4E-3	647014	
E-Diss.K	1.2E-4	1.1E-2	1187987	

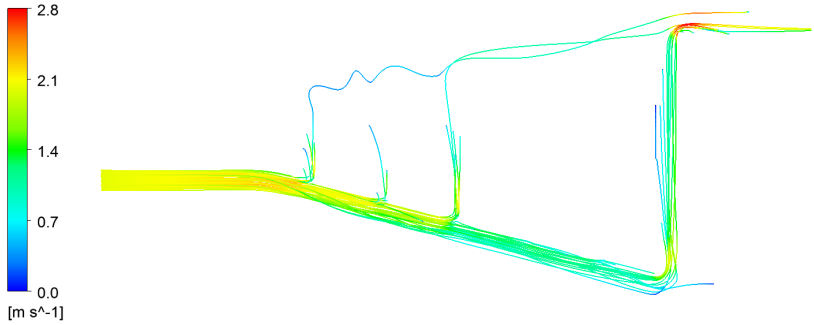

(a) Gas velocity

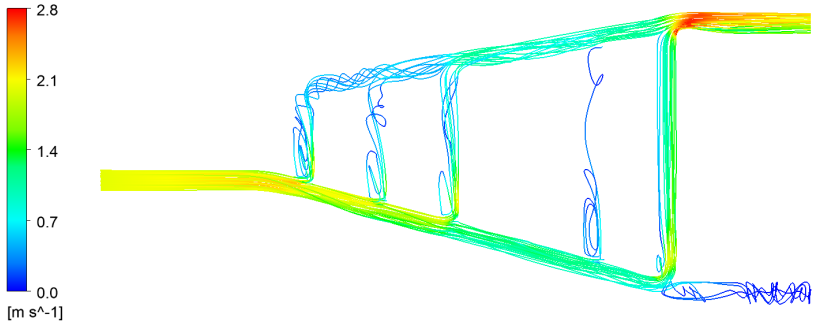

(b) Oil velocity

Figure C.4: Streamline plot of gas and oil velocity from case 4.1.2

Case 4.1.3

Table C.8: Residuals and imbalances for case 4.1.3

Equation	RMS	MAX	Location MAX - Node number	Imbalance [%]
U-Mom-oil	6.6E-4	1.8E-2	200452	-0.0021
V-Mom-oil	6.9E-4	1.4E-2	23823	-0.0003
W-Mom-oil	3.5E-4	1.2E-2	96371	0.0000
U-Mom-gas	3.2E-6	2.7E-3	983294	0.0009
V-Mom-gas	3.7E-6	3.9E-3	983294	0.0003
W-Mom-gas	7.3E-7	1.2E-4	983294	-0.0000
P-Vol	1.2E-9	3.2E-7	1192043	-25.2827
Mass-oil	1.4E-3	4.0E-2	735838	-30.0001
Mass-gas	2.0E-3	5.4E-2	1217930	100.000
K-TurbKE	2.5E-4	1.5E-2	891535	
E-Diss.K	2.5E-5	1.5E-2	891535	

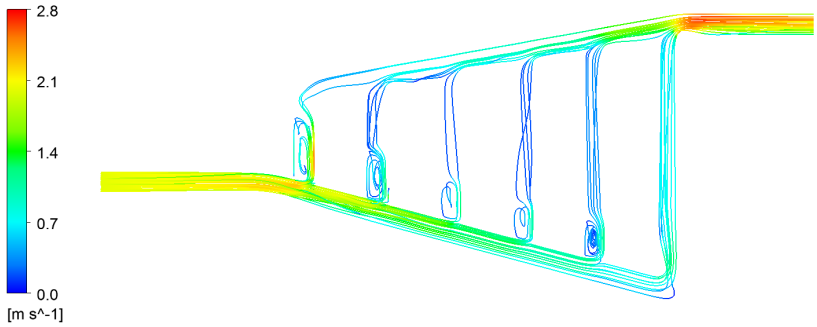

(a) Gas velocity

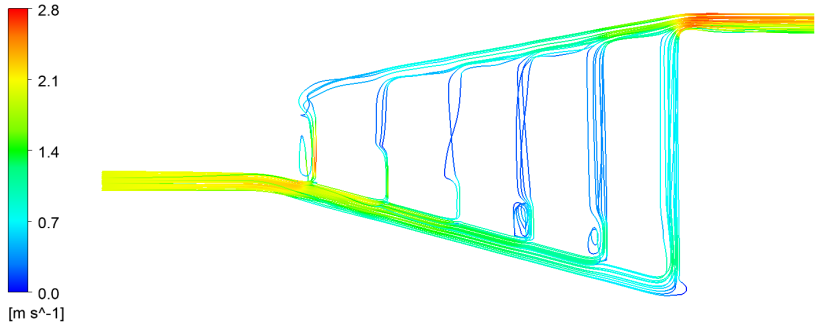

(b) Oil velocity

Figure C.5: Streamline plot of gas and oil velocity from case 4.1.3

Case 4.1.4

Table C.9: Residuals and imbalances for case 4.1.4

Equation	RMS	MAX	Location MAX - Node number	Imbalance [%]
U-Mom-oil	8.4E-4	2.5E-2	16467	-0.0014
V-Mom-oil	9.7E-4	2.6E-2	16055	0.0001
W-Mom-oil	4.2E-4	1.7E-2	118793	0.0000
U-Mom-gas	2.4E-6	9.2E-5	617357	0.0002
V-Mom-gas	3.7E-7	2.8E-5	529843	-0.0000
W-Mom-gas	6.2E-7	5.1E-5	355664	-0.0000
P-Vol	2.7E-9	2.4E-7	169029	-25.2826
Mass-oil	3.7E-3	3.1E-1	1222927	-30.0000
Mass-gas	4.1E-3	6.0E-1	1225589	100.0000
K-TurbKE	8.2E-4	2.8E-2	129016	
E-Diss.K	2.1E-4	7.0E-2	1222926	

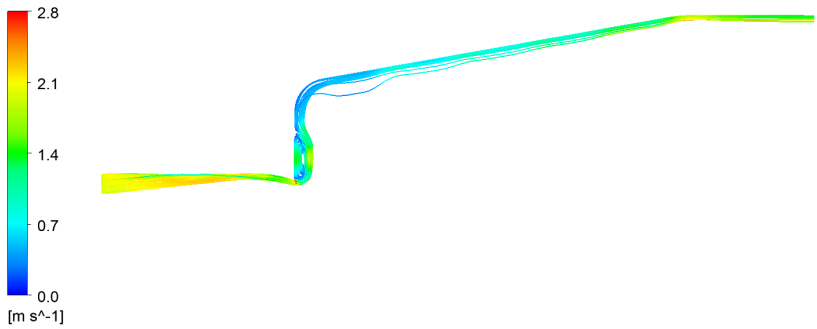

(a) Gas velocity

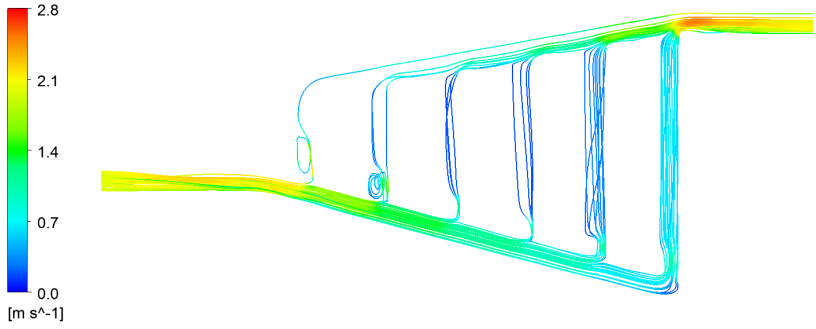

(b) Oil velocity

Figure C.6: Streamline plot of gas and oil velocity from case 4.1.4

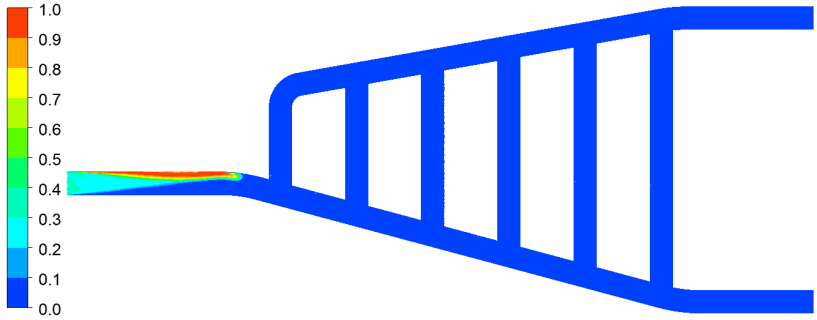

Figure C.7: GVF plot of case 4.1.4

Case 4.2.1

Table C.10: Residuals and imbalances for case 4.2.1

Equation	RMS	MAX	Location MAX - Node number	Imbalance [%]
U-Mom-oil	8.8E-3	5.1E-1	1083822	-0.0078
V-Mom-oil	1.0E-2	2.7E-1	448841	0.0108
W-Mom-oil	1.2E-2	3.0E-1	1084599	0.0002
U-Mom-gas	8.8E-3	5.1E-1	1083822	0.0075
V-Mom-gas	1.0E-2	2.7E-1	448841	-0.0109
W-Mom-gas	1.2E-2	3.0E-1	1084599	-0.0002
P-Vol	3.2E-7	1.4E-5	384381	-29.1534
Mass-oil	1.6E-2	1.0E+0	823280	-2.3369
Mass-gas	4.7E-2	6.5E+0	239437	89.2566
K-TurbKE	1.0E-4	6.3E-3	295738	
E-Diss.K	1.1E-4	2.7E-2	1191151	

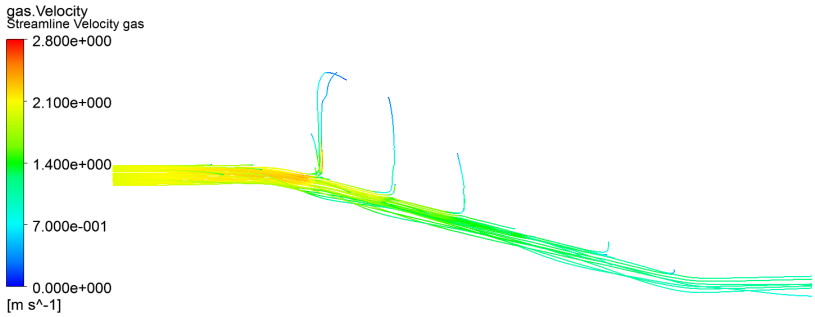

(a) Gas velocity

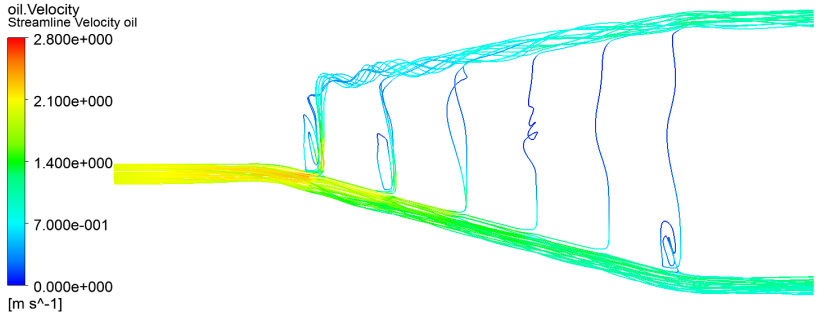

(b) Oil velocity

Figure C.8: Streamline plot of gas and oil velocity from case 4.2.1

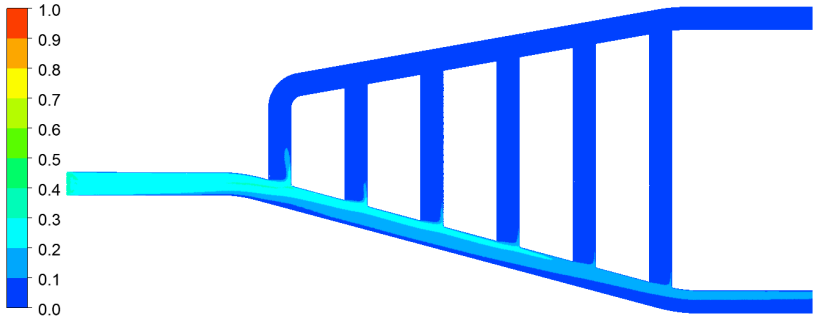

Figure C.9: GVF plot of case 4.2.1

Case 4.2.2

Table C.11: Residuals and imbalances for case 4.2.2

Equation	RMS	MAX	Location MAX - Node number	Imbalance [%]
U-Mom-oil	6.6E-4	1.8E-2	200452	-0.0021
V-Mom-oil	6.9E-4	1.4E-2	23825	-0.0003
W-Mom-oil	3.5E-4	1.2E-2	96371	0.0000
U-Mom-gas	3.2E-6	2.7E-3	983294	0.0009
V-Mom-gas	3.7E-6	3.9E-3	983294	0.0003
W-Mom-gas	7.3E-7	1.2E-4	983294	-0.0000
P-Vol	1.2E-9	3.2E-7	1192043	-25.2827
Mass-oil	1.4E-3	4.0E-2	735838	-30.0001
Mass-gas	2.0E-3	5.4E-2	1217930	100.0000
K-TurbKE	2.5E-4	1.5E-2	891535	
E-Diss.K	2.5E-5	1.5E-2	891535	

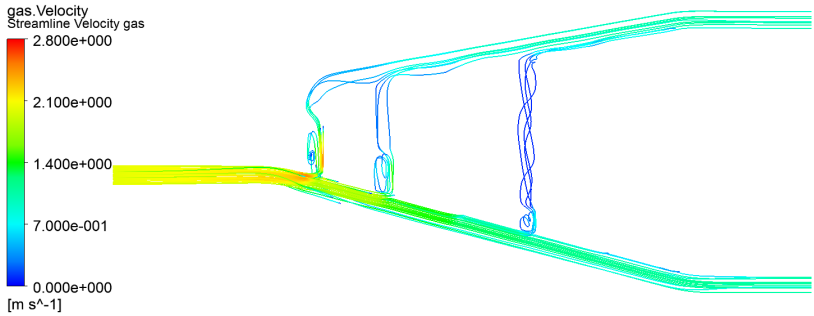

(a) Gas velocity

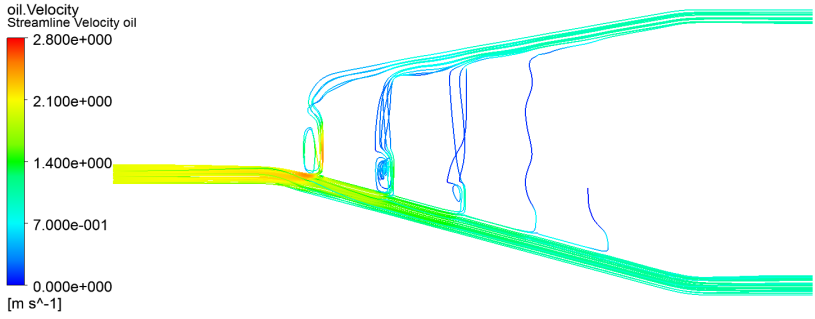

(b) Oil velocity

Figure C.10: Streamline plot of gas and oil velocity from case 4.2.2

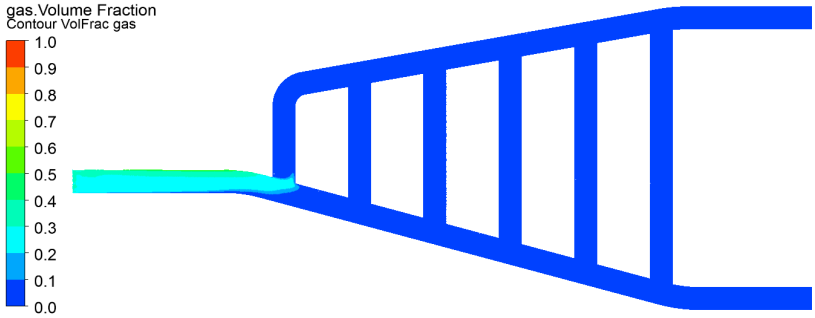

Figure C.11: GVF plot of case 4.2.2

Case 4.3

Table C.12: Residuals and imbalances for case 4.3

Equation	RMS	MAX	Location MAX - Node number	Imbalance [%]
U-Mom-oil	7.2E-3	4.4E-1	1082237	-0.0132
V-Mom-oil	8.9E-3	2.2E-1	448840	0.0149
W-Mom-oil	1.0E-2	2.9E-1	1084599	0.0018
U-Mom-gas	7.2E-3	4.4E-1	1082237	0.0129
V-Mom-gas	8.9E-3	2.2E-1	448840	-0.0151
W-Mom-gas	1.0E-2	2.9E-1	1084599	-0.0018
P-Vol	3.0E-7	1.1E-5	653207	-28.2199
Mass-oil	1.6E-2	1.0E+0	733846	-5.6028
Mass-gas	5.1E-2	2.1E+1	222981	86.7940
K-TurbKE	9.2E-5	6.1E-3	383225	
E-Diss.K	1.2E-4	2.0E-2	1191028	

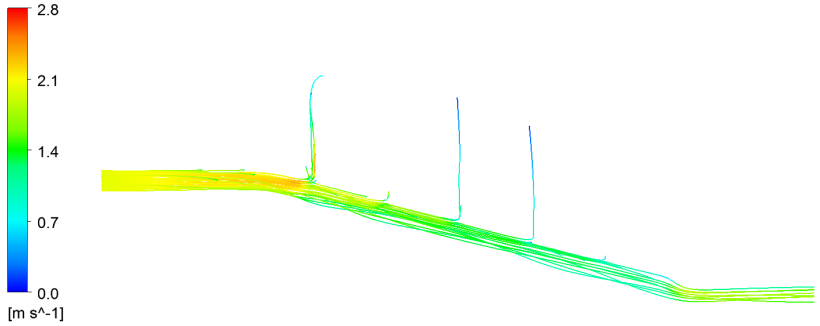

(a) Gas velocity

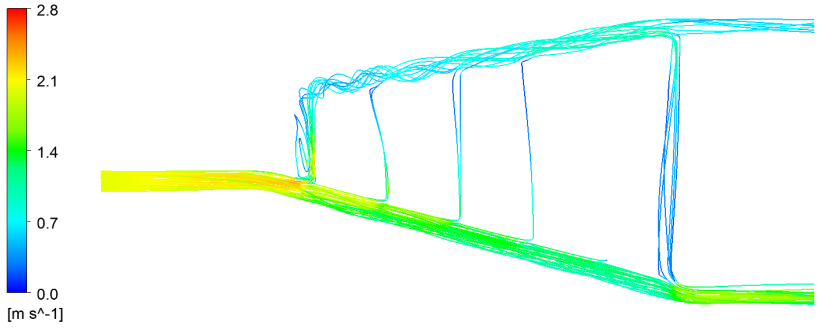

(b) Oil velocity

Figure C.12: Streamline plot of gas and oil velocity from case 4.3

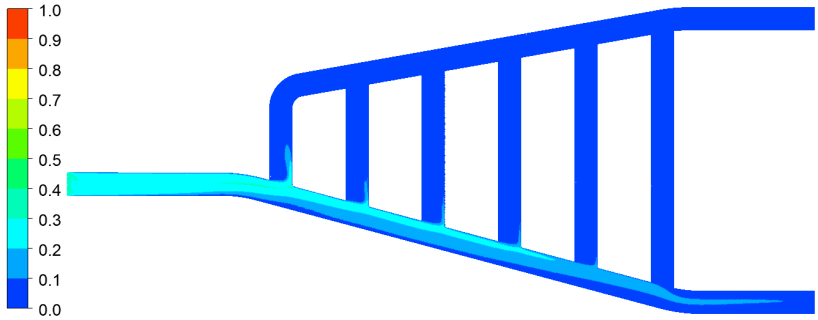

Figure C.13: GVF plot of case 4.3

Case 4.4

Table C.13: Residuals and imbalances for case 4.4

Equation	RMS	MAX	Location MAX - Node number	Imbalance [%]
U-Mom-oil	1.7E-4	7.3E-3	10533	-0.0001
V-Mom-oil	2.5E-4	5.6E-3	24109	-0.0000
W-Mom-oil	1.0E-4	3.7E-3	24112	0.0000
U-Mom-gas	7.7E-6	2.2E-4	10533	0.0000
V-Mom-gas	1.1E-5	2.8E-4	45168	0.0000
W-Mom-gas	4.5E-6	1.8E-4	13825	-0.0000
P-Vol	1.1E-9	1.9E-7	1149172	-5.0409
Mass-oil	2.2E-3	6.9E-2	1200470	-6.5232
Mass-gas	4.8E-3	2.0E-1	1200470	15.4914
K-TurbKE	2.4E-4	1.6E-2	70449	
E-Diss.K	1.1E-4	9.1E-3	1148971	

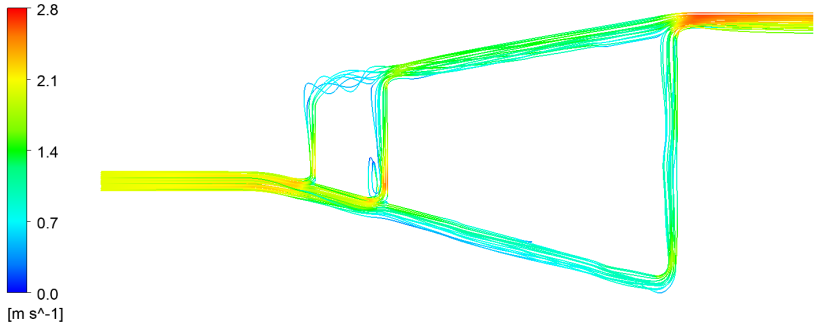

(a) Gas velocity

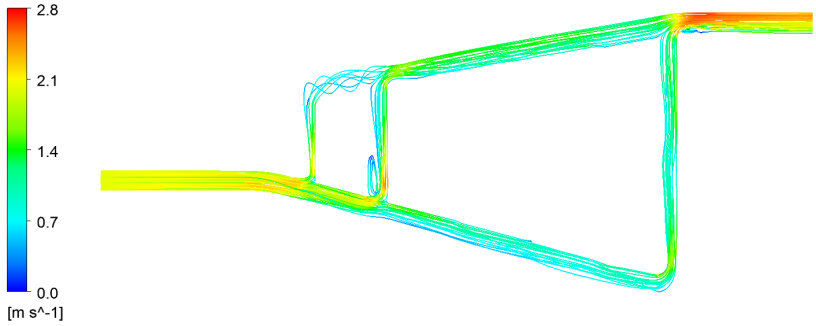

(b) Oil velocity

Figure C.14: Streamline plot of gas and oil velocity from case 4.4

Appendix D

Details on CFD simulations for performance evaluation

D.1 Case 5

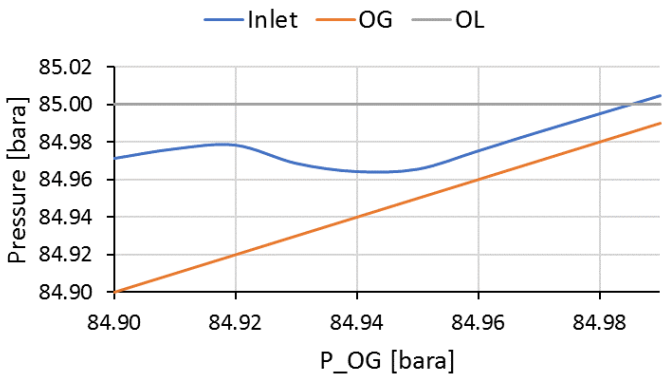

Figure D.1: Chart of boundary pressures for different P_{OG}

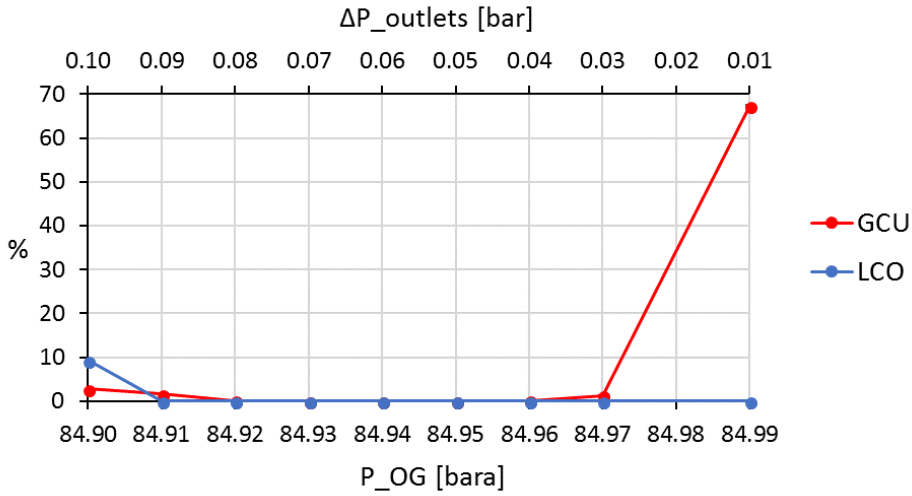

Figure D.2: Charts of LCO and GCU versus P_{OG}

Case 5.1: P_{OG} **= 84.90** $bara$

Table D.1: Residuals and imbalances for case 5.1

Equation	RMS	MAX	Location MAX - Node number	Imbalance [%]
U-Mom-oil	4.5E-5	3.5E-3	355517	0.0000
V-Mom-oil	3.5E-5	2.9E-3	1055466	-0.0000
W-Mom-oil	3.2E-5	3.1E-3	361295	-0.0000
U-Mom-gas	4.1E-5	7.4E-3	980807	0.0000
V-Mom-gas	2.3E-5	2.6E-3	796509	0.0000
W-Mom-gas	3.0E-5	4.9E-4	448053	-0.0000
P-Vol	1.8E-9	3.7E-7	950216	-0.0027
Mass-oil	1.6E-4	3.7E-2	981035	0.0312
Mass-gas	2.4E-4	1.8E-1	1209100	0.0148
K-TurbKE	1.2E-5	4.2E-3	1206680	
E-Diss.K	1.2E-5	7.0E-3	1215019	

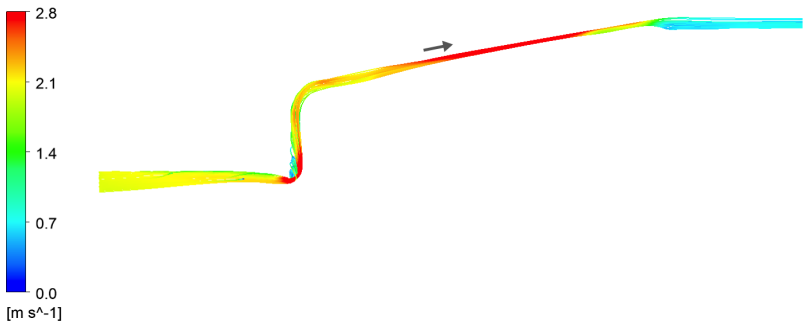

(a) Gas velocity

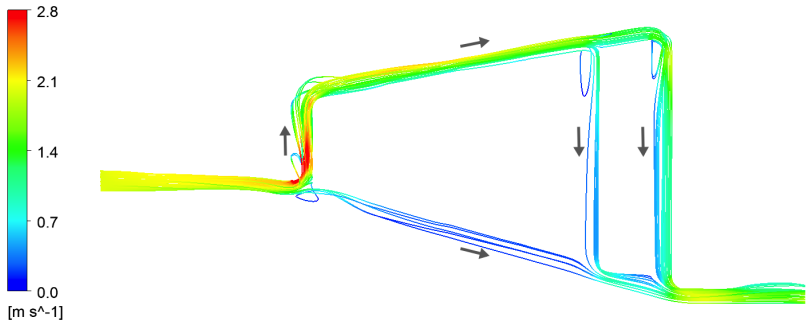

(b) Oil velocity

Figure D.3: Streamline plot of gas and oil velocity from case 5.1, with arrows indicating the main flow direction

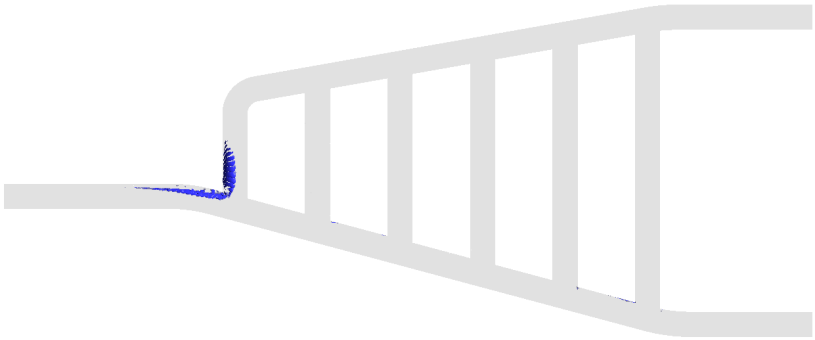

Figure D.4: Location of residuals with a value > 0.001 for case 5.1

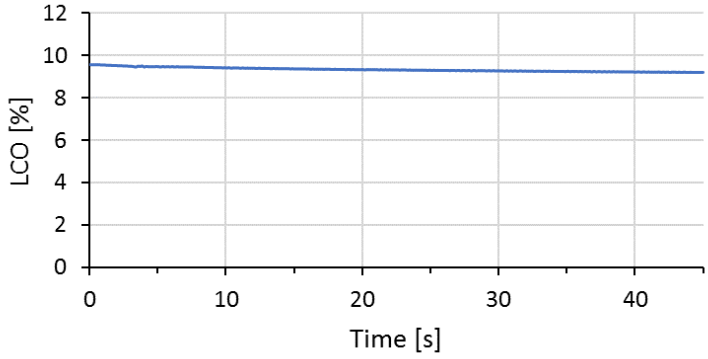

(a) LCO

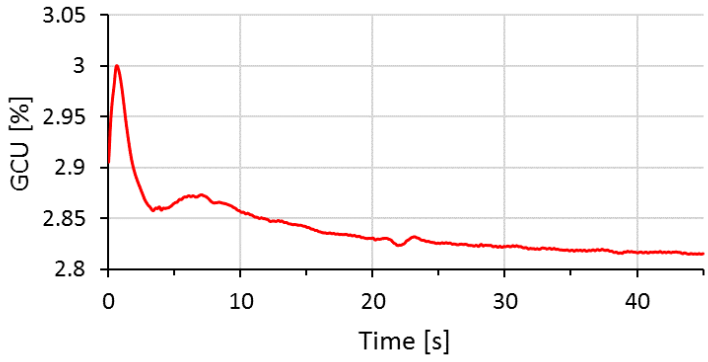

(b) GCU

Figure D.5: Transient behaviour of LCO and GCU for case 5.1

Case 5.2: OG pressure = 84.91 $bara$

Table D.2: Residuals and imbalances for case 5.1

Equation	RMS	MAX	Location MAX - Node number	Imbalance [%]
U-Mom-oil	1.3E-6	2.4E-4	1039714	0.0000
V-Mom-oil	7.1E-6	1.1E-3	1038660	-0.0000
W-Mom-oil	1.1E-6	1.5E-4	951130	-0.0000
U-Mom-gas	4.7E-6	1.6E-3	967506	-0.0000
V-Mom-gas	1.3E-5	2.0E-3	1146593	0.0000
W-Mom-gas	1.1E-6	3.5E-4	1141716	0.0000
P-Vol	9.7E-10	2.5E-7	1141931	0.0840
Mass-oil	3.6E-4	5.5E-2	1146673	0.0022
Mass-gas	4.8E-4	9.4E-2	1141703	0.0046
K-TurbKE	6.5E-6	2.1E-3	1146593	
E-Diss.K	5.3E-6	3.4E-3	1216425	

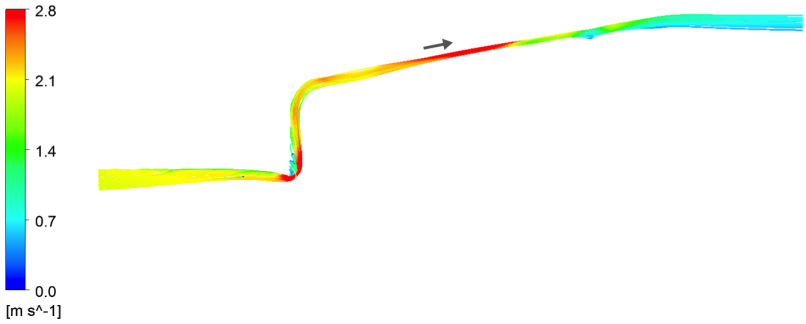

(a) Gas velocity

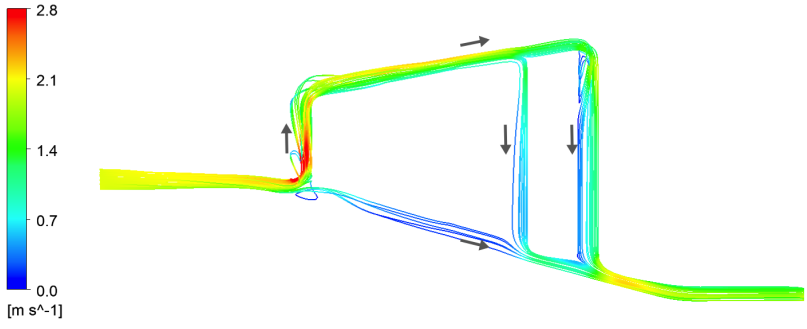

(b) Oil velocity

Figure D.6: Streamline plot of gas and oil velocity from case 5.2, with arrows indicating the main flow direction

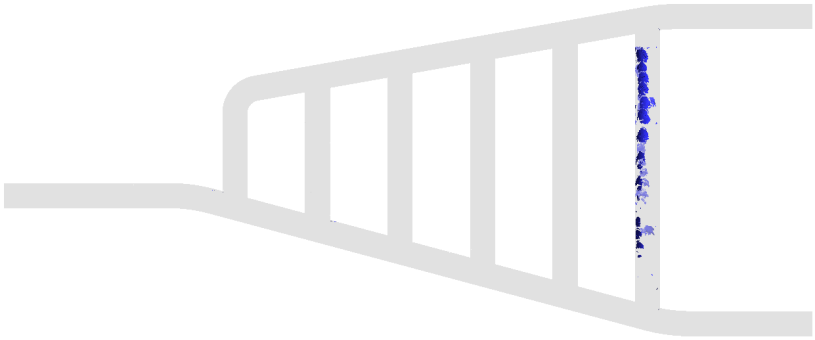

Figure D.7: Location of residuals with a value > 0.001 for case 5.2

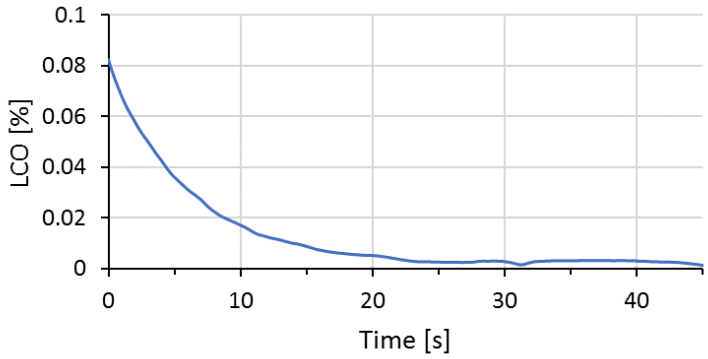

(a) LCO

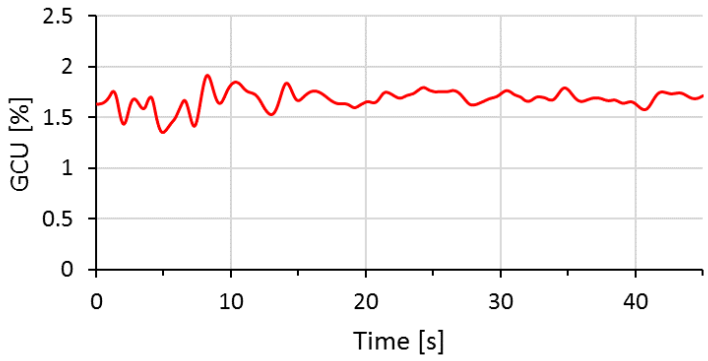

(b) GCU

Figure D.8: Transient behaviour of LCO and GCU for case 5.2

Case 5.3: OG pressure = 84.92 $bara$

Table D.3: Residuals and imbalances for case 5.3

Equation	RMS	MAX	Location MAX - Node number	Imbalance [%]
U-Mom-oil	1.7E-6	2.6E-4	1137295	0.0000
V-Mom-oil	7.4E-6	1.4E-3	1016608	-0.0000
W-Mom-oil	2.0E-6	5.3E-4	1016314	0.0000
U-Mom-gas	5.3E-6	1.6E-3	968299	-0.0000
V-Mom-gas	1.3E-5	2.4E-3	1174023	0.0000
W-Mom-gas	2.0E-6	4.5E-4	1174023	-0.0000
P-Vol	1.2E-9	2.1E-7	1174933	0.0991
Mass-oil	3.0E-4	5.7E-2	1173565	-0.0008
Mass-gas	4.6E-4	1.2E-1	1174958	0.0263
K-TurbKE	9.8E-6	5.2E-3	1175871	
E-Diss.K	7.1E-6	3.0E-3	1175871	

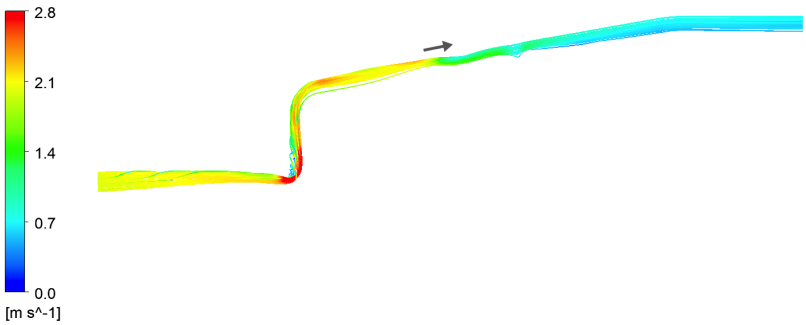

(a) Gas velocity

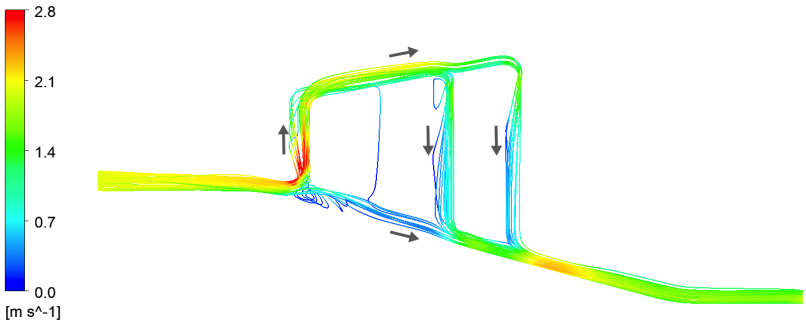

(b) Oil velocity

Figure D.9: Streamline plot of gas and oil velocity from case 5.3, with arrows indicating the main flow direction

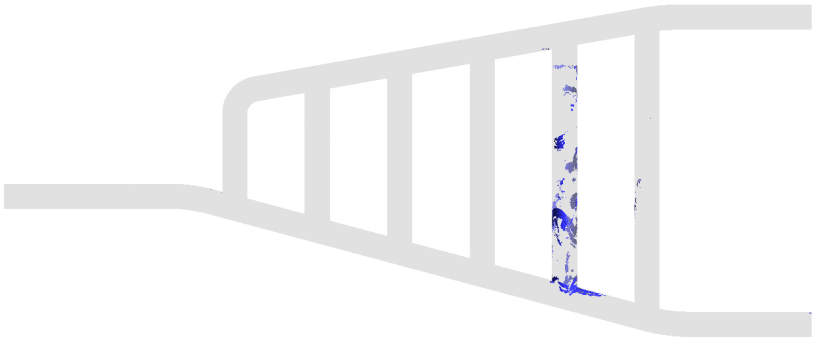

Figure D.10: Location of residuals with a value > 0.001 for case 5.3

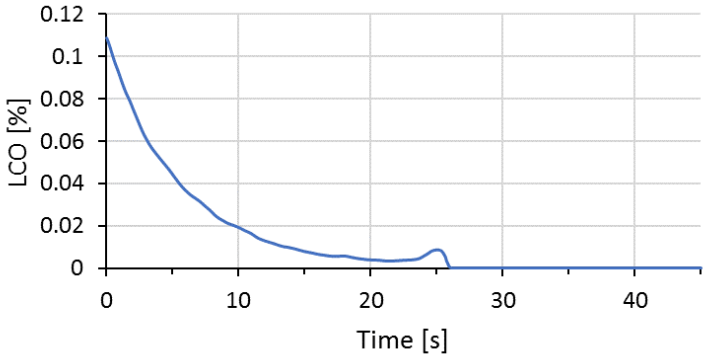

(a) LCO

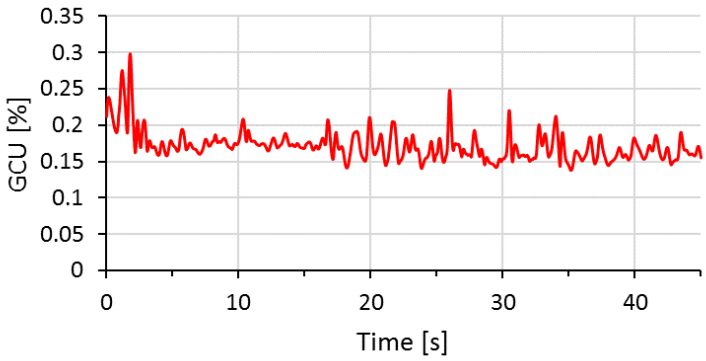

(b) GCU

Figure D.11: Transient behaviour of LCO and GCU for case 5.3

Case 5.4: OG pressure = 84.93 $bara$

Table D.4: Residuals and imbalances for case 5.1

Equation	RMS	MAX	Location MAX - Node number	Imbalance [%]
U-Mom-oil	1.0E-5	4.5E-3	632835	-0.0000
V-Mom-oil	1.3E-5	2.1E-3	1177873	0.0000
W-Mom-oil	4.3E-6	5.4E-4	1214481	-0.0000
U-Mom-gas	9.3E-6	1.8E-3	1193018	0.0000
V-Mom-gas	1.4E-5	2.1E-3	1181808	-0.0000
W-Mom-gas	5.9E-6	1.7E-3	1192528	-0.0000
P-Vol	3.7E-9	5.7E-7	1151005	0.1524
Mass-oil	2.5E-4	5.4E-2	1179458	-0.0802
Mass-gas	2.4E-4	4.3E-2	1193198	-0.1020
K-TurbKE	1.2E-4	3.4E-2	1192746	
E-Diss.K	8.4E-4	4.6E-1	1192746	

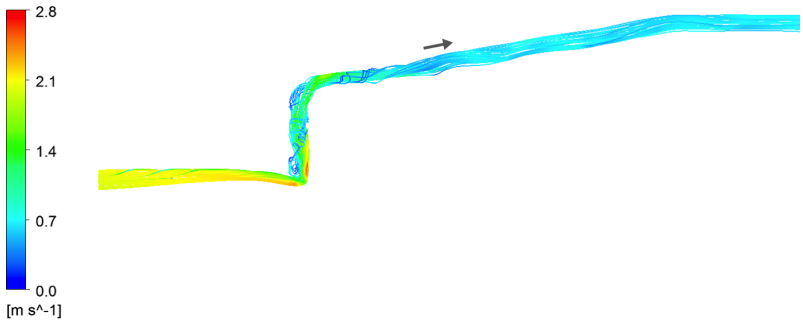

(a) Gas velocity

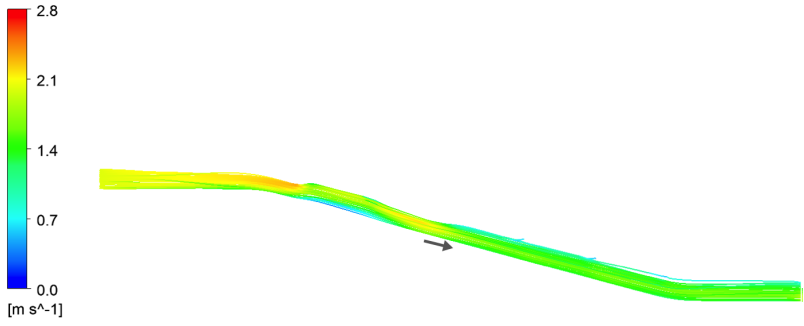

(b) Oil velocity

Figure D.12: Streamline plot of gas and oil velocity from case 5.4, with arrows indicating the main flow direction

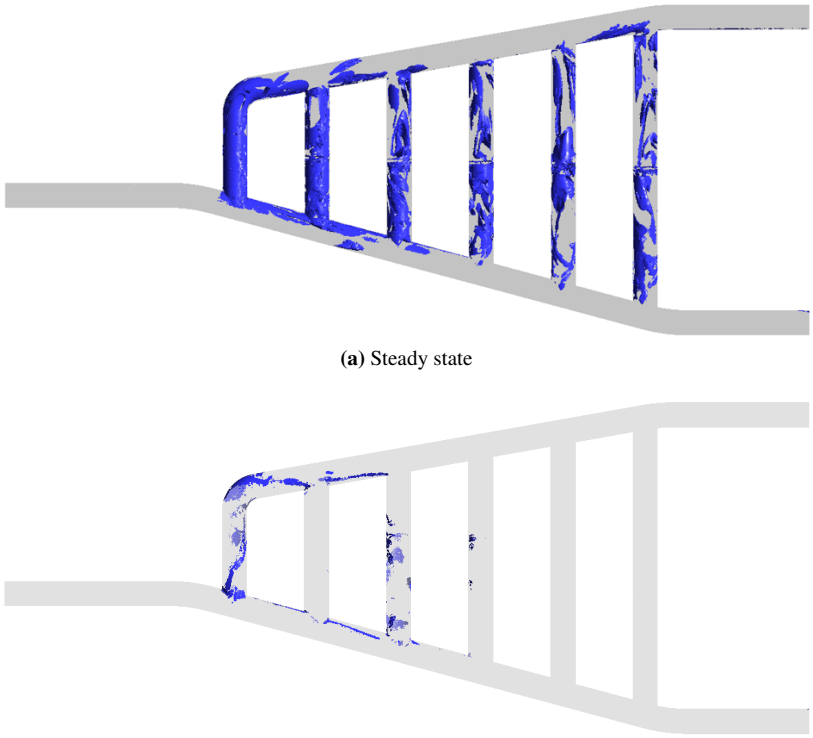

(a) Steady state

(b) Transient

Figure D.13: Location of residuals with a value > 0.001 for case 5.4

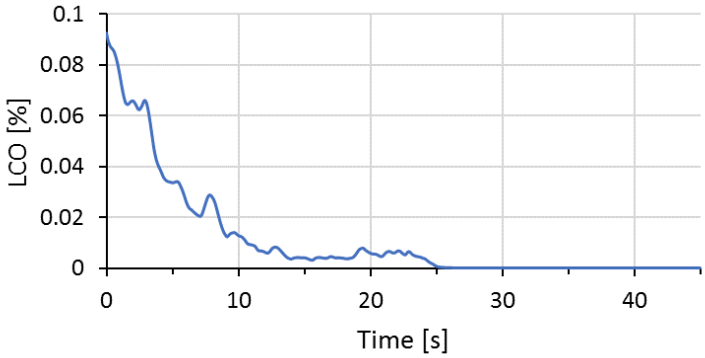

(a) LCO

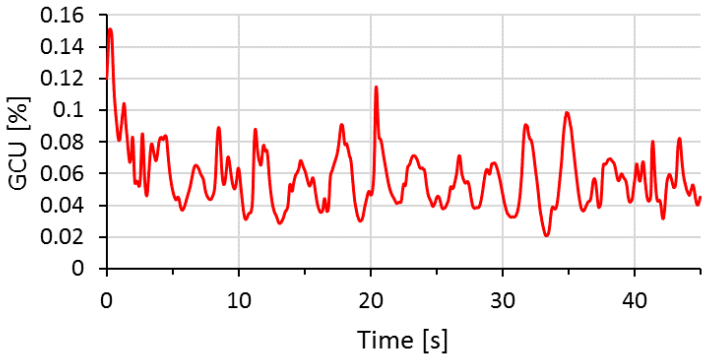

(b) GCU

Figure D.14: Transient behaviour of LCO and GCU for case 5.4

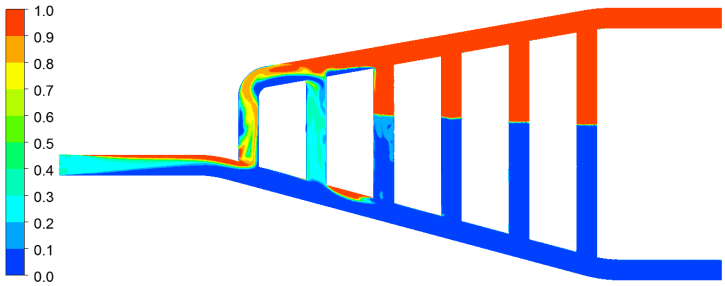

(a) 42 s

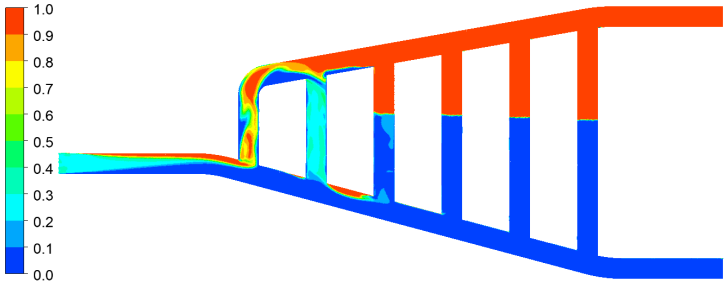

(b) 43 s

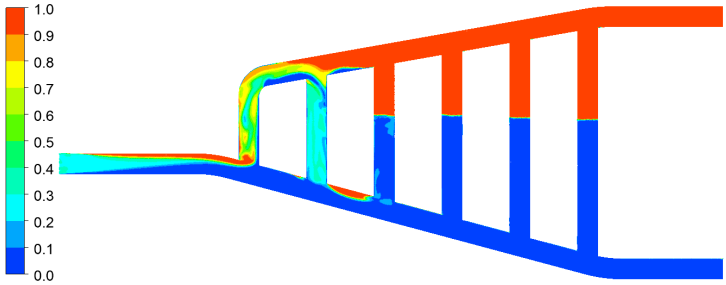

(c) 44 s

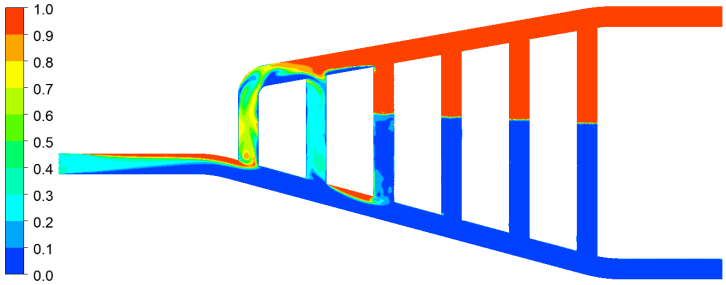

(d) 45 s

Figure D.15: GVF plot showing the transient behaviour of case 5.4

Case 5.5: OG pressure = 84.94 $bara$

Table D.5: Residuals and imbalances for case 5.5

Equation	RMS	MAX	Location MAX - Node number	Imbalance [%]
U-Mom-oil	1.6E-5	7.5E-3	632369	-0.0000
V-Mom-oil	8.3E-6	1.8E-3	1185760	0.0000
W-Mom-oil	3.8E-6	7.8E-4	1193112	-0.0000
U-Mom-gas	1.0E-5	2.8E-3	1193148	0.0000
V-Mom-gas	1.0E-5	2.0E-3	1185760	-0.0000
W-Mom-gas	4.4E-6	6.3E-4	1185760	0.0000
P-Vol	2.8E-9	3.5E-7	1159366	-0.0110
Mass-oil	1.9E-4	9.0E-2	1151463	-0.0126
Mass-gas	1.8E-4	5.5E-2	997996	-0.1000
K-TurbKE	9.4E-5	2.5E-2	1193148	
E-Diss.K	6.5E-4	3.1E-1	11931484	

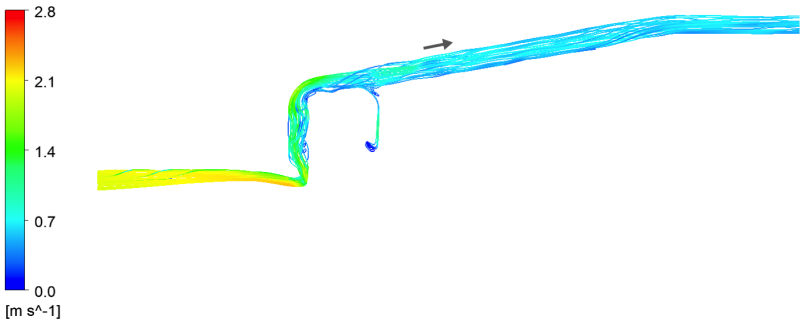

(a) Gas velocity

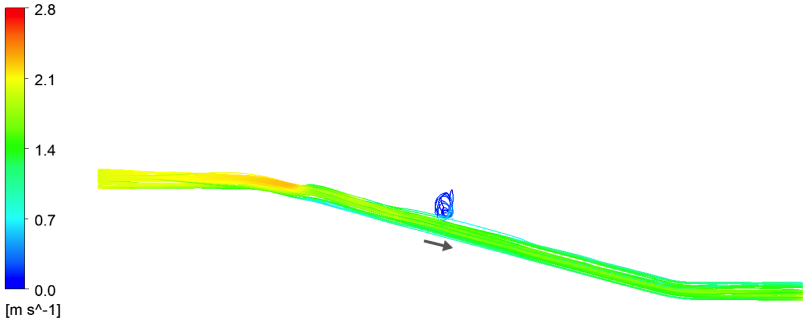

(b) Oil velocity

Figure D.16: Streamline plot of gas and oil velocity from case 5.5, with arrows indicating the main flow direction

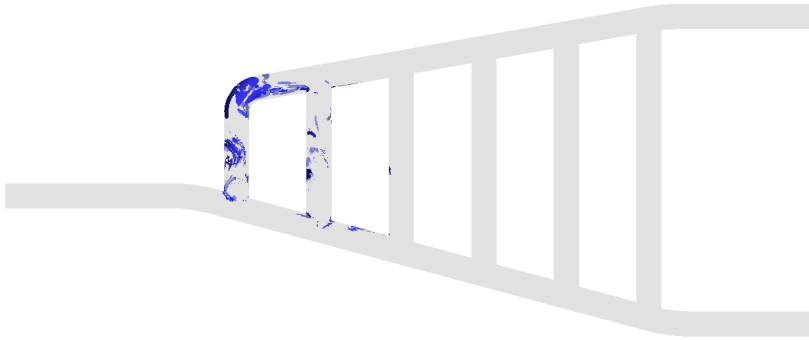

Figure D.17: Location of residuals with a value > 0.001 for case 5.5

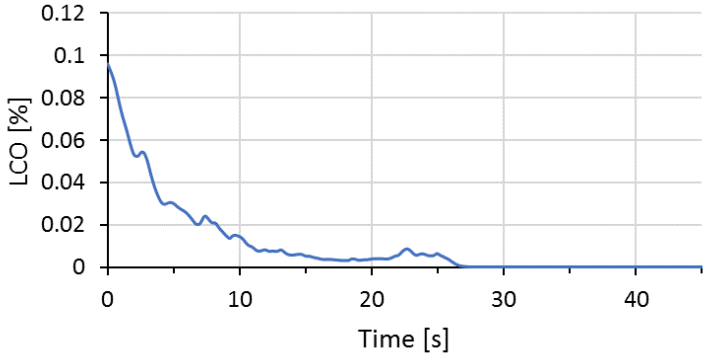

(a) LCO

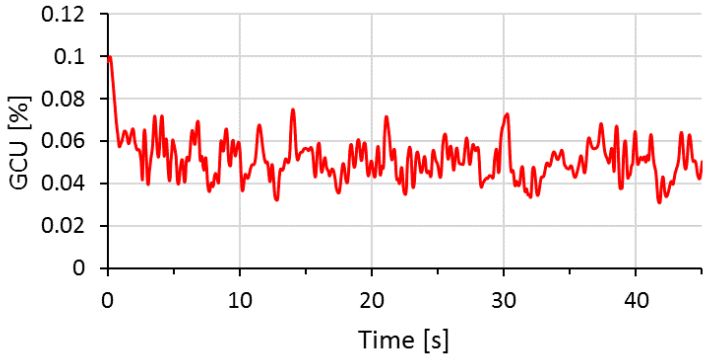

(b) GCU

Figure D.18: Transient behaviour of LCO and GCU for case 5.5

Case 5.6: OG pressure = 84.95 $bara$

Table D.6: Residuals and imbalances for case 5.6

Equation	RMS	MAX	Location MAX - Node number	Imbalance [%]
U-Mom-oil	2.7E-6	8.6E-4	1007079	0.0000
V-Mom-oil	7.9E-6	1.9E-3	1183567	-0.0000
W-Mom-oil	1.9E-6	3.5E-4	1005825	-0.0000
U-Mom-gas	2.3E-6	5.6E-4	1181314	-0.0000
V-Mom-gas	9.1E-6	2.8E-3	1183567	0.0000
W-Mom-gas	2.3E-6	9.5E-4	922122	0.0000
P-Vol	7.4E-10	2.2E-7	1178785	-0.0737
Mass-oil	2.0E-4	5.0E-2	1182729	0.0113
Mass-gas	2.4E-4	9.3E-2	1179179	0.0006
K-TurbKE	1.1E-5	5.5E-3	1191625	
E-Diss.K	3.3E-5	8.7E-3	1190180	

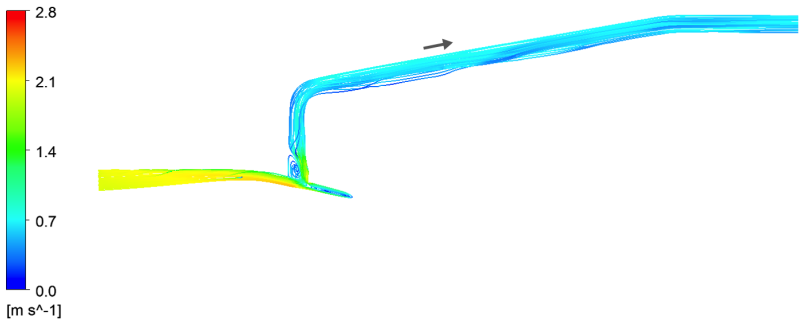

(a) Gas velocity

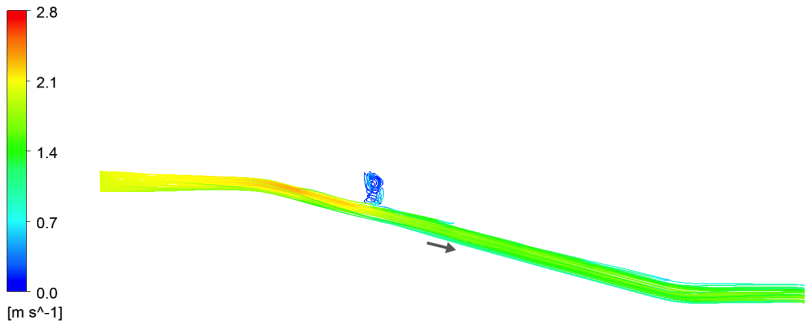

(b) Oil velocity

Figure D.19: Streamline plot of gas and oil velocity from case 5.6, with arrows indicating the main flow direction

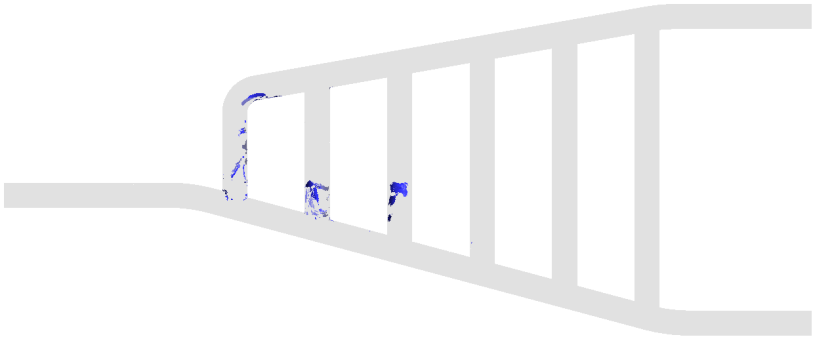

Figure D.20: Location of residuals with a value > 0.001 for case 5.6

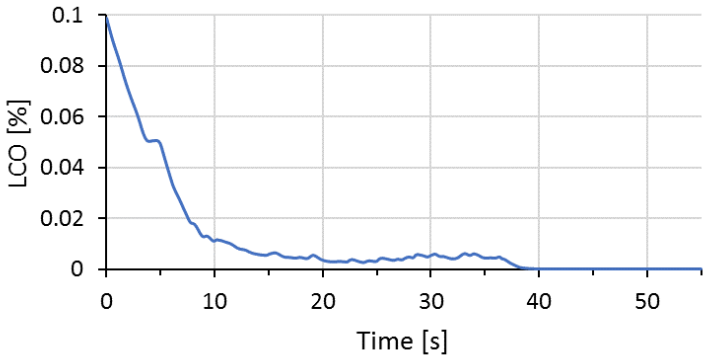

(a) LCO

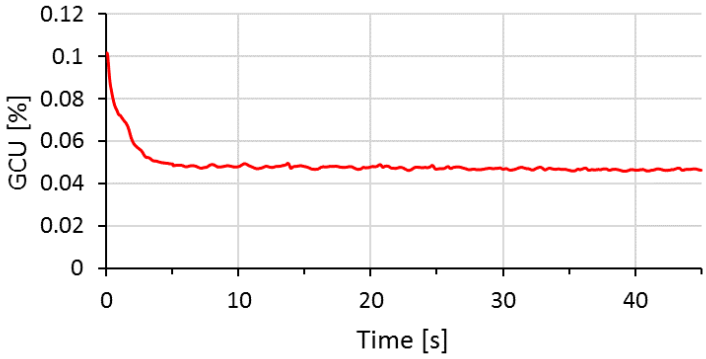

(b) GCU

Figure D.21: Transient behaviour of LCO and GCU for case 5.6

Case 5.7: P_{OG} **= 84.96** $bara$

Table D.7: Residuals and imbalances for case 5.7

Equation	RMS	MAX	Location MAX - Node number	Imbalance [%]
U-Mom-oil	1.1E-6	3.8E-4	941773	0.0000
V-Mom-oil	2.6E-6	1.1E-3	941773	0.0000
W-Mom-oil	1.4E-6	6.7E-4	1029260	0.0000
U-Mom-gas	2.4E-6	4.6E-4	941773	-0.0000
V-Mom-gas	4.9E-6	1.2E-3	941773	-0.0000
W-Mom-gas	1.6E-6	1.1E-3	941773	-0.0000
P-Vol	9.5E-10	7.4E-7	1152257	-0.0765
Mass-oil	9.5E-5	4.2E-2	1154456	-0.0003
Mass-gas	1.4E-4	4.6E-2	1152102	0.0087
K-TurbKE	3.3E-6	6.4E-4	1162859	
E-Diss.K	2.2E-5	1.2E-2	1215055	

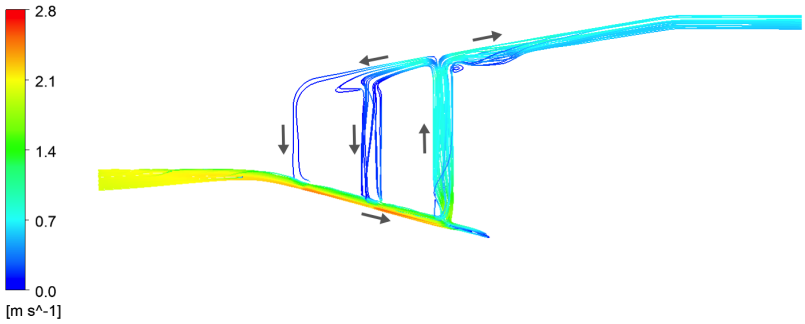

(a) Gas velocity

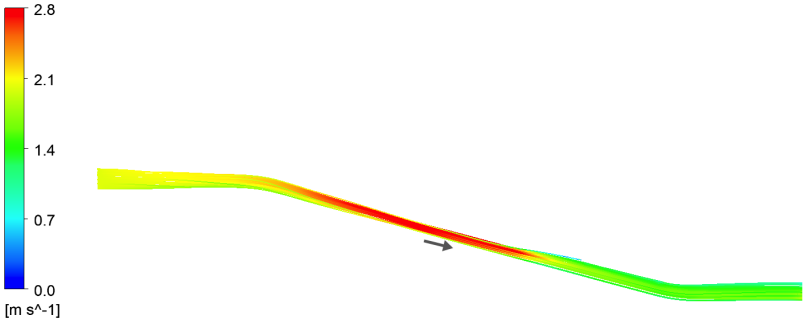

(b) Oil velocity

Figure D.22: Streamline plot of gas and oil velocity from case 5.7, with arrows indicating the main flow direction

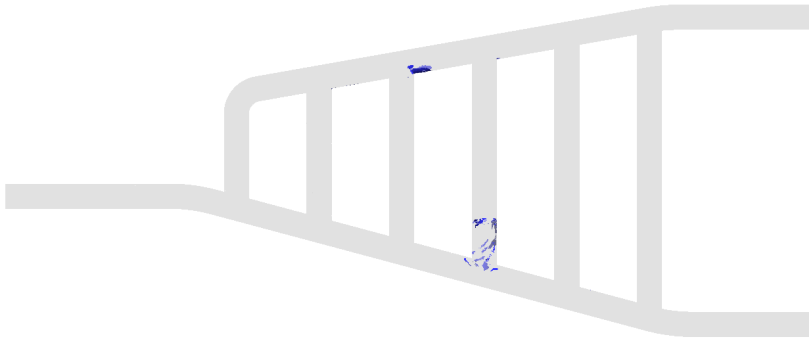

Figure D.23: Location of residuals with a value > 0.001 for case 5.7

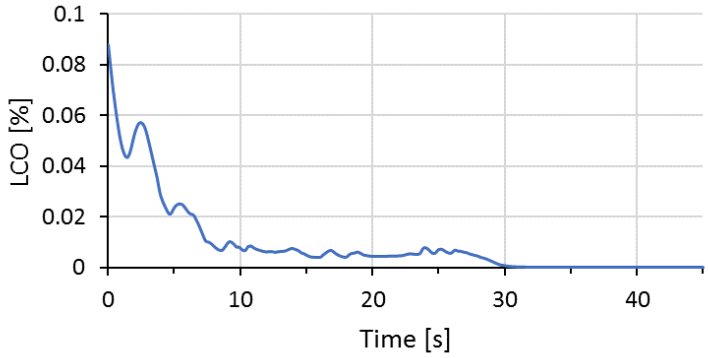

(a) LCO

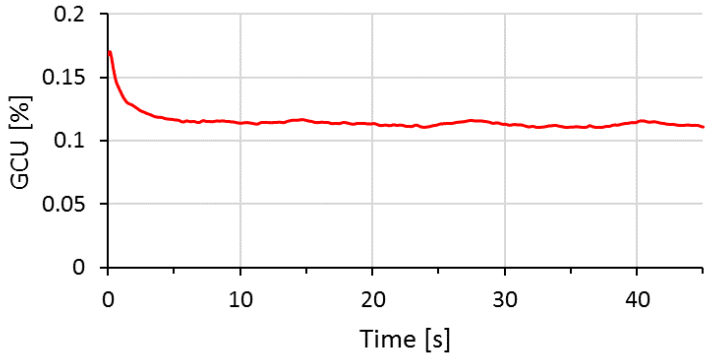

(b) GCU

Figure D.24: Transient behaviour of LCO and GCU for case 5.7

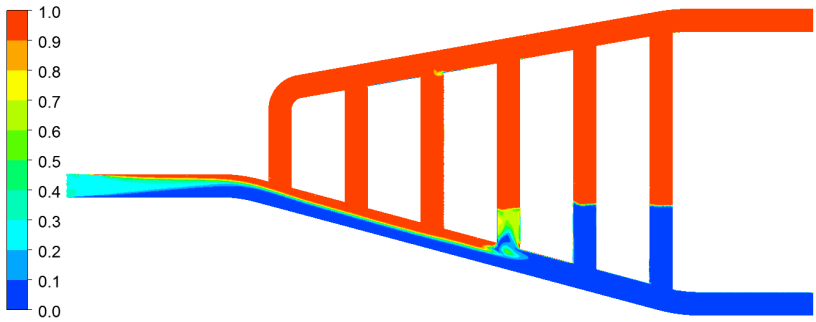

Figure D.25: Plot showing the GVF of case 5.7

Case 5.8: P_{OG} **= 84.97** $bara$

Table D.8: Residuals and imbalances for case 5.8

Equation	RMS	MAX	Location MAX - Node number	Imbalance [%]
U-Mom-oil	5.3E-7	9.2E-5	774380	-0.0000
V-Mom-oil	1.4E-6	5.0E-4	1143641	-0.0000
W-Mom-oil	3.2E-7	5.1E-5	1144925	-0.0000
U-Mom-gas	7.1E-7	9.3E-5	1160930	0.0000
V-Mom-gas	2.5E-6	6.2E-4	1145957	0.0000
W-Mom-gas	1.4E-6	8.0E-4	895753	0.0000
P-Vol	4.8E-10	2.4E-7	1144925	-0.0081
Mass-oil	8.2E-5	2.1E-2	1142065	0.0035
Mass-gas	1.0E-4	3.9E-2	1147032	0.0016
K-TurbKE	1.0E-6	1.5E-4	1144974	
E-Diss.K	6.6E-6	1.8E-3	1145957	

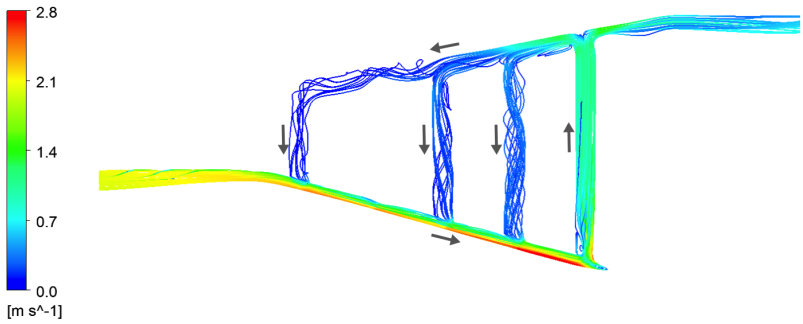

(a) Gas velocity

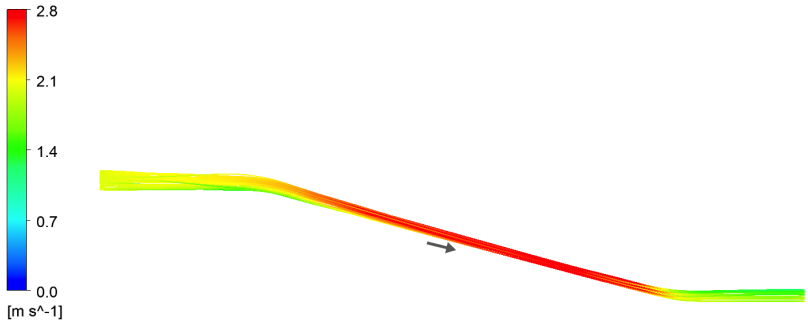

(b) Oil velocity

Figure D.26: Streamline plot of gas and oil velocity from case 5.8, with arrows indicating the main flow direction

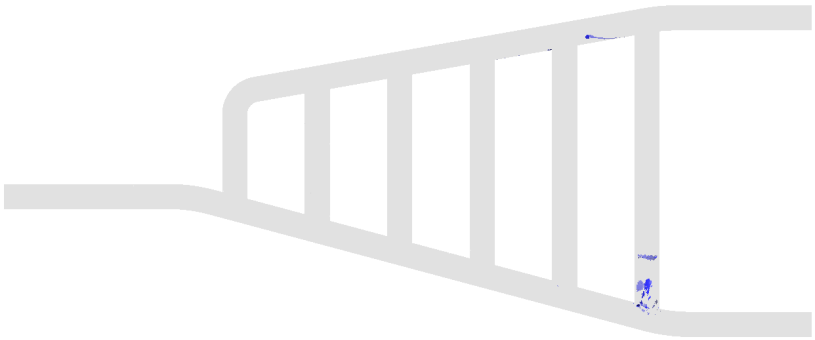

Figure D.27: Location of residuals with a value > 0.001 for case 5.8

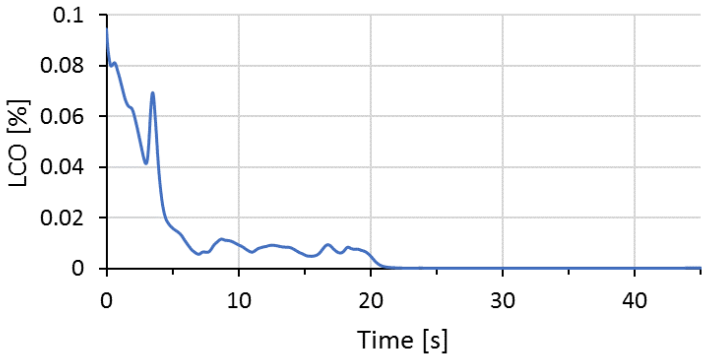

(a) LCO

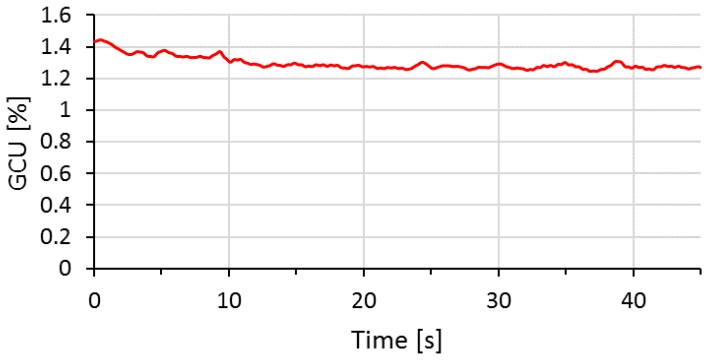

(b) GCU

Figure D.28: Transient behaviour of LCO and GCU for case 5.8

Case 5.9: P_{OG} **= 84.99** $bara$

Table D.9: Residuals and imbalances for case 5.9

Equation	RMS	MAX	Location MAX - Node number	Imbalance [%]
U-Mom-oil	4.4E-5	1.8E-3	1068059	0.0000
V-Mom-oil	1.8E-5	9.0E-4	1069500	0.0000
W-Mom-oil	1.5E-5	6.5E-4	1062199	0.0000
U-Mom-gas	3.2E-5	1.3E-2	895639	-0.0000
V-Mom-gas	1.6E-5	1.1E-3	946768	0.0000
W-Mom-gas	1.4E-5	5.0E-3	808266	0.0000
P-Vol	1.1E-9	2.5E-7	1157252	-0.1631
Mass-oil	1.6E-4	5.9E-2	939495	-0.1387
Mass-gas	2.3E-4	5.5E-2	1150909	0.6295
K-TurbKE	2.3E-5	1.8E-3	1125367	
E-Diss.K	1.1E-5	2.4E-3	1205047	

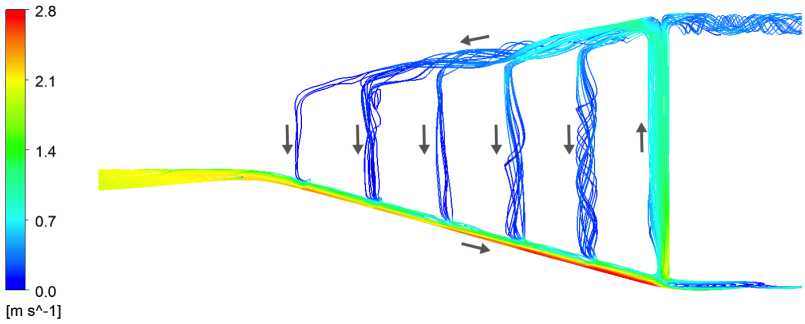

(a) Gas velocity

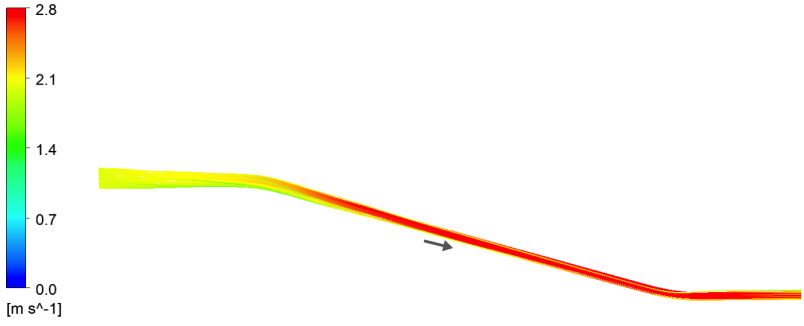

(b) Oil velocity

Figure D.29: Streamline plot of gas and oil velocity from case 5.9, with arrows indicating the main flow direction

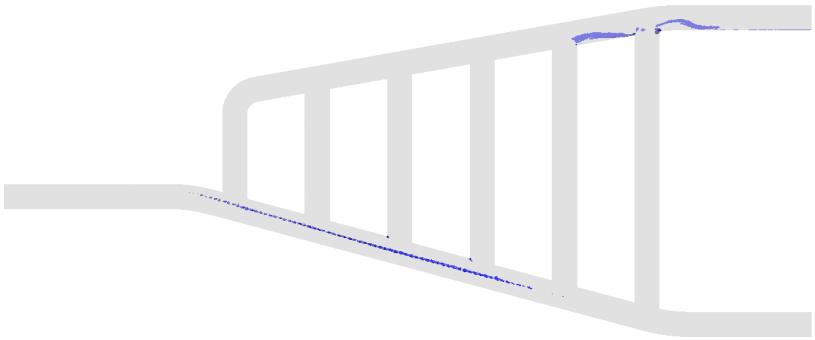

Figure D.30: Location of residuals with a value > 0.001 for case 5.9

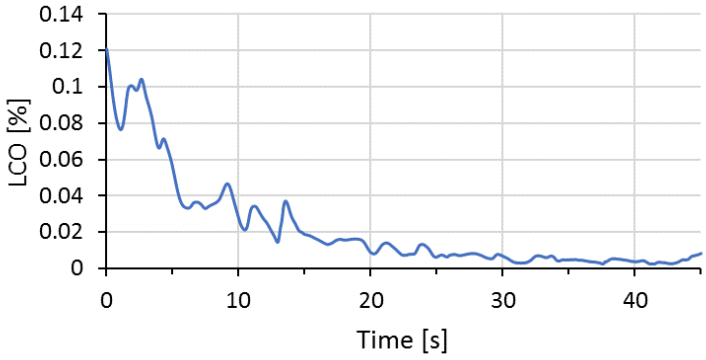

(a) LCO

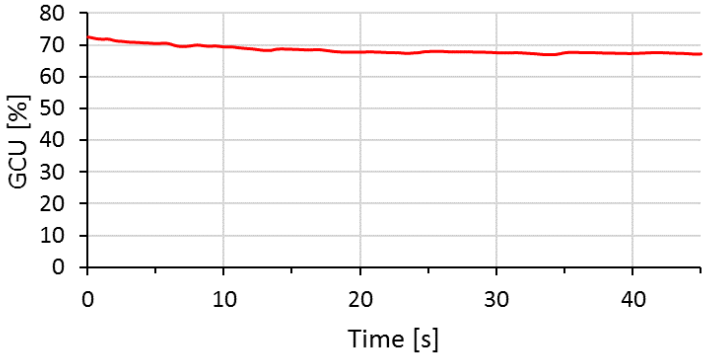

(b) GCU

Figure D.31: Transient behaviour of LCO and GCU for case 5.9

D.2 Case 6

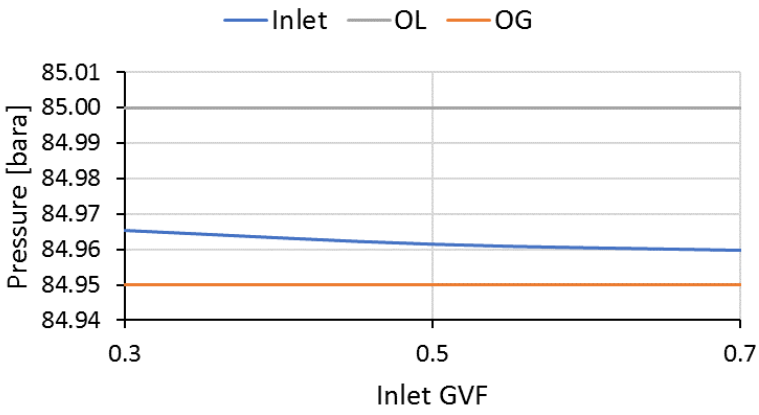

Figure D.32: Chart of boundary pressures for different P_{OG}

Case 6.1.1: α_G **= 0.5 &** P_{OG} **= 84.94** $bara$

Table D.10: Residuals and imbalances for case 6.1.1

Equation	RMS	MAX	Location MAX - Node number	Imbalance [%]
U-Mom-oil	1.1E-5	3.0E-3	983140	0.0000
V-Mom-oil	2.3E-5	7.0E-3	922056	-0.0000
W-Mom-oil	5.3E-6	1.6E-3	834569	-0.0000
U-Mom-gas	1.4E-5	2.7E-3	1085212	-0.0000
V-Mom-gas	3.0E-5	3.9E-3	1184981	0.0000
W-Mom-gas	5.3E-6	7.5E-4	1192071	0.0000
P-Vol	2.6E-9	5.1E-7	1158797	-0.0072
Mass-oil	4.7E-4	1.0E-1	1186095	-0.0504
Mass-gas	4.7E-4	1.3E-1	1188869	-0.0789
K-TurbKE	6.6E-5	1.8E-2	862437	
E-Diss.K	8.3E-4	2.7E-1	1192209	

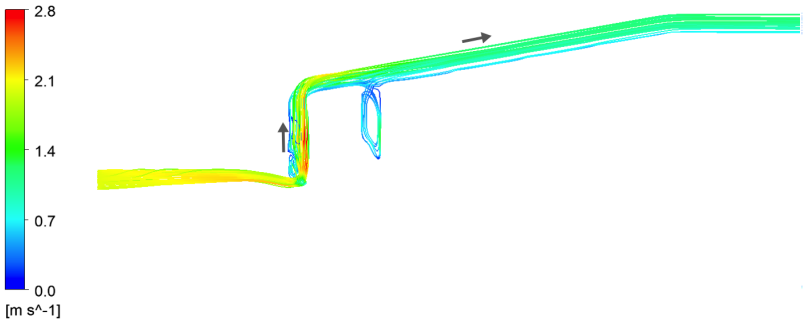

(a) Gas velocity

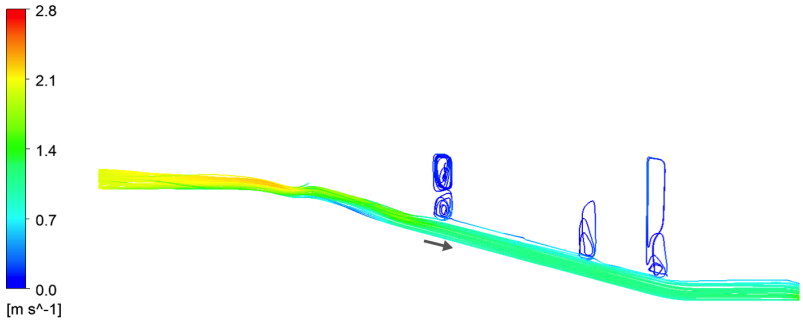

(b) Oil velocity

Figure D.33: Streamline plot of gas and oil velocity from case 6.1.1, with arrows indicating the main flow direction

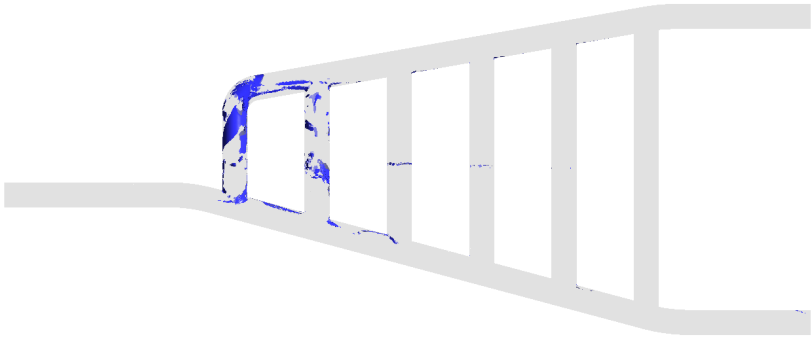

Figure D.34: Location of residuals with a value > 0.001 for case 6.1.1

Case 6.1.2: α_G **= 0.7 &** P_{OG} **= 84.94** $bara$

Table D.11: Residuals and imbalances for case 6.1.2

Equation	RMS	MAX	Location MAX - Node number	Imbalance [%]
U-Mom-oil	4.6E-6	1.6E-3	1192073	-0.0000
V-Mom-oil	1.2E-5	7.8E-3	1191559	0.0000
W-Mom-oil	3.1E-6	2.2E-3	1192073	0.0000
U-Mom-gas	4.0E-6	1.1E-3	910335	0.0000
V-Mom-gas	1.3E-5	1.0E-3	1186964	-0.0000
W-Mom-gas	2.5E-6	5.4E-4	1189845	-0.0000
P-Vol	2.0E-9	5.1E-7	1192073	-0.1837
Mass-oil	2.6E-4	3.6E-2	1007105	-0.0579
Mass-gas	2.2E-4	5.4E-2	1212693	-0.0005
K-TurbKE	1.1E-4	8.8E-3	1192073	
E-Diss.K	2.8E-4	3.0E-1	1192073	

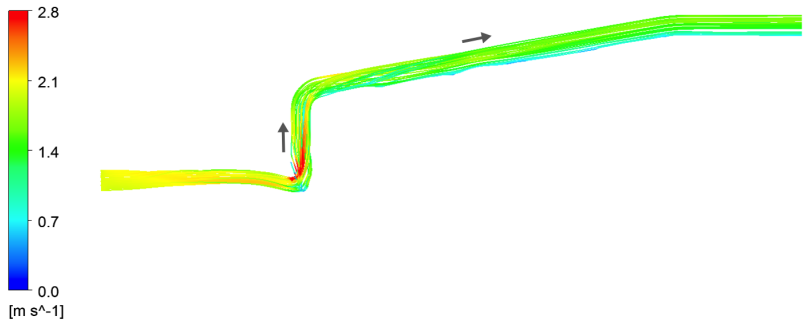

(a) Gas velocity

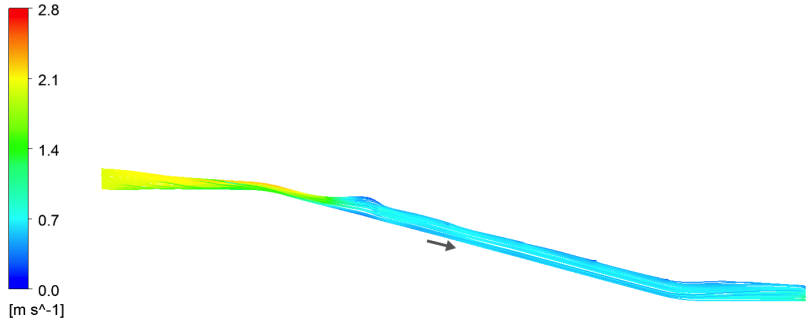

(b) Oil velocity

Figure D.35: Streamline plot of gas and oil velocity from case 6.1.2, with arrows indicating the main flow direction

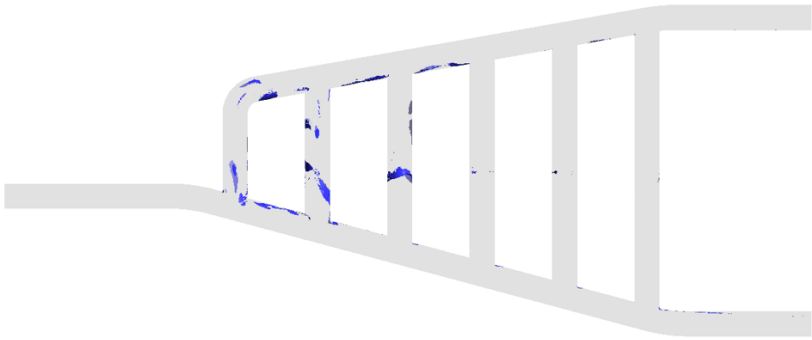

Figure D.36: Location of residuals with a value > 0.001 for case 6.1.2

Case 6.2.1: α_G **= 0.5 &** P_{OG} **= 84.95** $bara$

Table D.12: Residuals and imbalances for case 6.2.1

Equation	RMS	MAX	Location MAX - Node number	Imbalance [%]
U-Mom-oil	2.4E-6	4.0E-4	1002260	0.0000
V-Mom-oil	5.0E-6	1.0E-3	1001424	-0.0000
W-Mom-oil	1.6E-6	2.3E-4	1000205	-0.0000
U-Mom-gas	1.9E-6	5.2E-4	1188487	-0.0000
V-Mom-gas	1.4E-5	2.6E-3	1001424	-0.0000
W-Mom-gas	3.3E-6	1.7E-3	950192	0.0000
P-Vol	7.0E-10	2.6E-7	1184325	-0.0246
Mass-oil	1.1E-4	1.9E-2	911991	0.0070
Mass-gas	1.8E-4	3.6E-2	1185977	-0.0060
K-TurbKE	1.1E-5	2.8E-3	1186527	
E-Diss.K	1.1E-4	4.3E-2	1188452	

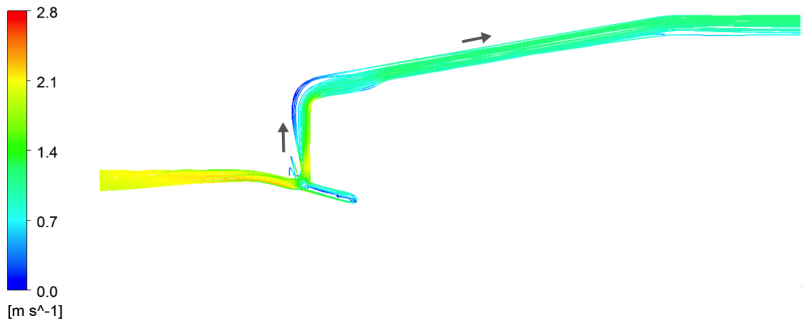

(a) Gas velocity

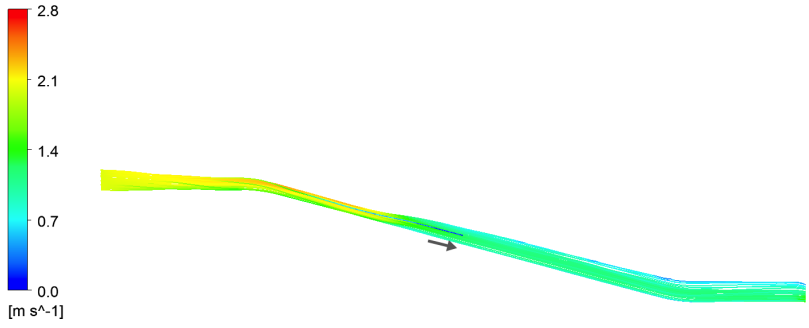

(b) Oil velocity

Figure D.37: Streamline plot of gas and oil velocity from case 6.2.1, with arrows indicating the main flow direction

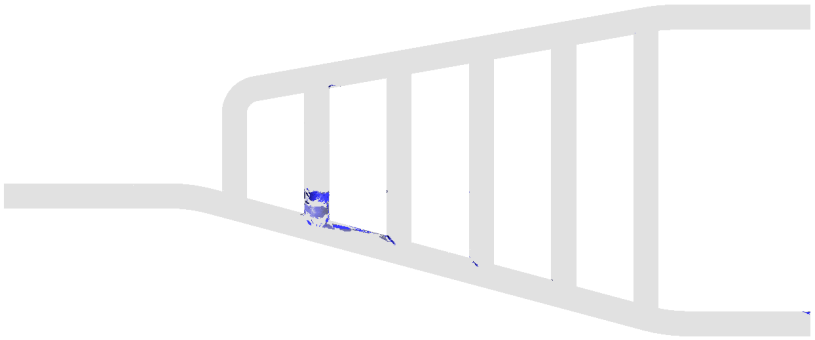

Figure D.38: Location of residuals with a value > 0.001 for case 6.2.1

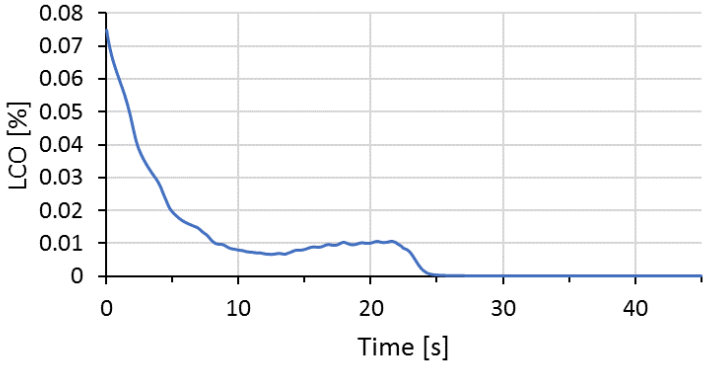

(a) LCO

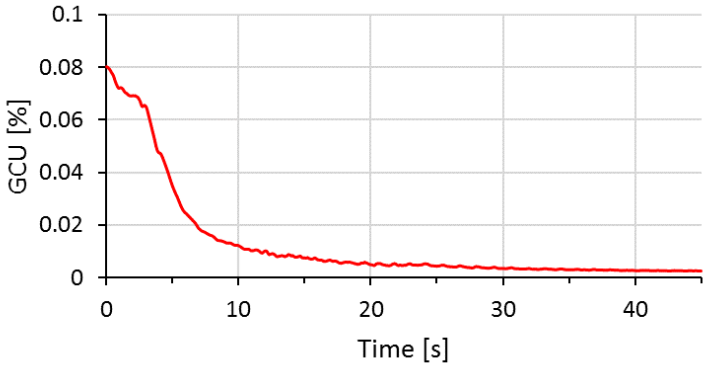

(b) GCU

Figure D.39: Transient behaviour of LCO and GCU for case 6.2.1

Case 6.2.2: α_G **= 0.7 &** P_{OG} **= 84.95** $bara$

Table D.13: Residuals and imbalances for case 6.2.2

Equation	RMS	MAX	Location MAX - Node number	Imbalance [%]
U-Mom-oil	8.4E-6	1.7E-3	1002992	0.0000
V-Mom-oil	3.4E-5	3.4E-3	1001152	-0.0000
W-Mom-oil	5.8E-6	1.1E-3	999376	-0.0000
U-Mom-gas	8.9E-6	1.8E-3	1186671	-0.0000
V-Mom-gas	3.1E-5	5.4E-3	1002992	0.0000
W-Mom-gas	8.8E-6	2.2E-3	1186213	-0.0000
P-Vol	2.4E-9	5.4E-7	1186017	0.2823
Mass-oil	2.8E-4	4.2E-2	1186017	0.0242
Mass-gas	4.1E-4	6.1E-2	1184052	0.0103
K-TurbKE	2.7E-5	5.8E-3	1186671	
E-Diss.K	3.2E-4	1.2E-1	1187494	

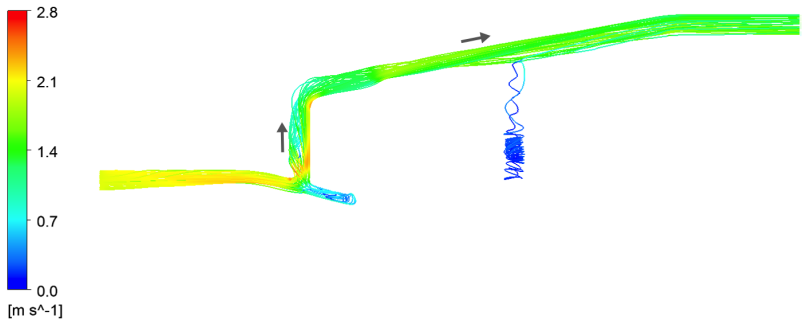

(a) Gas velocity

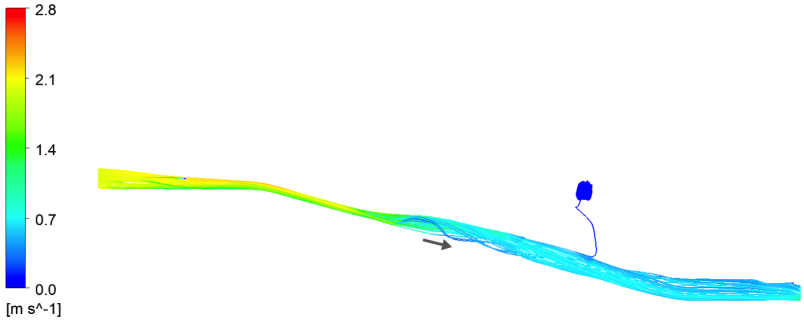

(b) Oil velocity

Figure D.40: Streamline plot of gas and oil velocity from case 6.2.2, with arrows indicating the main flow direction

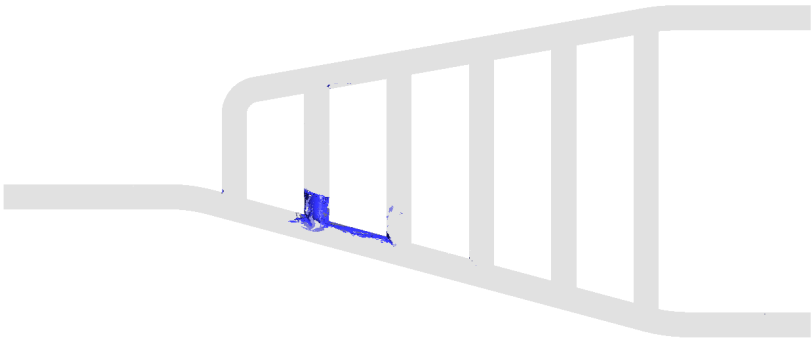

Figure D.41: Location of residuals with a value > 0.001 for case 6.2.2

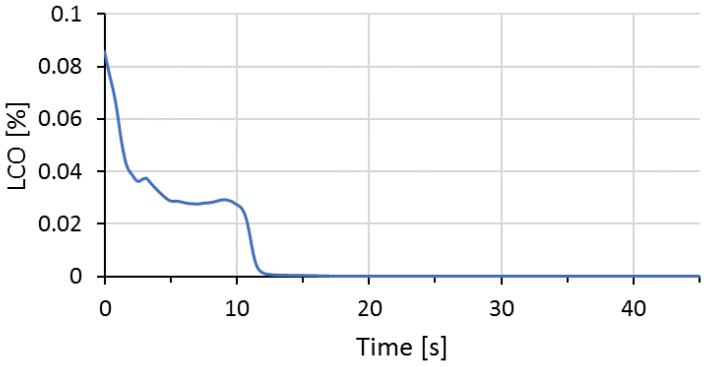

(a) LCO

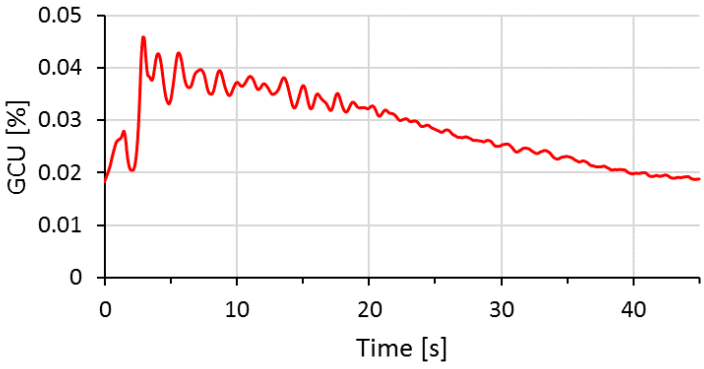

(b) GCU

Figure D.42: Transient behaviour of LCO and GCU for case 6.2.2

Appendix E

Details on CFD simulations for evaluation of slug handling

E.1 Case 7

Case 7.1: 2 meter slugs

Table E.1: Residuals and imbalances for case 7.1

Equation	RMS	MAX	Location MAX - Node number	Imbalance [%]
U-Mom-oil	1.5E-5	2.1E-3	1185514	0.0000
V-Mom-oil	2.8E-5	5.3E-3	1186017	-0.0000
W-Mom-oil	9.3E-6	3.2E-3	1188923	0.0000
U-Mom-gas	1.4E-5	2.2E-3	1001644	-0.0000
V-Mom-gas	2.4E-5	4.9E-3	1185295	-0.0000
W-Mom-gas	1.0E-5	1.7E-3	1188916	-0.0000
P-Vol	1.1E-8	2.2E-6	1184054	0.2423
Mass-oil	3.9E-4	9.4E-2	1186964	0.0588
Mass-gas	4.4E-4	1.4E-1	1217980	-0.3724
K-TurbKE	1.6E-4	4.8E-2	1185513	
E-Diss.K	4.1E-4	1.6E-1	1185513	

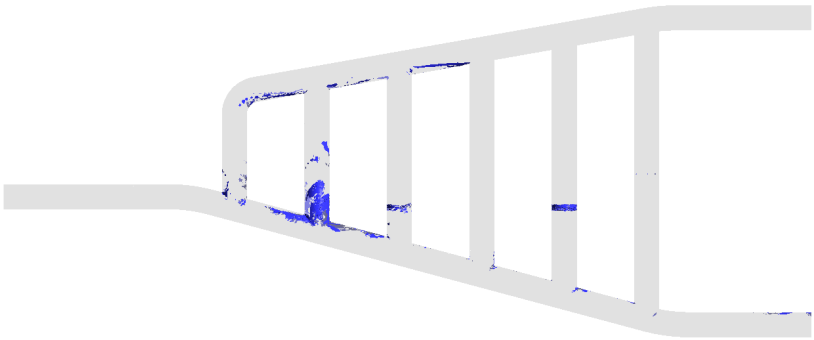

Figure E.1: Location of residuals with a value > 0.001 for case 7.1

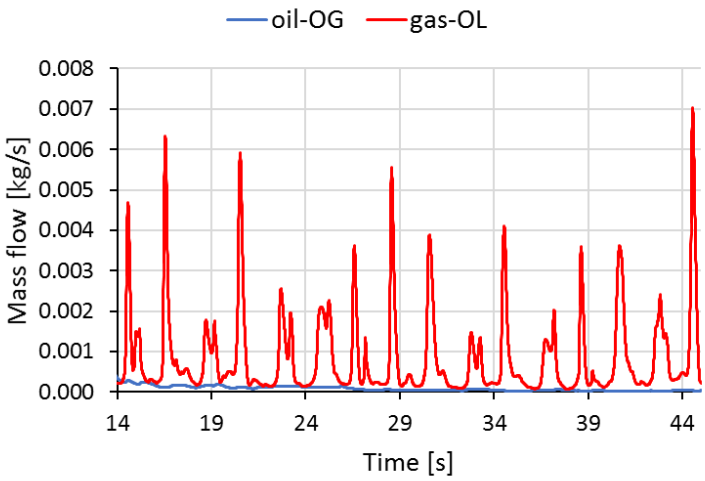

(a) Mass flow of oil carried over through OG and gas carried under through OL

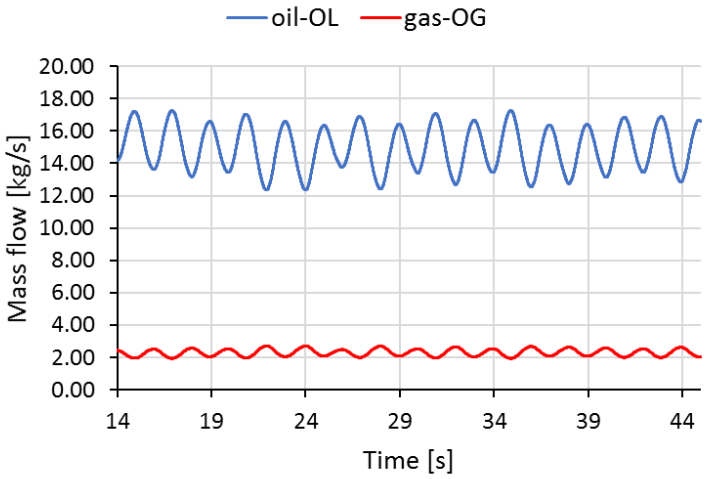

(b) Mass flow of oil flowing through OL and gas flowing through OG

Figure E.2: Charts of mass flow through outlets versus time for case 7.1

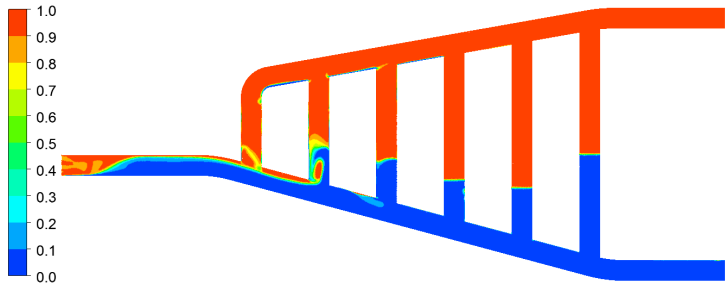

(a) 43.2 s

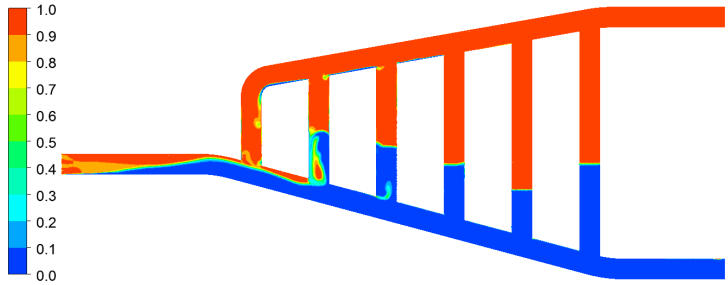

(b) 43.4 s

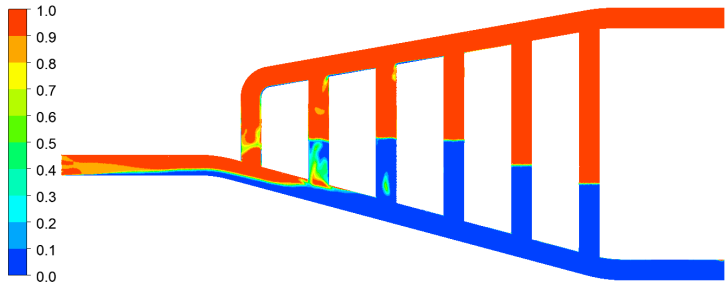

(c) 43.8 s

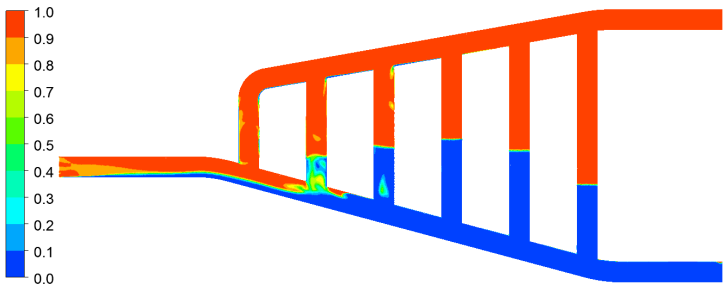

(d) 44 s

Figure E.3: GVF plots showing flow distribution for case 7.1 when a gas pocket arrives at the inlet

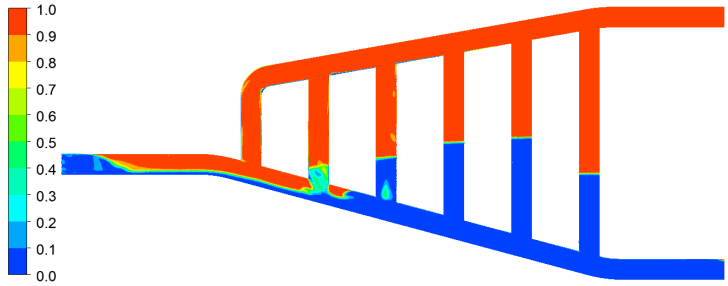

(a) 44.2 s

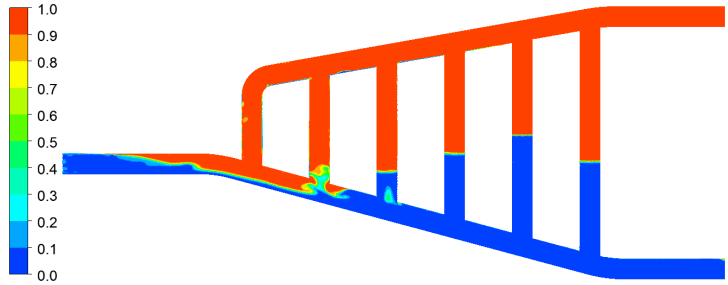

(b) 44.4 s

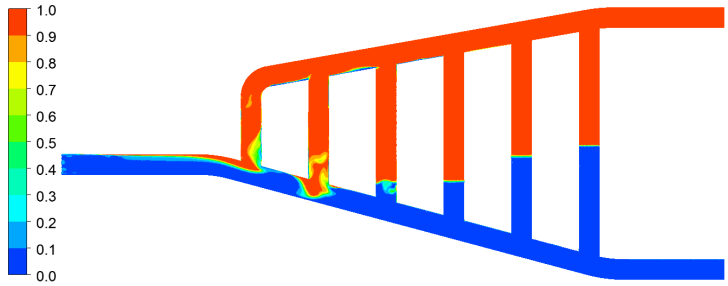

(c) 44.8 s

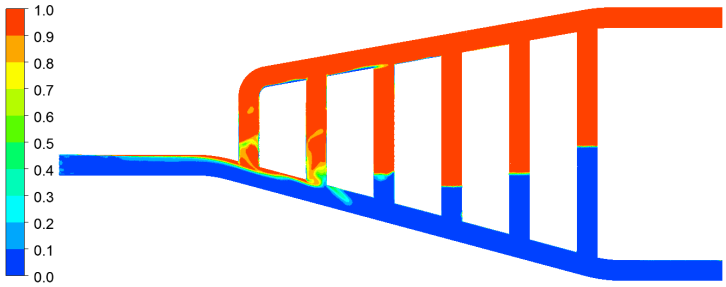

(d) 45 s

Figure E.4: GVF plots showing flow distribution for case 7.1 when a liquid slug arrives at the inlet

Case 7.2: 8 meter slugs

Table E.2: Residuals and imbalances for case 7.2

Equation	RMS	MAX	Location MAX - Node number	Imbalance [%]
U-Mom-oil	5.6E-6	2.2E-3	1136405	-0.0000
V-Mom-oil	4.8E-6	1.3E-3	843683	-0.0000
W-Mom-oil	1.9E-6	8.1E-4	843678	0.0000
U-Mom-gas	5.3E-6	3.8E-4	1152807	0.0000
V-Mom-gas	1.5E-5	1.0E-3	173807	-0.0000
W-Mom-gas	3.6E-6	1.4E-3	862705	-0.0000
P-Vol	4.6E-9	6.7E-7	1136405	1.8372
Mass-oil	1.7E-4	3.0E-2	633291	-0.7716
Mass-gas	2.0E-4	3.2E-2	1181049	0.0660
K-TurbKE	2.1E-5	1.4E-2	457864	
E-Diss.K	8.6E-5	4.6E-2	1183733	

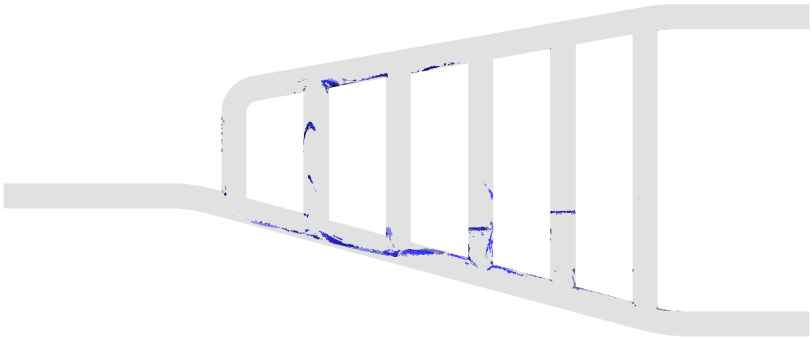

Figure E.5: Location of residuals with a value > 0.001 for case 7.1

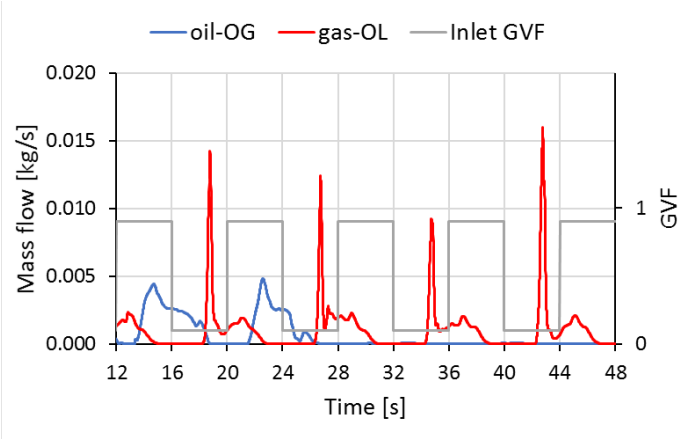

(a) Mass flow of oil carried over through OG and gas carried under through OL

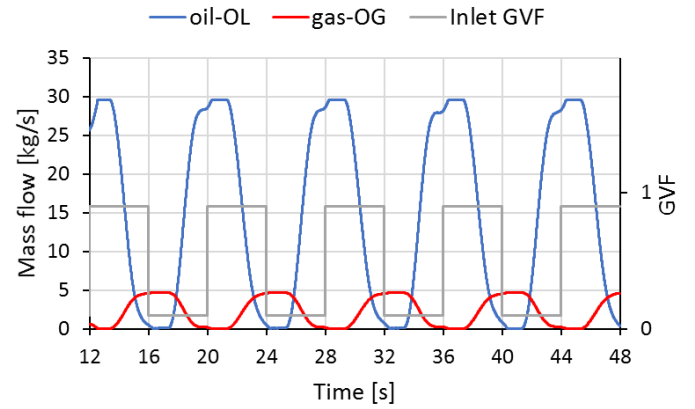

(b) Mass flow of oil flowing through OL and gas flowing through OG

Figure E.6: Charts showing mass flow through outlets versus time for case 7.2

Appendix F

ANSYS CFX simulation settings

F.1 Homogeneous free surface model

```
FLOW: Flow Analysis 1
SOLUTION UNITS:
  Angle Units = [rad]
  Length Units = [m]
  Mass Units = [kg]
  Solid Angle Units = [sr]
  Temperature Units = [K]
  Time Units = [s]
END
ANALYSIS TYPE:
  Option = Steady State
  EXTERNAL SOLVER COUPLING:
    Option = None
  END
END
DOMAIN: Default Domain
  Coord Frame = Coord 0
  Domain Type = Fluid
  Location = PART_1_1_1_SOLID
  BOUNDARY: Inlet
    Boundary Type = INLET
    Location = INLET
    BOUNDARY CONDITIONS:
      FLOW REGIME:
        Option = Subsonic
      END
      MASS AND MOMENTUM:
        Normal Speed = 2 [m s^-1]
        Option = Normal Speed
      END
      TURBULENCE:
        Option = Medium Intensity and Eddy Viscosity Ratio
      END
    END
    FLUID: gas
      BOUNDARY CONDITIONS:
        VOLUME FRACTION:
          Option = Value
          Volume Fraction = 0.3
        END
      END
    END
    FLUID: oil
```

```
    BOUNDARY CONDITIONS:
      VOLUME FRACTION:
        Option = Value
        Volume Fraction = 0.7
      END
    END
  END
END
BOUNDARY: Outlet Gas
  Boundary Type = OUTLET
  Location = OUTLET_GAS
  BOUNDARY CONDITIONS:
    FLOW REGIME:
      Option = Subsonic
    END
    MASS AND MOMENTUM:
      Option = Average Static Pressure
      Pressure Profile Blend = 0.05
      Relative Pressure = 84.906 [bar]
    END
    PRESSURE AVERAGING:
      Option = Average Over Whole Outlet
    END
  END
END
BOUNDARY: Outlet Liquid
  Boundary Type = OUTLET
  Location = OUTLET_LIQUID
  BOUNDARY CONDITIONS:
    FLOW REGIME:
      Option = Subsonic
    END
    MASS AND MOMENTUM:
      Option = Average Static Pressure
      Pressure Profile Blend = 0.05
      Relative Pressure = 85 [bar]
    END
    PRESSURE AVERAGING:
      Option = Average Over Whole Outlet
    END
  END
END
BOUNDARY: Walls
  Boundary Type = WALL
  Location = Primitive 2D
  BOUNDARY CONDITIONS:
    MASS AND MOMENTUM:
      Option = No Slip Wall
    END
    WALL ROUGHNESS:
      Option = Smooth Wall
    END
  END
  FLUID PAIR: gas | oil
    BOUNDARY CONDITIONS:
      WALL ADHESION:
        Option = None
      END
    END
  END
END
DOMAIN MODELS:
  BUOYANCY MODEL:
```

```
    Buoyancy Reference Density = 128 [kg m^-3]
    Gravity X Component = 0 [m s^-2]
    Gravity Y Component = -9.81 [m s^-2]
    Gravity Z Component = 0 [m s^-2]
    Option = Buoyant
    BUOYANCY REFERENCE LOCATION:
      Cartesian Coordinates = 3.7 [m], 1.16031 [m], 0 [m]
      Option = Cartesian Coordinates
    END
  END
  DOMAIN MOTION:
    Option = Stationary
  END
  MESH DEFORMATION:
    Option = None
  END
  REFERENCE PRESSURE:
    Reference Pressure = 85 [bar]
  END
END
FLUID DEFINITION: gas
  Material = Gas
  Option = Material Library
  MORPHOLOGY:
    Option = Continuous Fluid
  END
END
FLUID DEFINITION: oil
  Material = Oil
  Option = Material Library
  MORPHOLOGY:
    Option = Continuous Fluid
  END
END
FLUID MODELS:
  COMBUSTION MODEL:
    Option = None
  END
  FLUID: gas
    FLUID BUOYANCY MODEL:
      Option = Density Difference
    END
  END
  FLUID: oil
    FLUID BUOYANCY MODEL:
      Option = Density Difference
    END
  END
  HEAT TRANSFER MODEL:
    Homogeneous Model = True
    Option = None
  END
  THERMAL RADIATION MODEL:
    Option = None
  END
  TURBULENCE MODEL:
    Option = k epsilon
    BUOYANCY TURBULENCE:
      Option = None
    END
  END
  TURBULENT WALL FUNCTIONS:
```

```
        Option = Scalable
      END
    END
    FLUID PAIR: gas | oil
      Surface Tension Coefficient = 0.011 [N m^-1]
      INTERPHASE TRANSFER MODEL:
        Interface Length Scale = 1. [mm]
        Option = Mixture Model
      END
      MASS TRANSFER:
        Option = None
      END
      SURFACE TENSION MODEL:
        Option = Continuum Surface Force
        Primary Fluid = oil
      END
    END
    MULTIPHASE MODELS:
      Homogeneous Model = On
      FREE SURFACE MODEL:
        Option = Standard
      END
    END
  END
COMMAND FILE:
  Version = 17.2
  Results Version = 17.2
END
```

F.2 Inhomogeneous mixture model

```
FLOW: Flow Analysis 1
   SOLUTION UNITS:
     Angle Units = [rad]
     Length Units = [m]
     Mass Units = [kg]
     Solid Angle Units = [sr]
     Temperature Units = [K]
     Time Units = [s]
   END
   ANALYSIS TYPE:
     Option = Transient
     EXTERNAL SOLVER COUPLING:
       Option = None
     END
     INITIAL TIME:
       Option = Automatic with Value
       Time = 0 [s]
     END
     TIME DURATION:
       Option = Total Time
       Total Time = 45 [s]
     END
     TIME STEPS:
       Option = Timesteps
       Timesteps = 0.008 [s]
     END
   END
   DOMAIN: Default Domain
     Coord Frame = Coord 0
     Domain Type = Fluid
     Location = PART_1_1_1_SOLID
     BOUNDARY: Inlet
       Boundary Type = INLET
       Location = INLET
       BOUNDARY CONDITIONS:
         FLOW REGIME:
           Option = Subsonic
         END
         MASS AND MOMENTUM:
           Normal Speed = 2 [m s^-1]
           Option = Normal Speed
         END
         TURBULENCE:
           Option = Medium Intensity and Eddy Viscosity Ratio
         END
       END
       FLUID: gas
         BOUNDARY CONDITIONS:
           VOLUME FRACTION:
             Option = Value
             Volume Fraction = 0.3
           END
         END
       END
       FLUID: oil
         BOUNDARY CONDITIONS:
           VOLUME FRACTION:
```

```
        Option = Value
        Volume Fraction = 0.7
      END
    END
  END
END
BOUNDARY: Outlet Gas
  Boundary Type = OUTLET
  Location = OUTLET_GAS
  BOUNDARY CONDITIONS:
    FLOW REGIME:
      Option = Subsonic
    END
    MASS AND MOMENTUM:
      Option = Average Static Pressure
      Pressure Profile Blend = 0.05
      Relative Pressure = 84.95 [bar]
    END
    PRESSURE AVERAGING:
      Option = Average Over Whole Outlet
    END
  END
END
BOUNDARY: Outlet Liquid
  Boundary Type = OUTLET
  Location = OUTLET_LIQUID
  BOUNDARY CONDITIONS:
    FLOW REGIME:
      Option = Subsonic
    END
    MASS AND MOMENTUM:
      Option = Average Static Pressure
      Pressure Profile Blend = 0.05
      Relative Pressure = 85 [bar]
    END
    PRESSURE AVERAGING:
      Option = Average Over Whole Outlet
    END
  END
END
BOUNDARY: Walls
  Boundary Type = WALL
  Location = Primitive 2D
  BOUNDARY CONDITIONS:
    MASS AND MOMENTUM:
      Option = No Slip Wall
    END
    WALL CONTACT MODEL:
      Option = Use Volume Fraction
    END
    WALL ROUGHNESS:
      Option = Smooth Wall
    END
  END
END
DOMAIN MODELS:
  BUOYANCY MODEL:
    Buoyancy Reference Density = 128 [kg m^-3]
    Gravity X Component = 0 [m s^-2]
    Gravity Y Component = -9.81 [m s^-2]
    Gravity Z Component = 0 [m s^-2]
    Option = Buoyant
    BUOYANCY REFERENCE LOCATION:
```

```
      Cartesian Coordinates = 3 [m], 1.16031 [m], 0 [m]
      Option = Cartesian Coordinates
    END
  END
  DOMAIN MOTION:
    Option = Stationary
  END
  MESH DEFORMATION:
    Option = None
  END
  REFERENCE PRESSURE:
    Reference Pressure = 0 [bar]
  END
END
FLUID DEFINITION: gas
  Material = Gas
  Option = Material Library
  MORPHOLOGY:
    Option = Continuous Fluid
  END
END
FLUID DEFINITION: oil
  Material = Oil
  Option = Material Library
  MORPHOLOGY:
    Option = Continuous Fluid
  END
END
FLUID MODELS:
  COMBUSTION MODEL:
    Option = None
  END
  FLUID: gas
    FLUID BUOYANCY MODEL:
      Option = Density Difference
    END
  END
  FLUID: oil
    FLUID BUOYANCY MODEL:
      Option = Density Difference
    END
  END
  HEAT TRANSFER MODEL:
    Homogeneous Model = Off
    Option = None
  END
  THERMAL RADIATION MODEL:
    Option = None
  END
  TURBULENCE MODEL:
    Homogeneous Model = On
    Option = k epsilon
    BUOYANCY TURBULENCE:
      Option = None
    END
  END
  TURBULENT WALL FUNCTIONS:
    Option = Scalable
  END
END
FLUID PAIR: gas | oil
  Surface Tension Coefficient = 0.011 [N m^-1]
  INTERPHASE TRANSFER MODEL:
```

```
        Interface Length Scale = 1. [mm]
        Option = Mixture Model
      END
      MASS TRANSFER:
        Option = None
      END
      MOMENTUM TRANSFER:
        DRAG FORCE:
          Drag Coefficient = 0.44
          Option = Drag Coefficient
        END
      END
    END
    MULTIPHASE MODELS:
      Homogeneous Model = Off
      FREE SURFACE MODEL:
        Option = None
      END
    END
  END
COMMAND FILE:
  Version = 17.2
  Results Version = 17.2
END
```

F.3 Inhomogeneous particle model

```
FLOW: Flow Analysis 1
   SOLUTION UNITS:
     Angle Units = [rad]
     Length Units = [m]
     Mass Units = [kg]
     Solid Angle Units = [sr]
     Temperature Units = [K]
     Time Units = [s]
   END
   ANALYSIS TYPE:
     Option = Steady State
     EXTERNAL SOLVER COUPLING:
       Option = None
     END
   END
   DOMAIN: Default Domain
     Coord Frame = Coord 0
     Domain Type = Fluid
     Location = PART_1_1_1_SOLID
     BOUNDARY: Inlet
       Boundary Type = INLET
       Location = INLET
       BOUNDARY CONDITIONS:
         FLOW REGIME:
           Option = Subsonic
         END
         MASS AND MOMENTUM:
           Normal Speed = 2 [m s^-1]
           Option = Normal Speed
         END
         TURBULENCE:
           Option = Medium Intensity and Eddy Viscosity Ratio
         END
       END
       FLUID: gas
         BOUNDARY CONDITIONS:
           VOLUME FRACTION:
             Option = Value
             Volume Fraction = 0.3
           END
         END
       END
       FLUID: oil
         BOUNDARY CONDITIONS:
           VOLUME FRACTION:
             Option = Value
             Volume Fraction = 0.7
           END
         END
       END
     END
     BOUNDARY: Outlet Gas
       Boundary Type = OUTLET
       Location = OUTLET_GAS
       BOUNDARY CONDITIONS:
         FLOW REGIME:
           Option = Subsonic
         END
```

```
    MASS AND MOMENTUM:
      Option = Average Static Pressure
      Pressure Profile Blend = 0.05
      Relative Pressure = 84.906 [bar]
    END
    PRESSURE AVERAGING:
      Option = Average Over Whole Outlet
    END
  END
END
BOUNDARY: Outlet Liquid
  Boundary Type = OUTLET
  Location = OUTLET_LIQUID
  BOUNDARY CONDITIONS:
    FLOW REGIME:
      Option = Subsonic
    END
    MASS AND MOMENTUM:
      Option = Average Static Pressure
      Pressure Profile Blend = 0.05
      Relative Pressure = 85 [bar]
    END
    PRESSURE AVERAGING:
      Option = Average Over Whole Outlet
    END
  END
END
BOUNDARY: Walls
  Boundary Type = WALL
  Location = Primitive 2D
  BOUNDARY CONDITIONS:
    MASS AND MOMENTUM:
      Option = No Slip Wall
    END
    WALL CONTACT MODEL:
      Option = Use Volume Fraction
    END
    WALL ROUGHNESS:
      Option = Smooth Wall
    END
  END
END
DOMAIN MODELS:
  BUOYANCY MODEL:
    Buoyancy Reference Density = 814 [kg m^-3]
    Gravity X Component = 0 [m s^-2]
    Gravity Y Component = -9.81 [m s^-2]
    Gravity Z Component = 0 [m s^-2]
    Option = Buoyant
    BUOYANCY REFERENCE LOCATION:
      Cartesian Coordinates = 3 [m], 1.16031 [m], 0 [m]
      Option = Cartesian Coordinates
    END
  END
  DOMAIN MOTION:
    Option = Stationary
  END
  MESH DEFORMATION:
    Option = None
  END
  REFERENCE PRESSURE:
    Reference Pressure = 85 [bar]
```

```
  END
END
FLUID DEFINITION: gas
  Material = Gas
  Option = Material Library
  MORPHOLOGY:
    Mean Diameter = 0.1 [mm]
    Option = Dispersed Fluid
  END
END
FLUID DEFINITION: oil
  Material = Oil
  Option = Material Library
  MORPHOLOGY:
    Option = Continuous Fluid
  END
END
FLUID MODELS:
  COMBUSTION MODEL:
    Option = None
  END
  FLUID: gas
    FLUID BUOYANCY MODEL:
      Option = Density Difference
    END
  END
  FLUID: oil
    FLUID BUOYANCY MODEL:
      Option = Density Difference
    END
  END
  HEAT TRANSFER MODEL:
    Homogeneous Model = Off
    Option = None
  END
  THERMAL RADIATION MODEL:
    Option = None
  END
  TURBULENCE MODEL:
    Homogeneous Model = On
    Option = k epsilon
    BUOYANCY TURBULENCE:
      Option = None
    END
  END
  TURBULENT WALL FUNCTIONS:
    Option = Scalable
  END
END
FLUID PAIR: gas | oil
  Surface Tension Coefficient = 0.011 [N m^-1]
  INTERPHASE TRANSFER MODEL:
    Option = Particle Model
  END
  MASS TRANSFER:
    Option = None
  END
  MOMENTUM TRANSFER:
    DRAG FORCE:
      Option = Ishii Zuber
    END
    LIFT FORCE:
```

```
          Option = Tomiyama
        END
        TURBULENT DISPERSION FORCE:
          Option = Favre Averaged Drag Force
          Turbulent Dispersion Coefficient = 1.0
        END
        VIRTUAL MASS FORCE:
          Option = None
        END
        WALL LUBRICATION FORCE:
          Option = Tomiyama
          Pipe Diameter = 6 [in]
        END
      END
      TURBULENCE TRANSFER:
        ENHANCED TURBULENCE PRODUCTION MODEL:
          Option = None
        END
      END
    END
    MULTIPHASE MODELS:
      Homogeneous Model = Off
      FREE SURFACE MODEL:
        Option = None
      END
    END
  END
COMMAND FILE:
  Version = 17.2
  Results Version = 17.2
```

Appendix G

ANSYS CFX materials settings

G.1 Gas

```
MATERIAL: Gas
  Material Description = Air at 25 C and 1 atm (dry)
  Material Group = Air Data,Constant Property Gases
  Option = Pure Substance
  Thermodynamic State = Gas
  PROPERTIES:
    Option = General Material
    EQUATION OF STATE:
      Density = 128 [kg m^-3]
      Molar Mass = 28.96 [kg kmol^-1]
      Option = Value
    END
    SPECIFIC HEAT CAPACITY:
      Option = Value
      Specific Heat Capacity = 1.0044E+03 [J kg^-1 K^-1]
      Specific Heat Type = Constant Pressure
    END
    REFERENCE STATE:
      Option = Specified Point
      Reference Pressure = 1 [atm]
      Reference Specific Enthalpy = 0. [J/kg]
      Reference Specific Entropy = 0. [J/kg/K]
      Reference Temperature = 25 [C]
    END
    DYNAMIC VISCOSITY:
      Dynamic Viscosity = 1.6e-05 [kg m^-1 s^-1]
      Option = Value
    END
    THERMAL CONDUCTIVITY:
      Option = Value
      Thermal Conductivity = 2.61E-02 [W m^-1 K^-1]
    END
    ABSORPTION COEFFICIENT:
      Absorption Coefficient = 0.01 [m^-1]
      Option = Value
    END
    SCATTERING COEFFICIENT:
      Option = Value
      Scattering Coefficient = 0.0 [m^-1]
    END
    REFRACTIVE INDEX:
      Option = Value
      Refractive Index = 1.0 [m m^-1]
```

```
    END
    THERMAL EXPANSIVITY:
      Option = Value
      Thermal Expansivity = 0.003356 [K^-1]
    END
  END
END
```

G.2 Oil

```
  MATERIAL: Oil
    Material Description = Water (liquid)
    Material Group = Water Data,Constant Property Liquids
    Option = Pure Substance
    Thermodynamic State = Liquid
    PROPERTIES:
      Option = General Material
      EQUATION OF STATE:
        Density = 814 [kg m^-3]
        Molar Mass = 18.02 [kg kmol^-1]
        Option = Value
      END
      SPECIFIC HEAT CAPACITY:
        Option = Value
        Specific Heat Capacity = 4181.7 [J kg^-1 K^-1]
        Specific Heat Type = Constant Pressure
      END
      REFERENCE STATE:
        Option = Specified Point
        Reference Pressure = 1 [atm]
        Reference Specific Enthalpy = 0.0 [J/kg]
        Reference Specific Entropy = 0.0 [J/kg/K]
        Reference Temperature = 25 [C]
      END
      DYNAMIC VISCOSITY:
        Dynamic Viscosity = 0.0095 [kg m^-1 s^-1]
        Option = Value
      END
      THERMAL CONDUCTIVITY:
        Option = Value
        Thermal Conductivity = 0.6069 [W m^-1 K^-1]
      END
      ABSORPTION COEFFICIENT:
        Absorption Coefficient = 1.0 [m^-1]
        Option = Value
      END
      SCATTERING COEFFICIENT:
        Option = Value
        Scattering Coefficient = 0.0 [m^-1]
      END
      REFRACTIVE INDEX:
        Option = Value
        Refractive Index = 1.0 [m m^-1]
      END
      THERMAL EXPANSIVITY:
        Option = Value
        Thermal Expansivity = 2.57E-04 [K^-1]
      END
    END
  END
END
```